Understanding Diffusion Through Microscopic Models

By

Anjan Roy

A thesis submitted to the Jawaharlal Nehru University
for the degree of Doctor of Philosophy

Department of Theoretical Physics
Raman Research Institute
Bangalore 560 080
October 2015

Typeset in LaTeX 2_ε.

Dedicated to my parents

Declaration:

I hereby declare that the work reported in this thesis is a record of my original work carried out at the Raman Research Institute under the supervision of Prof. Abhishek Dhar. In keeping with the ethical practice in reporting scientific information, due acknowledgements have been made wherever the findings of others have been cited. I further declare that the subject matter presented in this thesis has not formed the basis for the award of any other degree or diploma, in this or any other Institution or University. I also declare that I have run this thesis through the turnitin plagiarism software.

Prof. Abhishek Dhar
(Thesis Supervisor)

Anjan Roy
(Student)

Certificate:

This is to certify that the thesis entitled **"Tagged Particle Diffusion in One-Dimensional Systems With Hamiltonian Dynamics"** submitted by Anjan Roy for the award of the degree of Doctor of Philosophy of Jawaharlal Nehru University is his original work. The contents of this thesis have not been published or submitted to any other Institution or University for the award of any degree or diploma.

Prof. Ravi Subrahmanyan
(Centre Chairperson)
Director
Raman Research Institute
Bangalore 560 080
India

Prof. Abhishek Dhar
(Thesis Supervisor)

Acknowledgements

Firstly, I thank my supervisor Abhishek Dhar for giving me the opportunity to work with him and guiding me throughout the period of my PhD. His dedication, hard work and work ethics will always be a benchmark for me. I am also grateful to Sanjib and Onuttom for their important contributions to the work presented in this thesis. I also express my sincere gratitude towards other faculties of the institute with whom I have interacted. In particular, interactions with Sam, Supurna, Ranjini, Pramod, Madhavan, Yashodhan, Madan, Arun and Sadiq have been enriching. I would like to extend my gratitude towards faculties in nearby institutes whose courses, lectures and seminars I have attended.

I am thankful to the administrative staff of RRI for making things smooth for me. Special thanks to our group secretary Manjunath who has constantly worked towards that. Special thanks also goes to Krishnamaraju, Shailaja, Marisa and Radha for patiently helping me out in various administrative and official work. I extend my sincere thanks to Jacob and Krishnamurthy for helping me with computer issues throughout my stay in RRI. Special acknowledgement should also go to the rrihpc for enabling me to perform my simulations. I thank the library staff for helping me out whenever I needed their help. Special thanks also to the mess, canteen and clinic staff for keeping me healthy and alive during this period.

This period would not have been pleasant without the wonderful friends I made in RRI. From seniors, to batch-mates, to juniors, I had the good fortune to be with some very nice people. I express my heartfelt gratitude to my amazing seniors, especially Arif, Antara, Wasim, Nandan, Arijit, Bibhu, Deepak, Anirban, Pragya, Anagha, Rajib, Debasish and Renu for taking care of

me in my early days in the hostel. I also thank my other seniors with whom I have interacted like Dibyendu, Rahul and Abhijit for their advises. My heartiest thanks go to my batch-mates Prasad, Chaitra, Arnab, Suman, Mahavir, Samim, Jyothi, Jagdish, Avinash and Swamy for rich discussions on various academic and non-academic topics and all the wonderful time together. I also extend my heartiest thanks to Harsha, Tridib, Jagdish, Nazma, Mriganko, Gayatri, Madhuri, Rahul, Shafi and others. Special thanks to Amruta and Amrita for treating me like family. Special thanks also to Rajib for teaching me cooking. Further, I thank my friends in other institutes and all my friends from Masters who have still kept the friendship warm and alive.

Finally, I express my deepest and heartfelt gratitude and love to my parents who have been staying away from me, now already for a decade. I also extend my heartfelt gratitude to other members of my family members for their love, support and constant encouragement.

List of Publications

I. Articles in journals/Unpublished eprints:

[1] Anjan Roy, Onuttom Narayan, Abhishek Dhar and Sanjib Sabhapandit.
Tagged Particle Diffusion in One-Dimensional Gas With Hamiltonian Dynamics.
J. Stat. Phys. **150**, 851 (2013).

[2] Anjan Roy, Abhishek Dhar, Onuttom Narayan and Sanjib Sabhapandit.
Tagged Particle Diffusion in One-Dimensional Systems With Hamiltonian Dynamics - II.
J. Stat. Phys. **160**, 73 (2015).

Synopsis

The aim of this thesis is to obtain and understand the nature of diffusion of a tagged particle in classical one-dimensional systems, starting from microscopic equations of motion. Though the general problem of tagged-particle diffusion in a fluid has been studied theoretically for more than a century, the problem came to be studied for microscopic models in one-dimension only in the second half of the last century. The major attention has been on stochastic models, where individual particles execute stochastic diffusive motion (hopping/random walk/Brownian motion). For a one-dimensional system of such particles interacting via hard-core collisions or general short ranged interactions, one interesting observation is that of *sub-diffusion* of the tagged particle. This came to be known as Single-File Diffusion (SFD) and has subsequently been verified by experiments on particles diffusing in zeolites, lithographically and optically prepared one-dimensional channels and carbon nanotubes.

Though theoretical studies on such microscopic models have been extremely successful, it has to be appreciated that they still are coarse grained descriptions, in the sense that the source of stochasticity of the individual particle dynamics is unaccounted for. Thus, for a deeper understanding, it is desirable to study tagged particle diffusion from purely deterministic equations of motion. Moreover, in the very few studies that have concentrated on one-dimensional Hamiltonian systems, most of them being on integrable models of harmonic chain and equal mass hard particle gas, tagged particle diffusion has been found to be normal. This is in striking contrast to the sub-diffusive behaviour observed in stochastic systems. The question of whether this normal-diffusion survives when the integrability is broken is a fundamentally interesting question which has, surprisingly, not been investigated much. Also, how the boundary effect sets in has not been

studied in these deterministic systems. In this thesis we present extensive study on tagged-particle diffusion in various one-dimensional Hamiltonian systems with two major aims. Firstly, to study the robustness of this normal-diffusion in Hamiltonian systems and secondly, to study the effect of boundary conditions on tagged-particle diffusion.

We obtain various auto-correlation functions of the central tagged-particle in various one-dimensional Hamiltonian systems. We consider classical point particles in a finite box interacting with their nearest neighbours through various Hamiltonians. The system is prepared in thermal equilibrium and starting from this initial state, the system is allowed to evolve through Hamiltonian dynamics. The systems we study are: (i) a gas of hard particles of equal masses, (ii) a similar gas of hard particles, but with alternate masses, (iii) a chain of particles interacting via nearest neighbour harmonic potential, (iv) a chain of particles interacting via nearest neighbour Fermi-Pasta-Ulam (FPU) potential, both the β and the $\alpha-\beta$ case, and (v) a chain of particles interacting via nearest neighbour Lennard-Jones (LJ) potential at different densities. We also study some special cases of these systems.

In all the systems studied we find normal-diffusion for the tagged particle asymptotically, before boundary effect sets in. The exact nature of the correlation functions, however, is found to be system specific. The boundary effect is studied for both reflecting/fixed and periodic boundary conditions. We see that for the fixed boundary case, the mean squared displacement of the tagged-particle saturates at long times. For the periodic case, due to the presence of centre of mass motion, the tagged-particle motion goes from diffusive to ballistic rather than saturating. In both the cases, we see oscillations in the correlation functions when boundary effect sets in. This we assign to disturbances generated by particle fluctuations travelling in the system as sound wave, interfering with the motion of the tagged particle periodically.

The structure of the thesis is as follows. In Chapter 1, we begin with a historical overview of the subject of diffusion and introduce the systems and problems studied in the thesis. In Chapter 2, we begin our study on tagged-particle diffusion with the equal mass hard particle gas, where we evaluate the correlation functions both analytically and through molecular dynamics (MD) simulations. We then study the alternate mass hard particle gas. This case cannot be solved analytically, so we obtain the correlations through MD simulations only. In Chapter 3 we move to the study of various soft chains. We begin with the harmonic chain which we study both

analytically and through MD simulations. We then study the anharmonic potentials through MD simulations. We study the FPU chain for both β and the $\alpha - \beta$ models to see if the difference between the two models, found in the studies of heat conduction, is found here too. We study the LJ chain for various densities because the potential is highly inter-particle spacing dependent and we expected it to show different density dependent behaviour. In Chapter 4 we present an effective harmonic model for the non-linear Hamiltonians and compare its predictions with the simulation results of the various nonlinear systems studied in the previous chapters. Finally, in Chapter 5, we study some special cases of the systems studied above. In particular, we study the effect of periodic boundary condition, the random mass hard particle gas, mass ratio dependence of the alternate mass hard particle gas, dynamics of a heavy particle in the centre of a light equal mass system and dynamics of a heavy particle in a special configuration of hard particle system.

Contents

1

Introduction

1.1 Historical introduction to diffusion

Philosophy of physics throughout its history has mostly been reductionist. Understanding the nature of complex physical occurrences through the nature of its constituents has occupied human minds for centuries. Such wish-fullness is reflected in the following piece of scientific poem of Lucretius, dating 60 BC [1]:

"Observe what happens when sunbeams are admitted into a building and shed light on its shadowy places. You will see a multitude of tiny particles mingling in a multitude of ways... their dancing is an actual indication of underlying movements of matter that are hidden from our sight... It originates with the atoms which move of themselves [i.e., spontaneously]. Then those small compound bodies that are least removed from the impetus of the atoms are set in motion by the impact of their invisible blows and in turn cannon against slightly larger bodies. So the

movement mounts up from the atoms and gradually emerges to the level of our senses, so that those bodies are in motion that we see in sunbeams, moved by blows that remain invisible."

But such ideas of atomistic/molecular basis of matter remained only that, fragments of wishful thinking, for centuries to come. Solids and fluids were seen mainly as continuous matter without any internal structure, whose statics and dynamics are governed by deterministic laws such as Newton's equations, Pascal's law, Archimedes' principle, Bernoulli's principle, etc. Hence when Ingenhousz in 1785 [2] and Brown in 1827 [3] observed the highly zig-zag motion of mesoscopic particles in fluids, they could not explain its origin. Although in 19^{th} century great minds like that of Gibbs, Boltzmann and Avogadro, among others, came up with explicit ideas of molecular basis of fluids, the biggest success for such ideas came when Einstein in 1905 [4, 5] and Smoluchowski in 1906 [6] applied the molecular ideas to successfully describe this zig-zag motion, known as the Brownian motion. Their idea was that the incessant molecular bombardments that a mesoscopic particle feels in the fluid medium results in net unbalanced forces acting on the particle at every instant of time which in turn causes the particle to do a random walk [7]. Einstein further used the concept of osmotic pressure of suspended particles in fluid medium and, by balancing the diffusion current with the drift current, obtained the diffusion constant of the Brownian particle in terms of the fluid temperature and the fluid viscosity (through Stokes law),

$$D = RT/6\pi\eta aN \ , \tag{1.1}$$

where D is the diffusion constant of the Brownian particle in the fluid medium, R is the gas constant, T is the temperature of the surrounding fluid medium, η is the viscosity, a is the radius of the Brownian particle and N is the Avogadro number. This relation, known as the Einstein relation, was later generalized in terms of the famous regression hypothesis by Onsager [8], the quantum fluctuation-dissipation theorem by Callen and Welton [9], and with the linear response theory by Green [10, 11] and Kubo [12–14]. It is worth noting that this Einstein relation was independently obtained and reported earlier (in 1904) by Sutherland. This work was actually submitted for publication even somewhat earlier (March 1905) as compared to Einstein's paper (May 11, 1905) [15], see also [16, 17]. In these papers Einstein and Smoluchowski also heuristically derived the (overdamped) diffusion equation,

$$\frac{\partial\rho(\vec{r},t)}{\partial t} = D\nabla^2\rho(\vec{r},t) \ , \tag{1.2}$$

where $\rho(\vec{r},t)$ is the density of such particles at position $\vec{r}$ at time t. Note that, even though the above equation is written for concentration of the diffusing particles, it can be carried forward to the case of an individual Brownian particles in the fluid, by replacing the concentration with the probability of finding the particle at position $\vec{r}$ at time t. This above equation, on assuming that the Brownian particles start at origin, has the solution :

$$\rho(\vec{r},t) = \frac{1}{\sqrt{12\pi Dt}} \exp\left(-\frac{\Delta r^2}{12Dt}\right) \ , \tag{1.3}$$

where $\Delta r^2 = \left(\vec{r}(t) - \vec{r}(0)\right)^2$. From this he deduced the famous prediction that the root mean square displacement of suspended particles is proportional to the square root of time, or

$$\left\langle \Delta r^2 \right\rangle = 6Dt \ . \tag{1.4}$$

Einstein also noted that the trajectories of such Brownian particles would be memory-less and non-differentiable [18], a concept made more precise by work of Weiner [19, 20].

A crucial consequence of Einsteins theory was that from the measurement of the diffusion constant it would have been possible to extract an independent estimate of the atomistically important, and much debated Avogadro number. Perrin and his students, in a series of experiments from 1908-1911, not only verified Einstein's equations for the mean square displacement and the probability distribution function of the Brownian particles but also obtained the then most accurate estimate of the Avogadro number, Fig. (1.1) [21, 22]. The immediate validation of his theory finally vindicated the ideas of atomistic/molecular basis of matter; the remaining critics, such as Ostwald, and in particular Mach [the latter being famous for his cynical remark against such ideas of atomistic/molecular basis: "haben wirs denn gesehen?"(die Atome/Moleküle), meaning "have we actually seen it?"(the atoms/molecules)] had thus no choice left but to concede [17].

An alternative and more general treatment of Brownian motion came with the work of Langevin who introduced a continuous, coarse grained equation of motion, now called the Langevin equation, to describe the individual trajectories of the Brownian particles [23]. His equation, which is a stochastic differential equation can be written in the modern form:

$$m\ddot{\vec{r}} = \vec{\eta}(t) - \gamma\dot{\vec{r}} \ . \tag{1.5}$$

Here the effect of net unbalanced force of multitude of molecular bombardments is modelled as random uncorrelated noise ($\vec{\eta}$) and phenomenological damping constant (γ), related to each

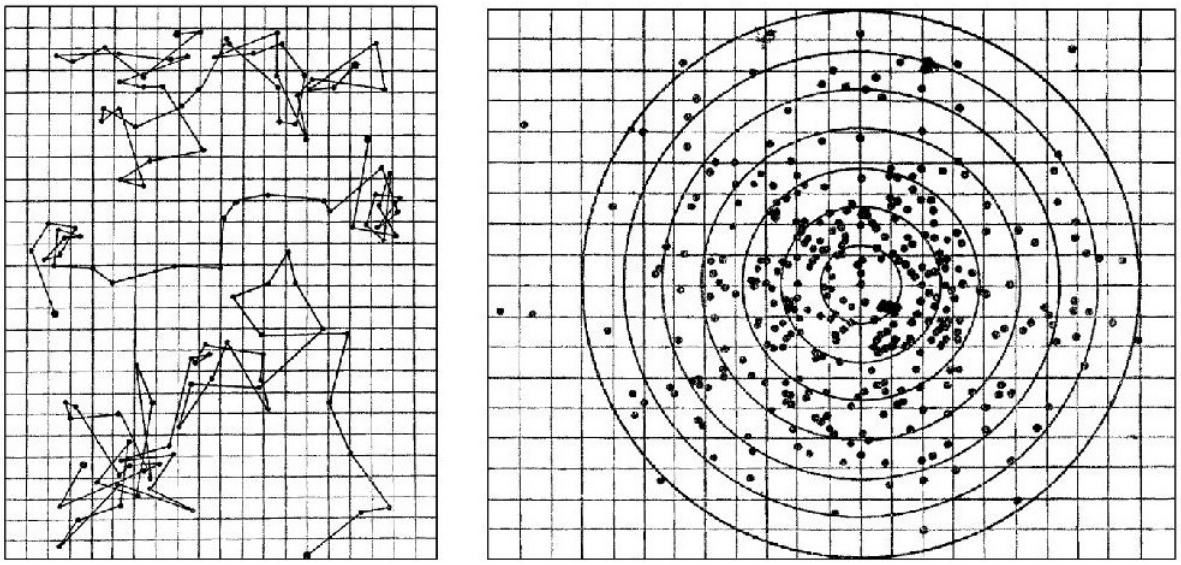

FIGURE 1.1: Recorded random walk trajectories by J B Perrin [21]. Left: three trajectories obtained by tracing a small grain of putty at intervals of 30 seconds. Right: the starting point of each motion event is shifted to the origin. The figure illustrates the probability distribution function of the travelled distance to be Gaussian, in accordance with Eq. (1.3).

other by the fluctuation-dissipation relation

$$\langle \eta_\alpha(t)\eta_\beta(t')\rangle = 2k_B T\gamma\delta(t-t')\delta_{\alpha\beta} \ , \tag{1.6}$$

where k_B is the Boltzmann constant ($k_B = R/N$). This relation, which fixes the strength of the noise and dissipation (damping) is chosen such that the Brownian particle reaches an equilibrium with the fluid medium in the long time, its velocity distribution function then being given by the Maxwell-Boltzmann distribution at temperature T. This equation gives, for the velocity auto-correlation function of the Brownian particle, the form $\langle v(0)v(t)\rangle \sim \exp(-\gamma t/m)$. In the overdamped limit, i.e. when the coefficient γ is large, this equation also gives Eqs. (1.2−1.4) at long times.

One should, however, draw attention to the fact that in the above description a strong assumption has been made, that the description of the phenomenon can be separated into two parts. This is an ad-hoc assumption that is based on the intuition that there is a separation of time scales in the problem, i.e., the time interval dt of the particle trajectory is small enough so that it has

executed only a small displacement while it is large enough that it has undergone large number of collisions with the fluid molecules, thereby validating the assumption of delta-correlated noise, and it is justified on the basis of the a posteriori success that the hypothesis enjoys in describing real phenomena. Clearly, it is desirable to derive the phenomenological Eqs. (1.5, 1.6), starting from a completely microscopic dynamical point of view. Real systems containing a large number of particles, however, are complicated in general and difficult to handle in full rigour. In order to understand the dynamical behaviour of such systems, it is important to have a number of sample systems in which the dynamical equations can be handled exactly. An interesting problem, thus, is to derive Eq. (1.5) and Eq. (1.6), starting from a completely Hamiltonian description of the system. This entails integrating out the degrees of freedom of the smaller particles (fluid molecules) and writing an effective equation for the larger particle (Brownian particle). A related problem is to understand self-diffusion, where all the particles are of similar size (no big separation of scales) and one is interested in the effective motion of one of the particles. An interesting question will then be whether and how this self-diffusion is different from Brownian diffusion. We will also be interested in understanding if a single labeled/tagged particle motion is always diffusive or if it can be anomalous in the sense that $\langle \Delta r^2 \rangle \sim t^\alpha \text{ with } \alpha \neq 1$. In the next section we shall review such attempts of microscopic dynamical derivation of tagged-particle diffusion in various model systems, mainly concentrating on studies in 1-dimension.

1.2 Dynamical/kinetic studies of diffusion in one-dimension

As mentioned in the previous section, microscopic dynamical derivations for the diffusion phenomena were sought for and various theoretical works were directed towards it in the second half of the 20^{th} century. This pursuit got further accelerated in the last couple of decades due to increased interest and advancements in single-molecule experiments. These experiments used fluorescence microscopy techniques to study dynamics of individual labeled or tagged components in various synthetic and natural systems, viz. fluorescence imaging of dye molecules in silica gel glasses to study microscopic inhomogeneities [24], study of dynamics of lipid molecules in biological membranes [25, 26], studying anomalous diffusion of fluorescent proteins in cells [27, 28] and observation of anomalous diffusion of hydra cells in cellular aggregates [29], see also [30, 31]. The

advantage of observing the dynamics of a single tagged particle is that it constitutes a simple way of probing the complex dynamics of an interacting many body system. As a result such studies have been made extensively, not only experimentally but also theoretically [32–34].

In particular, 1-dimensional systems started attracting major attention when it was found that the mean square displacement of a tagged particle in such systems grows as $\sim \sqrt{t}$ instead of $\sim t$ seen in normal-diffusive systems. The idea of such sub-diffusion in 1-dimensional systems, referred to as Single-File-Diffusion, though existed in the field of biological physics to account for the transport of water and ions through molecular-sized channels in membranes [35–40], experimental verification of the $\sqrt{t}$ scaling came much later due to lack of ideal experimentally accessible single-file systems. With progress in the synthesis of zeolitic materials, which consist of long quasi-cylindrical pores with diameters of several angstroms, came the first verification of this anomalous scaling, for methane/ethane molecules diffusing in the channel [41, 42]. However, because of the shortage of structural information on the atomic level, the mechanism of molecular diffusion in zeolites has been under constant debate [43–45]. An alternative and more straightforward verification came from experiments on colloidal systems which were confined to move in 1-dimensional physical/optical channels [46–48]. Recently such Single-File-Motion was also demonstrated in water molecules diffusing in carbon nanotube [49]. Theoretical studies that obtained this single-file scaling of the tagged-particle dynamics looked into various stochastic models [50–56], where the particles were assumed to undergo stochastic motion (Brownian motion/random walk/stochastic hopping) between hard elastic collisions. It was realized that the inability of the particles in these systems to cross each other leads to the tagged particle motion getting coupled to collective motion, which results in this interesting deviation from the normal-diffusion [56, 57].

For deterministic Hamiltonian systems in 1-dimension, the problem came to be theoretically studied first for two simple systems, (i) the harmonic chain [58–61] and (ii) the equal mass hard particle gas [62–67], both of which could be solved exactly analytically. One of the questions addressed in these papers was that of tagged-particle dynamics and it was proved that in both these systems the motion is normal-diffusive. This is in striking contrast to the anomalous diffusion seen for 1-dimensional stochastic systems. Moreover, the long time form of the velocity auto-correlation function was found to be $\sim 1/t^3$ for the hard particle gas and $\sin(\omega t)/\sqrt{t}$ for the

harmonic chain. Note that these functional forms are very different from the exponential form obtained from the Langevin dynamics. This may be seen as a signature of the self-diffusion being different than diffusion of a heavy particle. Also, note that both these systems are integrable models and an interesting problem would be to study tagged-particle dynamics in non-integrable models. Since the dynamics in the non-integrable models is expected to be ergodic, it would be interesting to see its implication on tagged-particle diffusion.

In the late 60's Alder and Wainwright published series of papers on the velocity auto-correlation of a hard particle gas in $3-$ and $2-$dimensions and obtained, through molecular dynamics computer simulations and hydrodynamic theory, the famous result that $\langle v(0)v(t)\rangle \sim t^{-d/2}$, where d is the dimensionality [68–70]. Notice that, given the Green-Kubo formula $D = \int_0^\infty \langle v(0)v(t)\rangle dt$, this would imply diverging diffusion constant in $1-$ and $2-$dimensions for $t \to \infty$. Moreover, this form for the velocity auto-correlation function is clearly not satisfied by the hard particle gas and the harmonic chain mentioned above. In fact, the hydrodynamic theory is based on vortex formations which is applicable only in the $3-$ and $2-$dimensions and should not hold in $1-$dimension.

Thus we see that there are lots of important questions that needs to be addressed in $1-$dimensional Hamiltonian systems :

(i) What is the effect of non-integrability on tagged-particle dynamics; does it remain normal-diffusive?

(ii) What is the nature of velocity auto-correlation function in general, when does one get Brownian motion like exponential decay for the velocity auto-correlation function and whether it ever decays so slow, so as to give rise to divergent diffusion constant?

(iii) Whether and when does one get Single-File-Diffusion like scaling of the mean square displacement in these systems?

(iv) Also, the question of how boundary conditions effect the dynamics at short and long times has remained mostly unattended.

While the problem of tagged-particle dynamics in stochastic systems were extensively studied for various situations of Brownian motion/random walk/hopping [57, 71–80], only few studies were done on non-integrable Hamiltonian systems like the alternate mass hard particle gas [81–83] and the Lennard-Jones chain [84–86]. Moreover, the computational studies suffered from

inadequate statistics. Thus, the question of robustness of the normal-diffusion in $1-$dimensional Hamiltonian systems remains poorly understood.

Notice that though there has been considerable work on these integrable and non-integrable systems in the context of heat conduction [87–89], this involves studying the propagation of conserved quantities as a function of position and time without reference to the identity of each particle. This changes things considerably: for instance, conserved quantities propagate ballistically for an equal mass hard particle gas, resulting in a thermal conductivity proportional to system size, while tagged particle dynamics in the same system is diffusive.

1.3 General introduction to the thesis

In this thesis we present a detailed study of tagged-particle dynamics in various $1-$dimensional Hamiltonian systems, like the hard particle gas (HPG) and various oscillator chains (OSC) like the harmonic (H) chain, the Fermi-Pasta-Ulam (FPU) chain and the Lennard-Jones (LJ) chain, with the aim of addressing the questions raised in the previous section [90–92]. The Hamiltonian of these systems are given by

$$H_{HPG} = \sum_{l=1}^{N} \frac{p_l^2}{2m_l} \tag{1.7}$$

$$H_{OSC} = \sum_{l=1}^{N} \frac{p_l^2}{2m} + \sum_{l=1}^{N+1} \left[\frac{k}{2}(q_l - q_{l-1})^2 \ + \frac{\alpha}{3}(q_l - q_{l-1})^3 \ + \frac{\beta}{4}(q_l - q_{l-1})^4 \right] \tag{1.8}$$

$$H_{LJ} = \sum_{l=1}^{N} \frac{p_l^2}{2m} + \sum_{l=1}^{N+1} \left[\frac{1}{(x_l - x_{l-1})^{12}} \ - \ \frac{1}{(x_l - x_{l-1})^6} \right], \tag{1.9}$$

where p_l is the momentum, q_l is the displacement about equilibrium position and x_l is the absolute position of the l^{th} particle in the system. For the harmonic chain we have $k \neq 0, \alpha = 0, \beta = 0$ while for the β FPU chain $k \neq 0, \alpha = 0, \beta \neq 0$ and for the $\alpha - \beta$ FPU chain $k \neq 0, \alpha \neq 0, \beta \neq 0$. We study both reflecting/fixed boundary condition, where $x_0 = 0, x_{N+1} = L$ or $q_0 = q_{N+1} = 0$ and periodic boundary condition, where $x_{N+1} = x_1$ or $q_{N+1} = q_1$. For the reflecting boundary we consider various correlation functions of the central particle (M) of the system which is our tagged particle. For periodic boundary all particles are equivalent and any particle can be chosen as the tagged particle. In particular, the correlation functions we compute are the mean square

displacement (MSD) $\langle[\Delta x(t)]^2\rangle$, the velocity auto-correlation function (VAF) $\langle v(0)v(t)\rangle$, and the time dependent diffusion constant $D(t) \equiv \langle \Delta x(t) v(0)\rangle$. Here $\Delta x(t) = x_M(t) - x_M(0)$ and $v(t) = v_M(t)$. Note that the three correlation functions are related to each other as

$$\begin{aligned} \frac{1}{2}\frac{d}{dt}\langle[\Delta x(t)]^2\rangle &= \langle \Delta x(t) v(0)\rangle \equiv D(t), \\ \frac{d}{dt}\langle \Delta x(t) v(0)\rangle &= \langle v(t) v(0)\rangle. \end{aligned} \tag{1.10}$$

The above equations follow from $\Delta x(t) = \int_0^t v(t')dt' \Rightarrow \langle \Delta x^2(t)\rangle = \int_0^t dt_1 \int_0^t dt_2 \langle v(t_1)v(t_2)\rangle = \int_0^t dt_1 \int_0^t dt_2 \langle v(t_1 - t_2)v(0)\rangle = 2\int_0^t d\tau \langle v(\tau)v(0)\rangle (t-\tau)$ and then taking time derivatives. The last equation on the first line of Eq. (1.10) defines the time dependent diffusivity $D(t)$. We note that in a finite closed box of size L, $\langle[\Delta x(t)]^2\rangle$ is bounded and so $\lim_{t\to\infty} D(t)$ would always either vanish or oscillate. However one is usually interested in the nature of the MSD of the particle before it sees the effect of the boundary, and it is then appropriate to study the limit $D_\infty(t) = \lim_{L\to\infty} D(t)$. We define the tagged particle motion as "normal diffusive" when $D_\infty(t \to \infty)$ is a constant, which is the diffusion constant. On the other hand, $D_\infty(t \to \infty)$ is zero for sub-diffusive, and divergent for super-diffusive behaviour.

For systems with Hamiltonian dynamics, the time evolution of the system is completely deterministic and all the randomness in the system is due to the randomness in the initial condition. Thus the averages $\langle \cdots \rangle$ are taken over the random initial configurations which we choose to be always taken from the equilibrium distribution.

The form of the correlations are examined at both "short times", when boundary effects are not felt and hence the correlation functions are system size independent, and at "long times", after boundary effects show up. At short times the form of the correlation functions is un-affected by the boundary conditions, *e.g.* periodic or reflecting boundary conditions. Hence in simulations we sometimes use periodic boundary conditions for short time studies, since one can then do an averaging over all particles, resulting in better statistics. The usage of boundary conditions will be specified again for each of the cases in their respective places.

The short time regime, as expected, typically has an initial ballistic regime with $\langle \Delta x^2(t)\rangle \sim t^2$, and we will find that this is always followed by an asymptotic diffusive regime, with $\langle \Delta x^2(t)\rangle \sim Dt$, before boundary effect sets in. We obtain exact value of this diffusion constant for the integrable cases, while for the nonlinear cases we obtain the diffusion constant through an effective

damped harmonic model.

The long time behaviour depends on boundary conditions. We see that the mean square displacement of the tagged particle saturates for the reflecting boundary case. For the periodic case, however, due to the presence of centre of mass (CoM) motion, the tagged particle motion goes from diffusive back to ballistic rather than saturating. In both the cases oscillations are seen in the correlation functions when boundary effect sets in. These are assigned to disturbances caused by particle fluctuations travelling as sound waves in the system and interfering with the motion of the tagged particle periodically. As we will see, the boundary effect typically shows up at times $t \sim L/c$ where L is the system size and c the sound speed in the system. We obtain this sound speed for our models and find it to match the period of oscillations too. In major part of this thesis we focus mainly on the reflecting boundary condition to see the long time boundary effect on tagged-particle diffusion. Only in chapter 5, we study in detail the effect of periodic boundary condition on the long time behaviour of the tagged particle.

The rest of the thesis is organized as follows:

In Chapter 2 the problem of tagged-particle diffusion is studied for the hard particle gas. Here we study both the equal mass case where all the particles are of the same mass m, as well as the alternate mass case where the particles are of masses m_1 and m_2 alternately. The equal mass case is special because the particles on collision just exchange velocities and this lends a mapping to the non-interacting picture, making it analytically tractable. We obtain analytic results for the various correlation functions in the short time diffusive regime and the long time approach to the saturation value. We also perform molecular dynamics (MD) simulations, via event-driven algorithm[93], on this system and confirm that it matches with the exact results. In the case where the masses are unequal, exact analytic evaluation of the correlation functions is no longer possible and here we only perform MD simulations. The numerical simulations for the alternate mass case indicate slow approach to normal-diffusive behaviour before saturating when the reflecting boundary effect sets in. The way it saturates, however, is very different from the equal mass case. The various correlation functions, involving the velocity and position of the tagged particle, show damped oscillations at long times after boundary effect sets in. This is due to the sound waves mentioned earlier in this section. We compute the speed of sound in this gas and find it to match the period of these oscillations. All these oscillations are however absent for

the equal mass case which doesn't support sound waves in equilibrium [64].

In Chapter 3 the problem of tagged-particle diffusion is studied for various oscillator chain systems. We start with the harmonic chain where we obtain the correlation functions both analytically, through normal mode analysis and computationally, through molecular dynamics (MD) simulations with velocity-verlet algorithm [93]. We find normal-diffusion in the intermediate time and size dependent oscillations after boundary effect sets in. We also find that even in times before the boundary effect plays role, there are oscillations in the $\langle v(0)v(t)\rangle$ and $D(t)$ correlation functions. These were absent in the hard particle gas and are due to the elastic nature of the system in the microscopic scale. For the non-linear FPU and LJ chains, where the equations of motion cannot be solved exactly, we obtain the correlation functions through MD simulations exclusively. We find the results for the FPU chain to be qualitatively similar to results for the harmonic chain, in the sense that the tagged particle shows normal-diffusion and that there are oscillations in the correlation functions, both at short times and at long times. However, there are important differences too in the details of the correlation functions. We study both the β and the $\alpha - \beta$ FPU chain and find similar behaviour between the two as far as tagged particle diffusion is concerned. The behaviour of LJ gas depends on its density. At low densities, it behaves like a hard-particle gas while at high densities, like an anharmonic chain. Importantly, this means that the tagged-particle diffusion is normal here as well. The long time oscillations are persistent for the harmonic chain while they damp out for the non-linear ones. Moreover, we find that the nature of the long time oscillations for the soft chains differ qualitatively from that for the alternate mass hard particle gas.

In Chapter 4 we attempt to tackle the problem of tagged-particle diffusion in non-linear systems analytically, by formulating a linearized equation where we model the non-linearity of the interaction potential in terms of momentum conserving noise and dissipation acting on a harmonic chain, thereby making the problem analytically tractable. The idea is that for any mode, all the other modes act as an internal heat bath. We solve this effective damped harmonic model analytically and compare its solutions with the simulation results of the various non-linear Hamiltonian systems studied in the earlier chapters. We find the effective model to describe the β FPU chain very well. For the $\alpha - \beta$ FPU chain and the high density LJ chain, though the effective model reproduces the qualitative features, the fits are not always very good. For the

alternate mass hard-particle gas or the low density LJ chain, this description fails altogether in describing the dynamics. These differences in the success of the effective model in describing the various non-linear systems shed some important light on the nature of 1-dimensional Hamiltonian systems which will be qualitatively discussed.

In Chapter 5 we consider some special cases of the models discussed in earlier chapters. In particular, we study the following problems:

(i) The long time effect of the periodic boundary condition on tagged particle dynamics. Here we focus our study on the hard particle gas and the harmonic chain and demonstrate the main general features. Among other things, we find that the centre of mass velocity, i.e. the zero mode, plays an important role.

(ii) The random mass hard particle gas where we do an averaging over the random particle masses and find the tagged particle motion to be normal-diffusive.

(iii) Mass ratio dependence in the alternate mass hard particle gas.

(iv) The case where the tagged particle is much heavier than the rest of the particles. Here, as should be expected, we re-obtain the short time exponential decay of the velocity auto-correlation function which is characteristic of regular Brownian motion.

(v) A hard particle configuration where heavy particles are separated by many light equal mass particles in-between. Our aim to study this configuration is to see if the heavy tagged particle, which reaches normal-diffusive regime quickly, shows any sign of transition from this normal-diffusion to single-file diffusion (which is subdiffusive).

2

Hard Particle Gases

2.1 Introduction

We begin our study of diffusion of a tagged particle in 1-dimensional Hamiltonian systems by considering N classical hard point particles in a 1-dimensional box of length L (see figures below). We consider the central particle of the system as the tagged particle. The particles move ballistic ally between collisions with their neighbours which are instantaneous and elastic in nature, conserving energy and momentum. The velocities of the colliding pair (say l and $l+1$) post-collision (primed variables) can be obtained from the pre-collision velocities (unprimed variables) from the two conservation principles,

$$m_l v_l' + m_{l+1} v_{l+1}' = m_l v_l + m_{l+1} v_{l+1} \tag{2.1}$$

and

$$\frac{1}{2}m_l v_l'^2 + \frac{1}{2}m_{l+1}v_{l+1}'^2 = \frac{1}{2}m_l v_l^2 + \frac{1}{2}m_{l+1}v_{l+1}^2. \tag{2.2}$$

Solving these equations we get,

$$\begin{aligned} v_l' &= \frac{(m_l - m_{l+1})}{(m_l + m_{l+1})}v_l + \frac{2m_{l+1}}{(m_l + m_{l+1})}v_{l+1}, \\ v_{l+1}' &= \frac{2m_l}{(m_l + m_{l+1})}v_l + \frac{(m_{l+1} - m_l)}{(m_l + m_{l+1})}v_{l+1} \ . \end{aligned} \tag{2.3}$$

The particles at the two ends ($l = 1, N$) collide elastically with the fixed walls so that their velocities simply reverse on collision.

Since the evolution of the system is completely deterministic, the only source of randomness will come from the initial conditions. We draw the initial state of the system from the canonical ensemble at temperature T. This implies that the initial velocities of the particles are chosen independently from the Gaussian distribution with zero mean and a variance $\overline{v_i}^2 = k_B T/m_i$ and that the initial positions of the particles are uniformly distributed in the box. Let x_i be the position of the i-th particle measured with respect to the "left" wall. Then, the order $0 < x_1 < x_2 < \cdots < x_{N-1} < x_N < L$ is maintained at all times. We study two main cases of hard particle gas in this chapter, namely the equal mass case where all the particles are of same mass m [Fig. (2.1)], and the alternate mass case where the particles are of masses m_1 and m_2 alternately [Fig. (2.2)].

In Sec. 2.2 we consider the equal mass case which is an integrable model. Here, as can be seen from Eq. (2.3) by putting $m_l = m_{l+1}$, the particles on collision just exchange velocities.

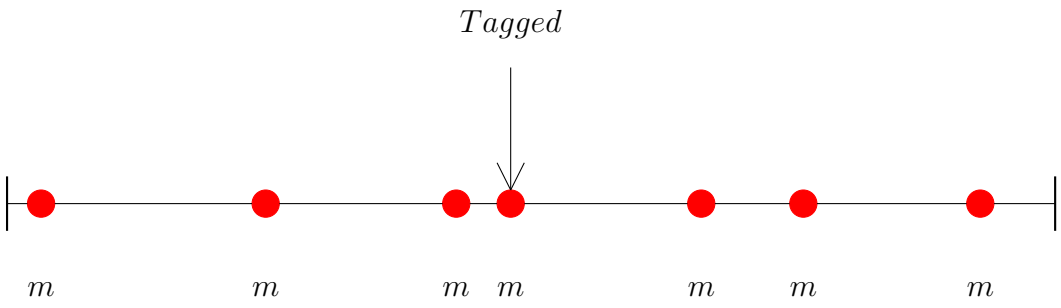

FIGURE 2.1: Schematic diagram of an equal mass hard particle gas with centre particle as tagged particle.

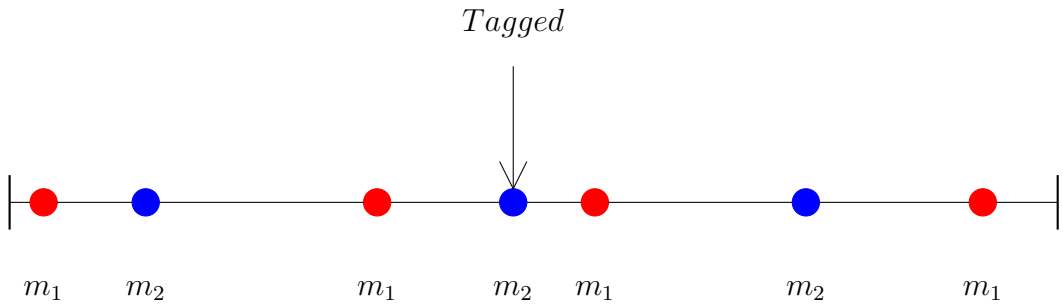

Figure 2.2: Schematic diagram of an alternate mass hard particle gas with centre particle as tagged particle.

This lends a mapping to the non-interacting picture, making it analytically tractable. This idea was first used by Jepsen [62]. For an infinite system at a fixed density of particles Jepsen had shown that the tagged-particle diffusion is normal, and that the velocity auto-correlation function at large times decay as

$$\langle v(0)v(t)\rangle \sim -1/t^3. \tag{2.4}$$

He further showed that the diffusion constant is given by

$$2D = nl^2, \tag{2.5}$$

where l (or a) is the step length (average inter-particle spacing) and n is the rate of jump given by

$$n = \rho \int_{-\infty}^{\infty} |v| g(v) dv, \tag{2.6}$$

where $\rho = N/L$ is the number density and $g(v)$ is the velocity distribution function. In our case where the initial distribution $g(v)$ is thermal, the diffusion constant becomes

$$2D = l\sqrt{2k_BT/m\pi}. \tag{2.7}$$

For a finite system, however, there must be corrections to Jepsen's result since the mean square displacement must saturate at long times (to a value that depends on the size of the system). This situation has been extensively studied for stochastic dynamics [54, 57, 76, 77, 79, 80] but not much for the Hamiltonian case [65–67]. Lebowitz and Sykes [65] considered finite size effects

for some special initial conditions. In Sec. 2.2 we study the problem for finite systems considering Boltzmann distributed initial conditions. We use an approach different and simpler than Jepsen's and obtain analytic expressions for the velocity auto-correlation function that are valid over the entire regime: both for $t << N$ diffusive regime (à la Jepsen) and $t >> N$ saturation regime (when boundary effect sets in). The short and long time analytic results are then confirmed through MD simulations.

In Sec. 2.3 we discuss the alternate mass case which is non-integrable. In this case there are no analytic results and we obtain the correlation functions through extensive MD simulations. Since the dynamics is expected to be ergodic, the correlation functions in this case should be very different from those of the equal mass case. Our motivation for studying this system would be to test the effect of this non-integrability on the tagged-particle diffusion. A similar case of binary mixture was studied by Masoliver and Marro [81, 82] who, based on MD simulations, obtained the velocity auto-correlation to decay as

$$\langle v(0)v(t)\rangle \sim -1/t. \tag{2.8}$$

This would, however, imply the diffusion constant to be going to $-\infty$. This negative infinite diffusion constant is not possible since $\langle[\Delta x(t)]^2\rangle$ is positive definite. Since their results were not statistically clean and conclusion was unphysical, we here try to understand this system better through improved statistics.

In this chapter we focus on the case with reflecting walls to study the long time boundary effect. The long time effect of periodic boundaries has lots of interesting features and will be presented separately in chapter 5. As mentioned in the previous chapter, before the boundary effect sets in, in the form of disturbances travelling through the system and interfering with the tagged-particle correlations, the correlation functions are un-affected by the nature of the boundary conditions. Thus, whenever better statistics are required for the short times study, we will use periodic boundary conditions. The advantage of using periodic periodic boundary condition is that in this case all the particles become equivalent and one can then do averaging over the particles thereby improving the statistics.

Before going into a detailed study of the two cases, we here point out that the long time saturation value of the mean square displacement can be exactly calculated and is independent of

the masses of the particles. This follows from the fact that the N-particle equilibrium measure is a product of momentum and position variables. The calculation is then based on the observation that the particles are uniformly distributed in the box and that their ordering is maintained at all times. For a system of N particles in a box of size L this gives,

$$\langle x_i \rangle = \frac{iL}{N+1}, \tag{2.9}$$

$$\langle x_i^2 \rangle = \frac{i(i+1)L^2}{(N+1)(N+2)}. \tag{2.10}$$

Hence at long times, when correlations vanish, we get

$$\begin{aligned}\langle \Delta x_i^2 \rangle &= \langle (x_i(t) - x_i(0))^2 \rangle = 2\left[\langle x_i^2 \rangle - \langle x_i \rangle^2\right] \\ &= 2\frac{i}{N+1}\left[\frac{(N+1)(i+1) - (N+2)i}{(N+1)(N+2)}\right] L^2 \\ &= 2\frac{i}{N+1}\left[\frac{(N+1-i)}{(N+1)(N+2)}\right] L^2. \end{aligned} \tag{2.11}$$

Thus we see that, for the central particle

$$MSD_{sat} \sim \frac{L}{2\rho}. \tag{2.12}$$

2.2 Equal mass hard particle gas

2.2.1 Analytic results for equal mass hard-particle gas

We begin this section by the analytic derivation of the velocity auto-correlation function for a system of N particles in a box of length L. We use reflecting boundary condition and obtain the correlation function for both short and long times, although as discussed earlier, the short time results are expected to be independent of whether the boundary conditions are periodic or reflecting. As mentioned in the previous section, by exchanging the identities of the particles emerging from collisions, one can effectively treat the actual interacting particle system [Fig. (2.3)] as non-interacting [Fig. (2.4)]. In the non-interacting particle picture, each particle executes an independent motion. The particles pass through each other when they 'collide' and reflect off the walls at $x = 0$ and $x = L$.

The initial condition is that each particle is independently chosen from the single particle distribution $p(x,v) = L^{-1}(2\pi\bar{v}^2)^{-1/2}e^{-v^2/2\bar{v}^2}$, where $\bar{v}^2 = k_BT/m$. To find the velocity auto-correlation function of the middle particle in the interacting-system from the dynamics of the non-interacting system, we note that there are two possibilities in the non-interacting picture: (1) the same particle is the middle particle at both times $t = 0$ and t [Fig. (2.5)], or (2) two different particles are at the middle position at times $t = 0$ and t respectively [Fig. (2.6)]. We denote the velocity auto-correlation function corresponding to these two cases by $\langle v_M(0)v_M(t)\rangle_1$ and $\langle v_M(0)v_M(t)\rangle_2$ respectively. The complete velocity auto-correlation function is given by

$$\langle v_M(0)v_M(t)\rangle = \langle v_M(0)v_M(t)\rangle_1 + \langle v_M(0)v_M(t)\rangle_2. \tag{2.13}$$

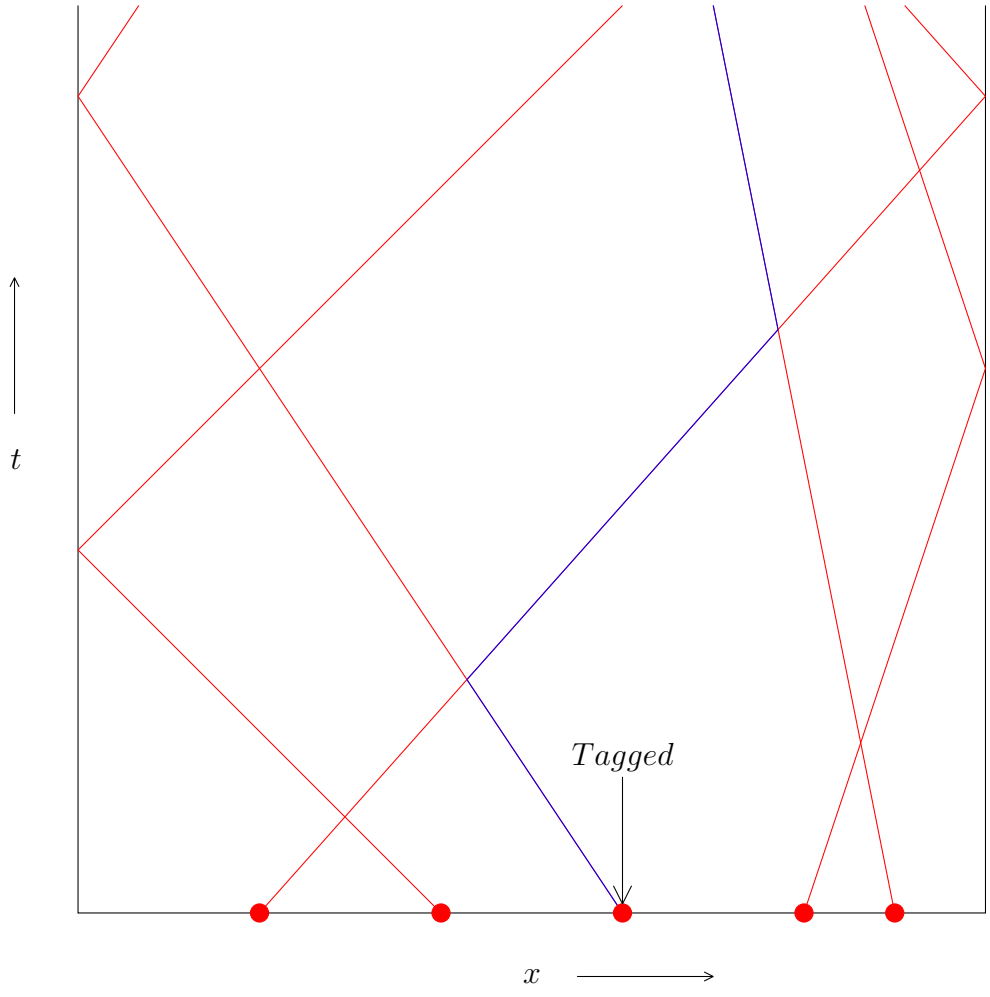

FIGURE 2.3: Equal mass hard particle gas in the interacting picture.

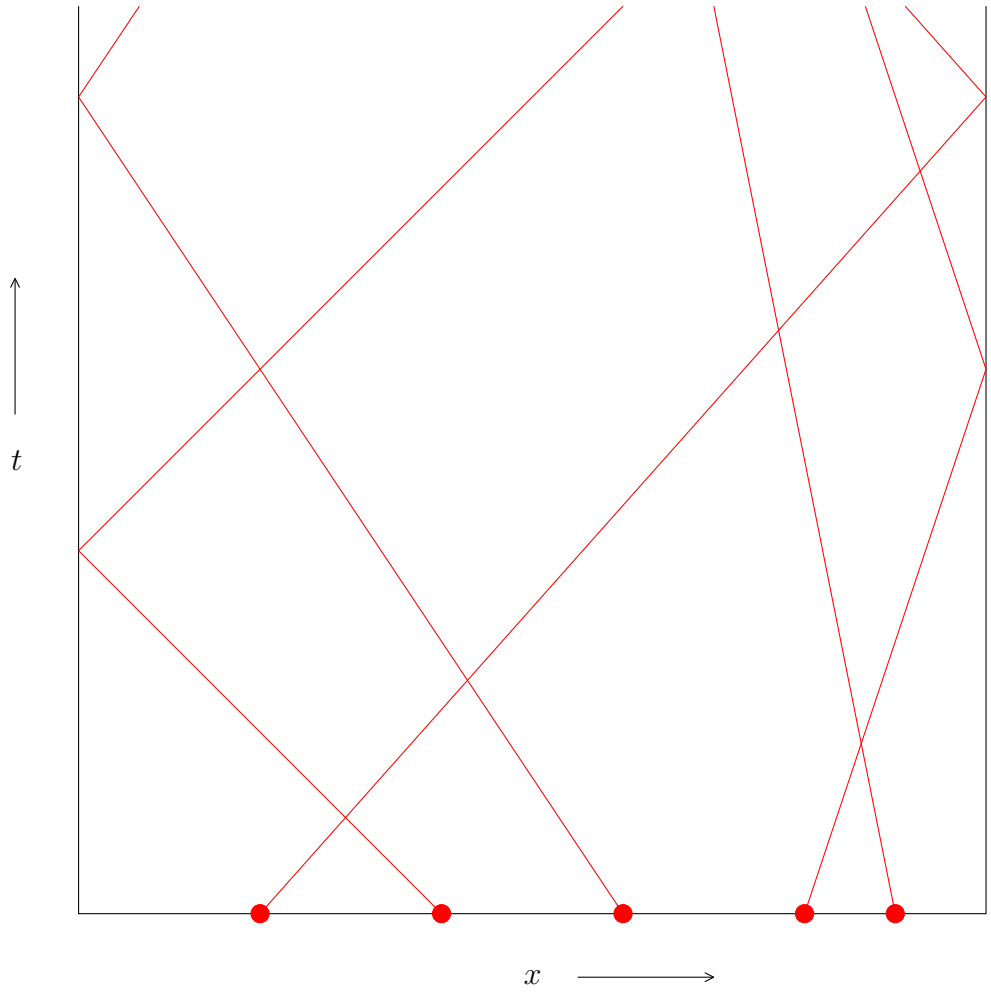

Figure 2.4: Equal mass hard particle gas in the non-interacting picture.

To compute $\langle v_M(0)v_M(t)\rangle_1$, we pick at time $t = 0$ one of the non-interacting particles at random from the distribution $p(x_0, v_0)$. At time t let the position and velocity of the particle be given by $x_t(x_0, v_0)$ and $v_t(x_0, v_0)$ respectively. We then calculate the probability, $P_N^{(1)}(x_0, x_t; t)$, that it has an equal number of particles to its left and right at both the initial and final times, *i.e.*, at $t = 0$ and t. For $\langle v_M(0)v_M(t)\rangle_2$, we pick two non-interacting particles from the distribution $p(x_0, v_0)\ p(\tilde{x}_0, \tilde{v}_0)$ and let them evolve to x_t, v_t and $\tilde{x}_t, \tilde{v}_t$ respectively. We then calculate the probability $P_N^{(2)}(x_0, \tilde{x}_t; t)$ that at time $t = 0$, the first particle x_0 is the middle particle while at

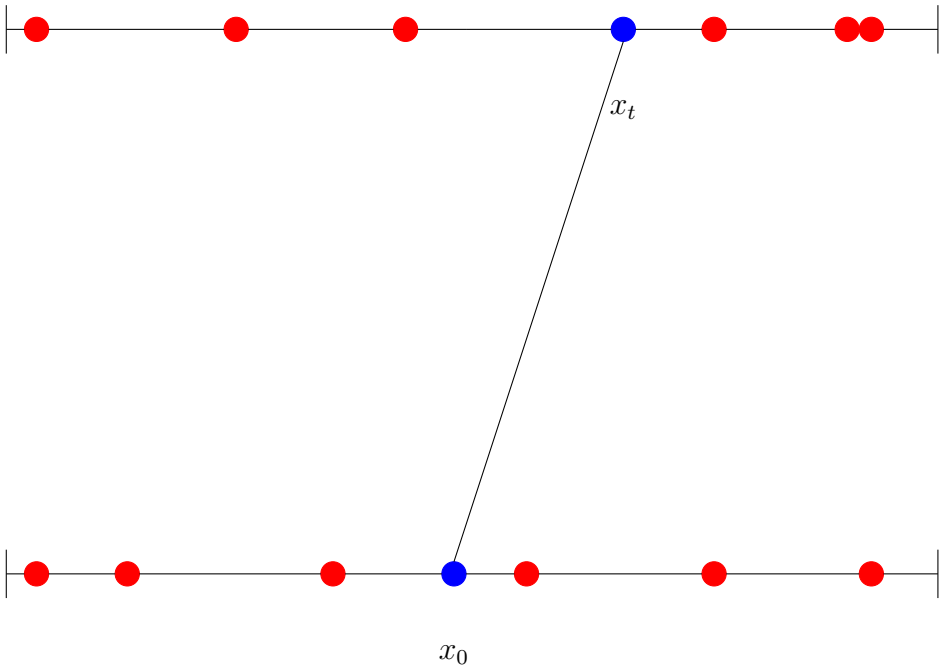

FIGURE 2.5: Diagram illustrating possibility (1)

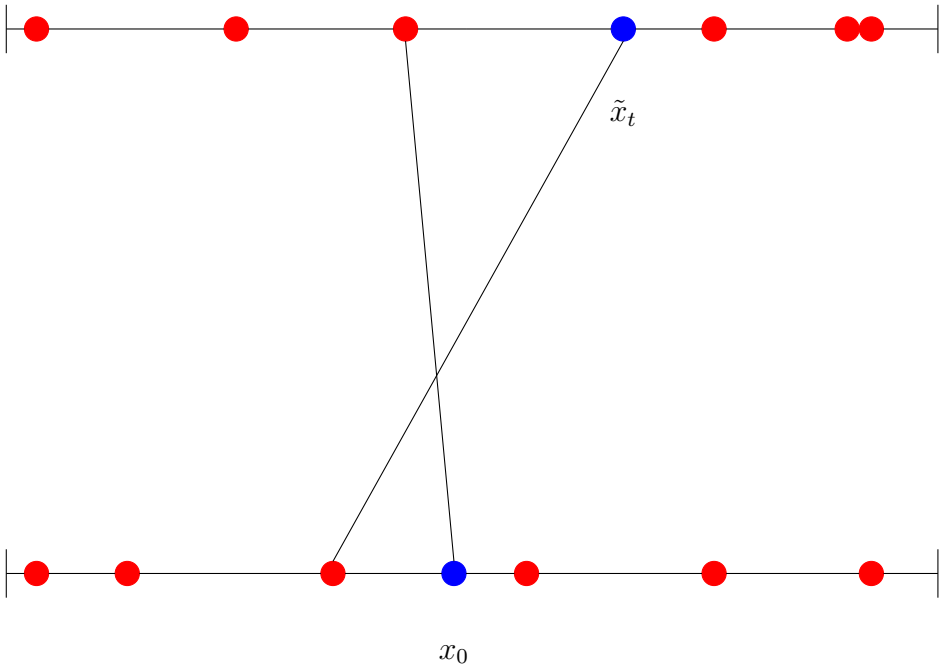

FIGURE 2.6: Diagram illustrating possibility (2)

time t the second particle $\tilde{x}_t$ is the middle particle. The normalized VAF is thus given by:

$$C_{vv}^{(1)}(t) = \frac{\langle v_M(0)v_M(t)\rangle_1}{\bar{v}^2} = \frac{N}{\bar{v}^2}\int_0^L \frac{dx_0}{L}\int_{-\infty}^{\infty}\frac{dv_0}{\sqrt{2\pi}\,\overline{v}}e^{-v_0^2/2\overline{v}^2}\, v_0 v_t\, P_N^{(1)}(x_0,x_t;t)\ , \tag{2.14}$$

$$\begin{aligned} C_{vv}^{(2)}(t) &= \frac{\langle v_M(t)v_M(0)\rangle_2}{\bar{v}^2} \\ &= \frac{N(N-1)}{\bar{v}^2}\int\cdots\int \frac{dx_0}{L}\frac{d\tilde{x}_0}{L}\frac{dv_0 d\tilde{v}_0}{2\pi\overline{v}^2}\, v_0\tilde{v}_t\, e^{-(v_0^2+\tilde{v}_0^2)/2\overline{v}^2}\ P_N^{(2)}(x_0,\tilde{x}_t;t)\ . \end{aligned} \tag{2.15}$$

In the non-interacting picture, x_t and v_t, as well as the number of collisions m, suffered by the particle with the walls upto time t, are completely determined by the initial configuration (x_0, v_0). The number of collisions with the wall is given by

$$m = \begin{cases} \left\lfloor \dfrac{x_0+v_0t}{L}\right\rfloor & \text{if } v_0>0, \\ \left\lfloor \dfrac{L-x_0-v_0t}{L}\right\rfloor & \text{if } v_0<0\ , \end{cases} \tag{2.16}$$

where $\lfloor x\rfloor$ is the integral part of x. When m is even, we have $v_t = v_0$ whereas $v_t = -v_0$ for odd m. The final position x_t is given by one of the following relations depending on m and v_0. When m is even, we have $x_0+v_0t = mL+x_t$ for $v_0>0$ and $L-x_0-v_0t = mL+L-x_t$ for $v_0<0$. On the other hand for odd m we get $x_0+v_0t = mL+L-x_t$ for $v_0>0$ and $L-x_0-v_0t = mL+x_t$ for $v_0<0$. Combining all these four cases, we can write $x_0+v_0t = 2nL\pm x_t$. Here $n=m/2$ and $-m/2$ respectively for the first two cases where m is even and the plus sign is taken. For the last two cases, where m is odd, $n=(m+1)/2$ and $-(m+1)/2$ respectively and the minus sign is taken. In other words, for a given values of x_0 and v_0 in the relations $x_0+v_0t = 2nL\pm x_t$ and $v_t=\pm v_0$, the values of n and x_t, and the signs taken from the $\pm$ are uniquely determined. Therefore, inserting the term $[\delta(x_0+v_0t-2nL-x_t)\delta(v_t-v_0)+\delta(x_0+v_0t-2nL+x_t)\delta(v_t+v_0)]$ in the integrand of Eq. (2.14) while integrating over x_t and v_t, and summing over all integer values of n, does not change the result, i.e.,

$$\begin{aligned} \langle v_M(t)v_M(0)\rangle_1 = N\int_0^L dx_t\int_{-\infty}^{\infty}dv_t\sum_{n=-\infty}^{\infty}\int_0^L\frac{dx_0}{L}\int_{-\infty}^{\infty}\frac{dv_0}{\sqrt{2\pi}\,\overline{v}} \\ \times e^{-v_0^2/2\overline{v}^2}\, v_0v_t\, P_N^{(1)}(x_0,x_t;t) \\ \times\big[\delta(x_0+v_0t-2nL-x_t)\delta(v_t-v_0)+\delta(x_0+v_0t-2nL+x_t)\delta(v_t+v_0)\big]. \end{aligned} \tag{2.17}$$

Now, carrying out the integrations over v_t and v_0, after some straightforward manipulation we obtain

$$C_{vv}^{(1)} = N \int_0^L dx_0 \int_0^L dx_t \; P_N^{(1)}(x_0, x_t; t) \;\; \partial_{\overline{v}} \; [\overline{v} P_-(x_0, x_t; t)], \tag{2.18}$$

where

$$P_\pm(x, y; t) = \frac{1}{L\sqrt{2\pi}\overline{v}t} \sum_{n=-\infty}^{\infty} \left\{ \exp\left[-\frac{(2nL + y - x)^2}{2\overline{v}^2 t^2} \right] \right. \\ \left. \pm \exp\left[-\frac{(2nL - y - x)^2}{2\overline{v}^2 t^2} \right] \right\}. \tag{2.19}$$

Using the Poisson resummation formula we can also write the above series in the form

$$P_-(x, y; t) = \frac{1}{L^2} \sum_{k=-\infty}^{\infty} \exp[-\overline{v}^2 t^2 k^2 \pi^2/(2L^2)] \sin\frac{\pi k x}{L} \sin\frac{\pi k y}{L} \;, \\ P_+(x, y; t) = \frac{1}{L^2} \sum_{k=-\infty}^{\infty} \exp[-\overline{v}^2 t^2 k^2 \pi^2/(2L^2)] \cos\frac{\pi k x}{L} \cos\frac{\pi k y}{L} \;. \tag{2.20}$$

The second part of the velocity auto-correlation function is given by Eq. (2.15) and in this case we trade the $v_0, \tilde{v}_0$ integrals for $x_t, \tilde{x}_t$ by introducing two sets of δ-function, one for each particle as in Eq. (2.17). After some manipulations we then get

$$C_{vv}^{(2)} = N(N-1) \int \cdots \int dx_0 d\tilde{x}_0 dx_t d\tilde{x}_t \; P_N^{(2)}(x_0, \tilde{x}_t; t) \\ \left[\overline{v}t \; \partial_{x_0} P_+(x_0, x_t; t)\right] \left[-\overline{v}t \; \partial_{\tilde{x}_t} P_+(\tilde{x}_0, \tilde{x}_t; t)\right], \tag{2.21}$$

Evaluation of $P_N^{(1)}(x_0, x_t; t)$: This gives the probability that, at $t = 0$ and at time t, the selected particle has an equal number of particles to its left and right. We note that the remaining $N - 1$ particles are independent of each other and the selected particle. Let $p_{-+}(x_0, x_t; t)$ be the probability that one of these particles is to the left of x_0 at $t = 0$ and to the right of x_t at time t. Let p_{+-}, p_{--} and p_{++} be similarly defined. Thus

$$p_{-+}(x, y; t) = \int_0^x dx' \int_y^L dy' P(x', y'; t) \;, \\ p_{+-}(x, y; t) = \int_x^L dx' \int_0^y dy' P(x', y'; t) \;, \\ p_{--}(x, y; t) = \int_0^x dx' \int_0^y dy' P(x', y'; t) \;, \\ p_{++}(x, y; t) = \int_x^L dx' \int_y^L dy' P(x', y'; t) \;. \tag{2.22}$$

where

$$\begin{aligned}
P(x,y;t) &= \langle \delta(x-x_0)\delta(y-x_t)\rangle \\
&= \int_0^L \frac{dx_0}{L}\int_{-\infty}^{\infty} dv_0\ \frac{e^{-v_0^2/2\bar{v}^2}}{\sqrt{2\pi}\bar{v}}\ \delta(x-x_0)\delta(y-x_t) \\
&= \int_0^L dx_t \int_{-\infty}^{\infty} dv_t \sum_{n=-\infty}^{\infty}\int_0^L \frac{dx_0}{L}\int_{-\infty}^{\infty} dv_0\ \frac{e^{-v_0^2/2\bar{v}^2}}{\sqrt{2\pi}\bar{v}}\ \delta(x-x_0)\delta(y-x_t) \\
&\times \left[\delta(x_0+v_0t-2nL-x_t)\ \delta(v_t-v_0)+\delta(x_0+v_0t-2nL+x_t)\ \delta(v_t+v_0)\right] \\
&= P_+(x,y;t)\ . \qquad (2.23)
\end{aligned}$$

In terms of these probabilities, it is easily seen that

$$P_N^{(1)} = \sum_{n_1+n_2+n_3+n_4=N-1} \frac{(N-1)!}{n_1!n_2!n_3!n_4!}\, p_{--}^{n_1}p_{-+}^{n_2}p_{+-}^{n_3}p_{++}^{n_4}\,\delta_{n_1,n_4}\delta_{n_2,n_3}, \qquad (2.24)$$

where in the summand, n_1 particles go from the left of x_0 to the left of x_t, n_2 particles from the left to the right, n_3 particles from the right to the left, and n_4 particles from the right to the right. The two Kronecker delta functions ensure that an equal number of particles cross the selected particle in both directions in time t and that an equal number of particles remain on either side of the selected particle. Together, these conditions are equivalent to an equal number of particles being on either side of the selected particle at time 0 and t, that is, $n_1+n_2=n_3+n_4$ and $n_1+n_3=n_2+n_4$. The multinomial coefficient takes care of all possible permutations among the particles. Now, after using the integral representation of the Kronecker delta, $\delta_{m,n} = (2\pi)^{-1}\int_0^{2\pi} e^{i(m-n)\theta}\,d\theta$ in the above equation, it immediately follows that

$$\begin{aligned}
P_N^{(1)} &= \int_{-\pi}^{\pi}\frac{d\phi}{2\pi}\int_{-\pi}^{\pi}\frac{d\theta}{2\pi}\ \left[p_{++}e^{i\phi}+p_{--}e^{-i\phi}+p_{+-}e^{i\theta}+p_{-+}e^{-i\theta}\right]^{N-1} \\
&= \frac{1}{(2\pi)^2}\int_{-\pi}^{\pi}d\phi\int_{-\pi}^{\pi}d\theta\ \Big[1-(1-\cos\phi)\ (p_{++}+p_{--})+i\sin\phi\ (p_{++}-p_{--}) \\
&- (1-\cos\theta)\ (p_{+-}+p_{-+})\ +i\sin\theta\ (p_{+-}-p_{-+})\Big]^{N-1} \\
&= \frac{1}{2\pi^2}\int_{-\pi/2}^{\pi/2}d\phi\int_{-\pi}^{\pi}d\theta\ \Big[1-(1-\cos\phi)\ (p_{++}+p_{--})+i\sin\phi\ (p_{++}-p_{--}) \\
&- (1-\cos\theta)\ (p_{+-}+p_{-+})\ +i\sin\theta\ (p_{+-}-p_{-+})\Big]^{N-1}\ . \qquad (2.25)
\end{aligned}$$

where we used the identity $p_{++}+p_{+-}+p_{-+}+p_{--}=1$. In the last step the range of the ϕ integral has been broken into two parts and, for even $N-1$, each of these contributes equally.

Evaluation of $P_N^{(2)}(x_0, \tilde{x}_t; t)$: In calculating $P_N^{(2)}$ we have to keep track of both the particles. There arise four situations: (a) $x_0 > \tilde{x}_0$ and $x_t < \tilde{x}_t$, (b) $x_0 > \tilde{x}_0$ and $x_t > \tilde{x}_t$, (c) $x_0 < \tilde{x}_0$ and $x_t > \tilde{x}_t$, and (d) $x_0 < \tilde{x}_0$ and $x_t < \tilde{x}_t$. Let there be n_1 particles go from the left of x_0 to the left of $\tilde{x}_t$, n_2 particles from the left to the right, n_3 particles from the right to the left, and n_4 particles from the right to the right. Since two of the particles are considered separately, the rest can be chosen $(N-2)!/(n_1!n_2!n_3!n_4!)$ different ways and $n_1+n_2+n_3+n_4 = N-2$. Now, in the first situation we have (a) $n_1+n_2+1 = n_3+n_4$ and $n_1+n_3+1 = n_2+n_4$. These conditions are equivalent to $n_2 = n_4$ and $n_1 = n_4 - 1$. Similarly one can work out the conditions for the other three situations which gives (b) $n_1 = n_4$ and $n_2 = n_3 - 1$, (c) $n_2 = n_3$ and $n_1 = n_4 + 1$, and (d) $n_1 = n_4$ and $n_2 = n_3 + 1$, respectively. Following the procedure used to evaluate $P_N^{(1)}$, it is easily found that

$$P_N^{(2)} = \int \frac{d\theta}{2\pi} \int \frac{d\phi}{2\pi} [p_{++}e^{i\phi} + p_{--}e^{-i\phi} + p_{+-}e^{i\theta} + p_{-+}e^{-i\theta}]^{N-2}\, \psi(\theta,\phi), \tag{2.26}$$

$$\begin{aligned} &= \frac{2}{(2\pi)^2} \int_{-\pi/2}^{\pi/2} d\phi \int_{-\pi}^{\pi} d\theta \, \Big[1 - (1-\cos\phi)\,(p_{++}+p_{--}) \\ &\qquad + i\sin\phi\,(p_{++}-p_{--}) - (1-\cos\theta)\,(p_{+-}+p_{-+}) \\ &\qquad + i\sin\theta\,(p_{+-}-p_{-+})\Big]^{N-2}\, \psi(\theta,\phi)\ . \end{aligned} \tag{2.27}$$

where the extra phase factor $\psi(\theta,\phi)$ originates from added ± 1 that appear in the relations among n_i's above, and $\psi(\theta,\phi) = e^{-i\phi}$, $e^{-i\theta}$, $e^{i\phi}$ and $e^{i\theta}$ for situations (a), (b), (c) and (d) respectively.

Using these we finally obtain

$$\begin{aligned} C_{vv}^{(1)} = N\frac{2}{(2\pi)^2} &\int_0^L dx \int_0^L dy \int_{-\pi/2}^{\pi/2} d\phi \int_{-\pi}^{\pi} d\theta\ \partial_{\overline{v}}[\overline{v}P_-(x,y,t)] \\ &\times \Big[1 - (1-\cos\phi)\,(p_{++}+p_{--}) + i\sin\phi\,(p_{++}-p_{--}) \\ &\quad - (1-\cos\theta)\,(p_{+-}+p_{-+}) + i\sin\theta\,(p_{+-}-p_{-+})\Big]^{N-1} \end{aligned} \tag{2.28}$$

and

$$\begin{aligned} C_{vv}^{(2)} = -N(N-1)\overline{v}^2t^2\frac{2}{(2\pi)^2} &\int_0^L dx \int_0^L d\tilde{y} \int_{-\pi/2}^{\pi/2} d\phi \int_{-\pi}^{\pi} d\theta\ P_-^2(x,\tilde{y},t) \\ &\times \Big[1 - (1-\cos\phi)\,(p_{++}+p_{--}) + i\sin\phi\,(p_{++}-p_{--}) \\ &\quad - (1-\cos\theta)\,(p_{+-}+p_{-+}) + i\sin\theta\,(p_{+-}-p_{-+})\Big]^{N-2} \\ &\times (2\cos\phi - 2\cos\theta). \end{aligned} \tag{2.29}$$

Short time regime : When $\bar{v}t << L$, the tagged particle does not feel the effect of the walls and we can make the following approximations

$$P(x,y;t) = P_+(x,y;t) = P_-(x,y;t) = \frac{1}{\sqrt{2\pi}\bar{v}tL}\exp\left[-\frac{(y-x)^2}{2\bar{v}^2t^2}\right] \ . \tag{2.30}$$

In this limit the expressions for p_{-+}, *etc.* given in Eq. (2.22) also simplify by using Eq. (2.30) and taking the limits of the y' integral to be from y to ∞ for p_{-+}, p_{++} and from $-\infty$ to y for p_{+-}, p_{--}, we then get

$$\begin{aligned}
Np_{++}(x,y;t) &\approx \frac{\rho}{\sqrt{2\pi}\bar{v}t}\int_x^L dx' \int_y^\infty dy' \ e^{-(y'-x')^2/2\bar{v}^2t^2} \ \approx \frac{N}{2} - \frac{\lambda z_+}{2} - \lambda q(z_-) \ , \\
Np_{--}(x,y;t) &\approx \frac{\rho}{\sqrt{2\pi}\bar{v}t}\int_0^x dx' \int_{-\infty}^y dy' \ e^{-(y'-x')^2/2\bar{v}^2t^2} \approx \frac{N}{2} + \frac{\lambda z_+}{2} - \lambda q(z_-) \ , \\
Np_{+-}(x,y;t) &\approx \frac{\rho}{\sqrt{2\pi}\bar{v}t}\int_x^L dx' \int_{-\infty}^y dy' \ e^{-(y'-x')^2/2\bar{v}^2t^2} \approx -\frac{\lambda z_-}{2} + \lambda q(z_-) \ , \\
Np_{-+}(x,y;t) &\approx \frac{\rho}{\sqrt{2\pi}\bar{v}t}\int_0^x dx' \int_y^\infty dy' \ e^{-(y'-x')^2/2\bar{v}^2t^2} \approx \frac{\lambda z_-}{2} + \lambda q(z_-) \ ,
\end{aligned} \tag{2.31}$$

$$\text{where } z_+ = \frac{x+y-L}{\bar{v}t}, \ z_- = \frac{x-y}{\bar{v}t} \ , \lambda = \rho\bar{v}t \ \text{ with } \rho = N/L,$$

$$\text{and } q(z_-) = \frac{e^{-z_-^2/2}}{\sqrt{2\pi}} + \frac{z_-}{2}\mathsf{Erf}(z_-/\sqrt{2}) \tag{2.32}$$

Hence we get $N(p_{++}+p_{--}) = N - 2\lambda q(z_-), \ N(p_{++}-p_{--}) = -\lambda z_+, \ N(p_{+-}+p_{-+}) = 2\lambda q(z_-), \ N(p_{+-}-p_{-+}) = -\lambda z_-$. Using these in Eqs. (2.28) and (2.29), and changing variables from x_0, x_t and $x_0, \tilde{x}_t$ to z_+, z_- we get, for large N

$$\begin{aligned}
C_{vv}^{(1)}(t) &= \frac{\lambda}{\sqrt{2\pi}(2\pi)^2}\int_{-\infty}^\infty dz_+ \int_{-\infty}^\infty dz_- z_-^2 e^{-z_-^2/2} \int_{-\pi/2}^{\pi/2} d\phi \int_{-\pi}^{\pi} d\theta \\
&\qquad \times e^{-N(1-\cos\phi)} e^{-i\lambda z_+ \sin\phi} e^{-2\lambda q(z_-)(1-\cos\theta)} e^{-i\lambda z_- \sin\theta} \ , \\
C_{vv}^{(2)}(t) &= -\frac{\lambda^2}{4\pi^3}\int_{-\infty}^\infty dz_+ \int_{-\infty}^\infty dz_- e^{-z_-^2} \int_{-\pi/2}^{\pi/2} d\phi \int_{-\pi}^{\pi} d\theta \ (\cos\phi - \cos\theta) \\
&\qquad \times e^{-N(1-\cos\phi)} e^{-i\lambda z_+ \sin\phi} e^{-2\lambda q(z_-)(1-\cos\theta)} e^{-i\lambda z_- \sin\theta} \ .
\end{aligned}$$

For large N, the major contribution of the integral over ϕ comes from the region around $\phi = 0$. Therefore, the ϕ integral can be performed by expanding around $\phi = 0$ to make it a Gaussian integral (while extending the limits to $\pm\infty$). Subsequently, one can also perform the Gaussian

integral over z_+. This leads to the following expressions:

$$C_{vv}^{(1)}(t) = \frac{1}{(2\pi)^{3/2}} \int_{-\infty}^{\infty} dz_- z_-^2 e^{-z_-^2/2} \int_{-\pi}^{\pi} d\theta e^{-2\lambda q(z_-)(1-\cos\theta)} e^{-i\lambda z_- \sin\theta} \ , \tag{2.33}$$

$$C_{vv}^{(2)}(t) = -\frac{\lambda}{2\pi^2} \int_{-\infty}^{\infty} dz_- e^{-z_-^2} \ \int_{-\pi}^{\pi} d\theta \ (1-\cos\theta) \ e^{-2\lambda q(z_-)(1-\cos\theta)} e^{-i\lambda z_- \sin\theta} \ . \tag{2.34}$$

Thus we have closed form expressions of the VAF which are valid in the entire short time regime. For any value of $\lambda = \rho\overline{v}t$, these integrals can be performed numerically, and as we see from Fig. (2.7), the results are in excellent agreement with the numerical simulation.

We now analyze the above expression in the large λ limit, i.e., $(\overline{v}\rho)^{-1} \ll t$. Together with the condition $\overline{v}t << L$ for being in the short time regime, this means that t is much larger than the typical time between inter-particle collisions, i.e. outside the ballistic regime, while being much smaller than the time it takes to see boundary effects. We first make a change of variables $\sqrt{\lambda}z_- = z$ and $\sqrt{\lambda}\theta = x$. The integrands can then be expanded as a power series in powers of $1/\lambda$. The integrals acquire the forms:

$$C_{vv}^{(1)}(t) = \frac{1}{(2\pi)^{3/2}} \int_{-\infty}^{\infty} dz \int_{-\sqrt{\lambda}\pi}^{\sqrt{\lambda}\pi} dx \, e^{-\frac{x^2}{\sqrt{2\pi}} - ixz} \sum_{n=2}^{\infty} a_n(x,z)\lambda^{-n}, \tag{2.35}$$

$$C_{vv}^{(2)}(t) = -\frac{1}{2\pi^2} \int_{-\infty}^{\infty} dz \int_{-\sqrt{\lambda}\pi}^{\sqrt{\lambda}\pi} dx \, e^{-\frac{x^2}{\sqrt{2\pi}} - ixz} \sum_{n=1}^{\infty} b_n(x,z)\lambda^{-n}, \tag{2.36}$$

where $a_n(x,z)$ and $b_n(x,z)$ are polynomials in x and z. For example, $a_2(x,z) = z^2$, $b_1(x,z) = x^2/2$, and so on. Now, integrating term by term (while extending the integrating limits of x to $\pm\infty$) we get

$$C_{vv}^{(1)}(t) = \frac{1}{\pi}\lambda^{-2} - \frac{2(\pi-3)}{(2\pi)^{3/2}}\lambda^{-3} + O(\lambda^{-5}), \tag{2.37}$$

$$C_{vv}^{(2)}(t) = -\frac{1}{\pi}\lambda^{-2} - \frac{1}{(2\pi)^{3/2}}\lambda^{-3} + O(\lambda^{-4}). \tag{2.38}$$

Therefore, adding the above two results, we recover Jepsen's result [62]

$$C_{vv}(t) = -\frac{(2\pi-5)}{(2\pi)^{3/2}}\lambda^{-3} + O(\lambda^{-4}). \tag{2.39}$$

Long time regime: In the limit $\bar{v}t >> L$ we use the series representation of $P_\pm$ given in

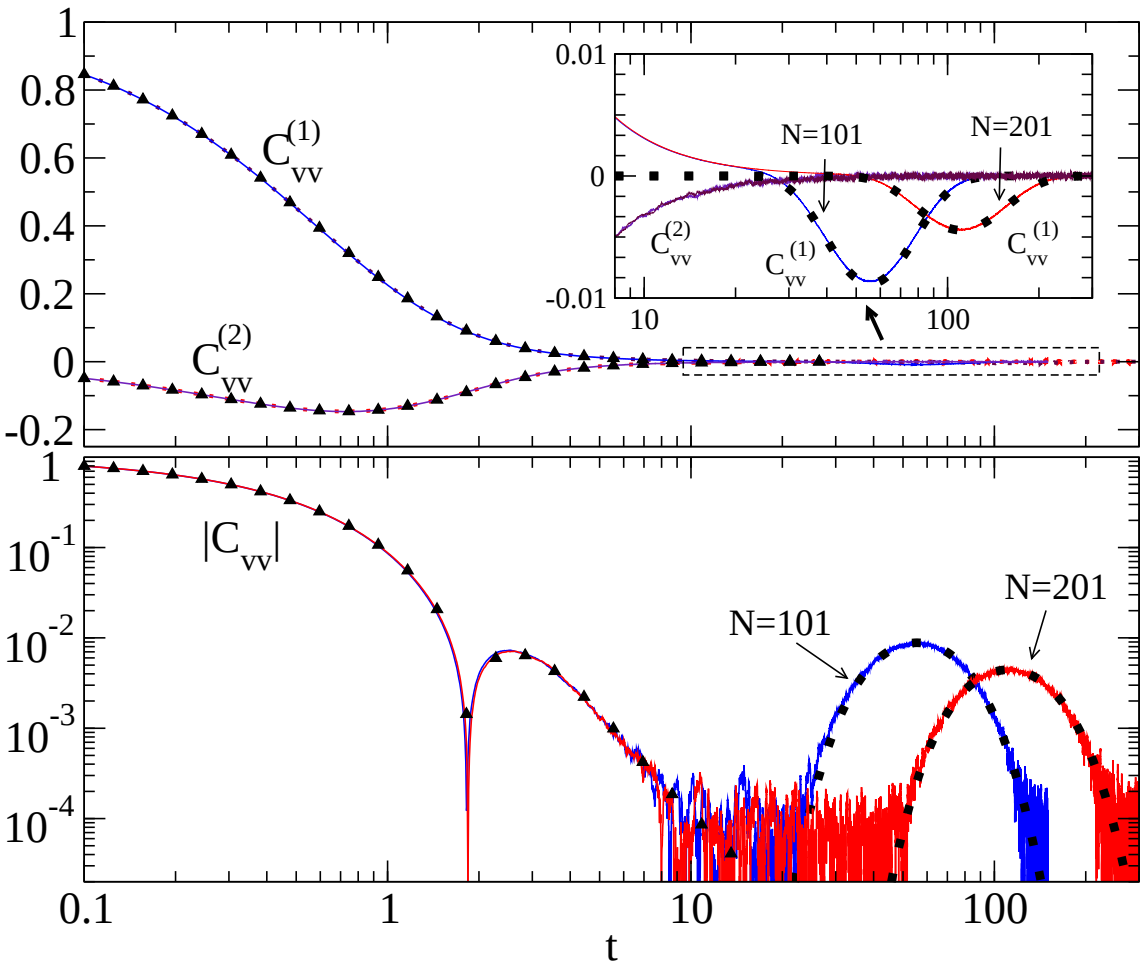

FIGURE 2.7: Plot of the separate contributions $C_{vv}^{(1)}$ and $C_{vv}^{(2)}$ to the velocity auto-correlation function of equal mass hard-particle gas, for two different system sizes ($N = 101, 201$) with fixed number density $\rho = 1$. The solid lines correspond to the simulation data, whereas the points are from the analytic results given by Eqs. (2.28) and (2.29) for short time behaviors (▲), and Eq. (2.45) for the long time behaviors (■). In the first panel, the dashed rectangle is enlarged in the inset.

Eqs. (2.20) . Integrating this expression over the appropriate ranges, we obtain

$$\begin{aligned} p_{--}(x_0, x_t; t) &= \frac{x_0 x_t}{L^2} + f(x_0, x_t; t) \\ p_{-+}(x_0, x_t; t) &= \frac{x_0(L - x_t)}{L^2} - f(x_0, x_t; t) \\ p_{+-}(x_0, x_t; t) &= \frac{x_t(L - x_0)}{L^2} - f(x_0, x_t; t) \\ p_{++}(x_0, x_t; t) &= \frac{(L - x_0)(L - x_t)}{L^2} + f(x_0, x_t; t) \end{aligned} \tag{2.40}$$

with

$$f(x_0, x_t; t) = \sum_{k\neq 0} \frac{1}{k^2\pi^2} \exp\left(-\frac{k^2\pi^2\overline{v}^2t^2}{2L^2}\right) \sin\left(\frac{k\pi x_0}{L}\right) \sin\left(\frac{k\pi x_t}{L}\right). \tag{2.41}$$

Expanding around $x = y = L/2$ we get to leading order $N(p_{++} + p_{--}) = N[1/2 + 2a(t)],\ N(p_{++} - p_{--}) = -Nw_+,\ N(p_{+-} + p_{-+}) = N[1/2 - 2a(t)],\ N(p_{+-} + p_{-+}) = -Nw_-$, where $w_+ = (x + y)/L - 1,\ w_- = (x - y)/L$ and

$$a(t) = f(L/2, L/2; t) = \sum_k \frac{1}{\pi^2(2k+1)^2} \exp\left[-\frac{(2k+1)^2\pi^2\overline{v}^2t^2}{2L^2}\right]. \tag{2.42}$$

Using these and the expression of P_- from Eq. (2.19) in Eqs. (2.28) and (2.29), we find the following results upto $O(1/N)$:

$$\begin{aligned} C^{(1)}_{vv}(t) =& N \sum_k \left(1 - \frac{(2k+1)^2\pi^2\overline{v}^2t^2}{L^2}\right) \exp\left(-\frac{(2k+1)^2\pi^2\overline{v}^2t^2}{2L^2}\right) \\ & \times \frac{1}{(2\pi)^2} \int_{-\infty}^{\infty} dw_+ \int_{-\infty}^{\infty} dw_- \int_{-\infty}^{\infty} d\phi \int_{-\infty}^{\infty} d\theta \\ & \times e^{-N[1/4+a(t)]\phi^2} e^{-iNw_+\phi} e^{-N[1/4-a(t)]\theta^2} e^{-iNw_-\theta}, \end{aligned} \tag{2.43}$$

$$\begin{aligned} C^{(2)}_{vv}(t) =& -N^2 \left(\frac{\bar{v}t}{L}\right)^2 \left[\sum_k \exp\left(-\frac{(2k+1)^2\pi^2\overline{v}^2t^2}{2L^2}\right)\right]^2 \\ & \times \frac{1}{(2\pi)^2} \int_{-\infty}^{\infty} dw_+ \int_{-\infty}^{\infty} dw_- \int_{-\infty}^{\infty} d\phi \int_{-\infty}^{\infty} d\theta \\ & \times e^{-N[1/4+a(t)]\phi^2} e^{-iNw_+\phi} e^{-N[1/4-a(t)]\theta^2} e^{-iNw_-\theta} \ (\theta^2 - \phi^2). \end{aligned} \tag{2.44}$$

Performing the Gaussian integrals we find that $C^{(2)}_{vv}$ vanishes and hence to $O(1/N)$ the velocity autocorrelation is given by

$$C_{vv}(t) = C^{(1)}_{vv}(t) = \frac{2}{N} \sum_{k=1,3,5\ldots} \left(1 - \frac{k^2\pi^2\overline{v}^2t^2}{L^2}\right) \exp\left(-\frac{k^2\pi^2\overline{v}^2t^2}{2L^2}\right). \tag{2.45}$$

As seen from Fig. (2.7), the above expression describes the numerical simulation data very well. The late time behaviour $C_{vv}(t) \sim \exp(-\pi^2\overline{v}^2t^2/2L^2)$ was earlier obtained in [66].

2.2.2 Simulation results for equal mass hard-particle gas

We now perform molecular dynamics simulation on this system of particles and show it to match the analytic results just obtained. Apart from the VAF $\equiv \langle v(0)v(t)\rangle$, we also obtain MSD

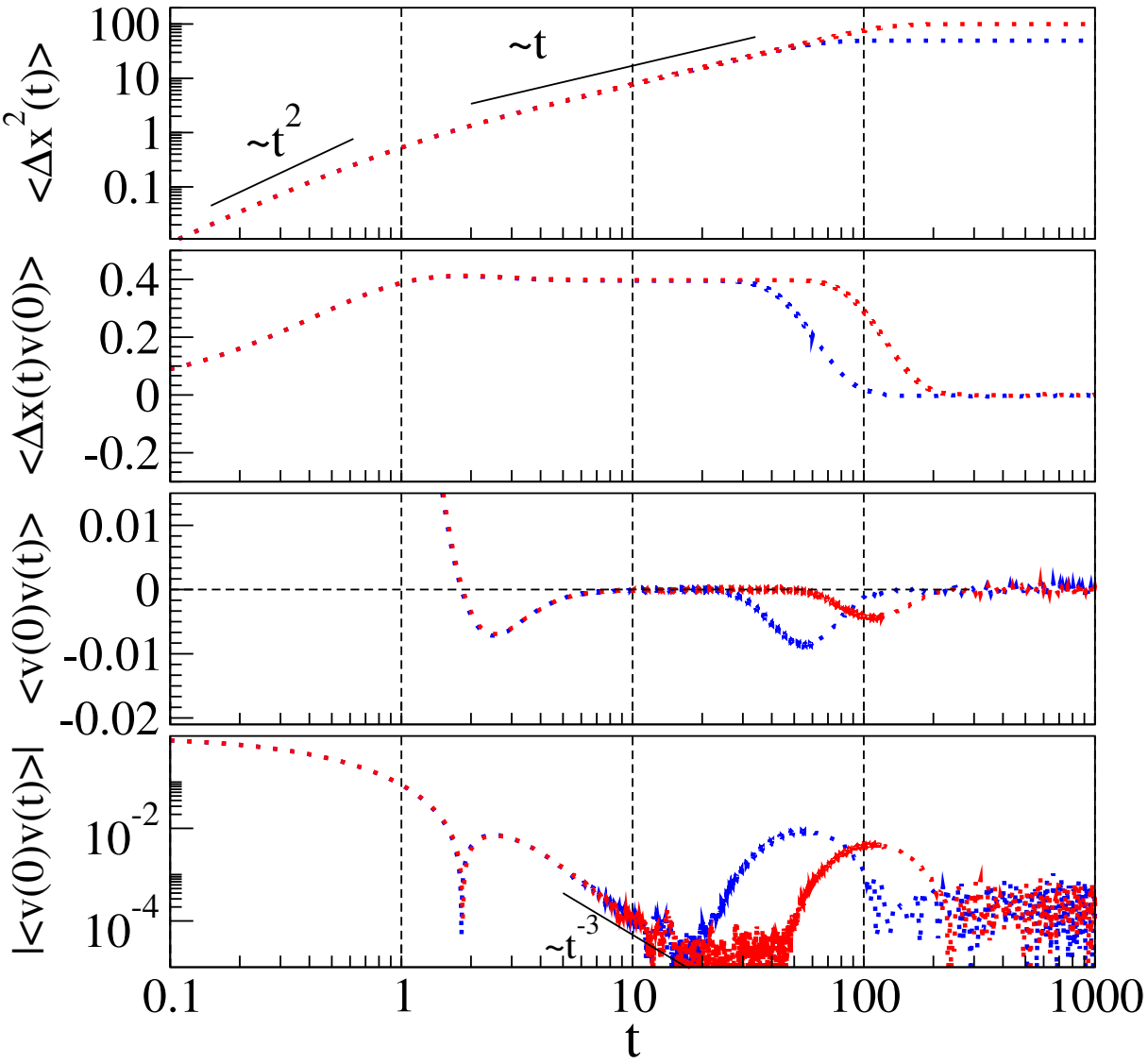

FIGURE 2.8: Various correlation functions for the equal mass hard particle gas with masses 1 (solid lines) for $N = 101$ (blue) and $N = 201$ (red) particles; number density $\rho = 1$ and $k_B T = 1$. The data is obtained by averaging over 10^9 equilibrium initial conditions.

$\equiv \langle [\Delta x(t)]^2 \rangle$ and $D(t) \equiv \langle \Delta x(t) v(0) \rangle$. The averaging $\langle \cdots \rangle$ is taken over initial configurations chosen from the equilibrium distribution, where the particles are uniformly distributed in the box with number density $\rho = N/L$, while the velocity of each particle is independently chosen from the distribution $(m/2\pi k_B T)^{1/2}\ e^{-mv^2/2k_B T}$. In the simulations for the equal mass hard particle gas reported here we take all $m = 1, k_B T = 1$ and and we take various N keeping $\rho = 1$.

Since the particles move freely between collisions, which are instantaneous in nature, we resort

to the event-driven molecular dynamics scheme [93]. In this scheme instead of a regular, step-by-step approach, as for continuous potentials, the program evolves on a collision-by-collision basis. The general scheme of the simulation is as follows. The next collision time between the different neighbouring pairs of particles is first evaluated. The program is then evolved to the minimum of these pair collision times, called T_{coll}, when one of the pairs collide. We then implement the collision dynamics of Eq. (2.3) for the colliding pair. This collision now changes three of the pair collision times. One for the colliding pair, which can be taken to be effectively infinite, and the other two of the two colliding particles with their other neighbours. Calculating these two collision times afresh, rest of the collision times being only reduced by T_{coll}, we then locate the next minimum of the collision times and repeat the process. It has to be noted that the correlation functions, however, has to be obtained at fixed time intervals, independent of the collision times which vary from one realization to the other.

As can be seen from Fig. (2.7), the simulation results for the velocity auto-correlation function matches the analytic results, both for $C_{vv}^{(1)}$ and $C_{vv}^{(2)}$. In Fig. (2.8) the other correlation functions obtained from the simulations are also shown. In particular, one can see the expected short time ballistic to diffusive crossover of the mean square displacement and $1/t^3$ decay of the velocity auto-correlation function. The observation of normal-diffusion can also be made from the plot of $D(t)$, which saturates to the fixed value of ≈ 0.4, as can be obtained from Jepsen's relation $2D = \sqrt{2/m\pi\beta}$. Moreover, the long time effect of the reflecting boundary can be seen as the mean square displacement of the tagged particle saturates to a value given by Eq. (2.11), thereby making $D(t) \to 0$. The anti-correlation seen in the velocity auto-correlation function on the onset of reflecting boundary effect is an interesting observation.

2.3 Alternate mass hard particle gas

For the alternate mass hard particle gas no exact result exist and we obtain the correlation functions through event-driven MD simulations, described in the previous section, exclusively. We choose all other parameters to be the same as the equal mass case apart from the mass of the particles which are set at 1.5 and 0.5 alternately. Here the data is shown for the case where the tagged particle has mass 1.5, and similar results are obtained for the case when the tagged

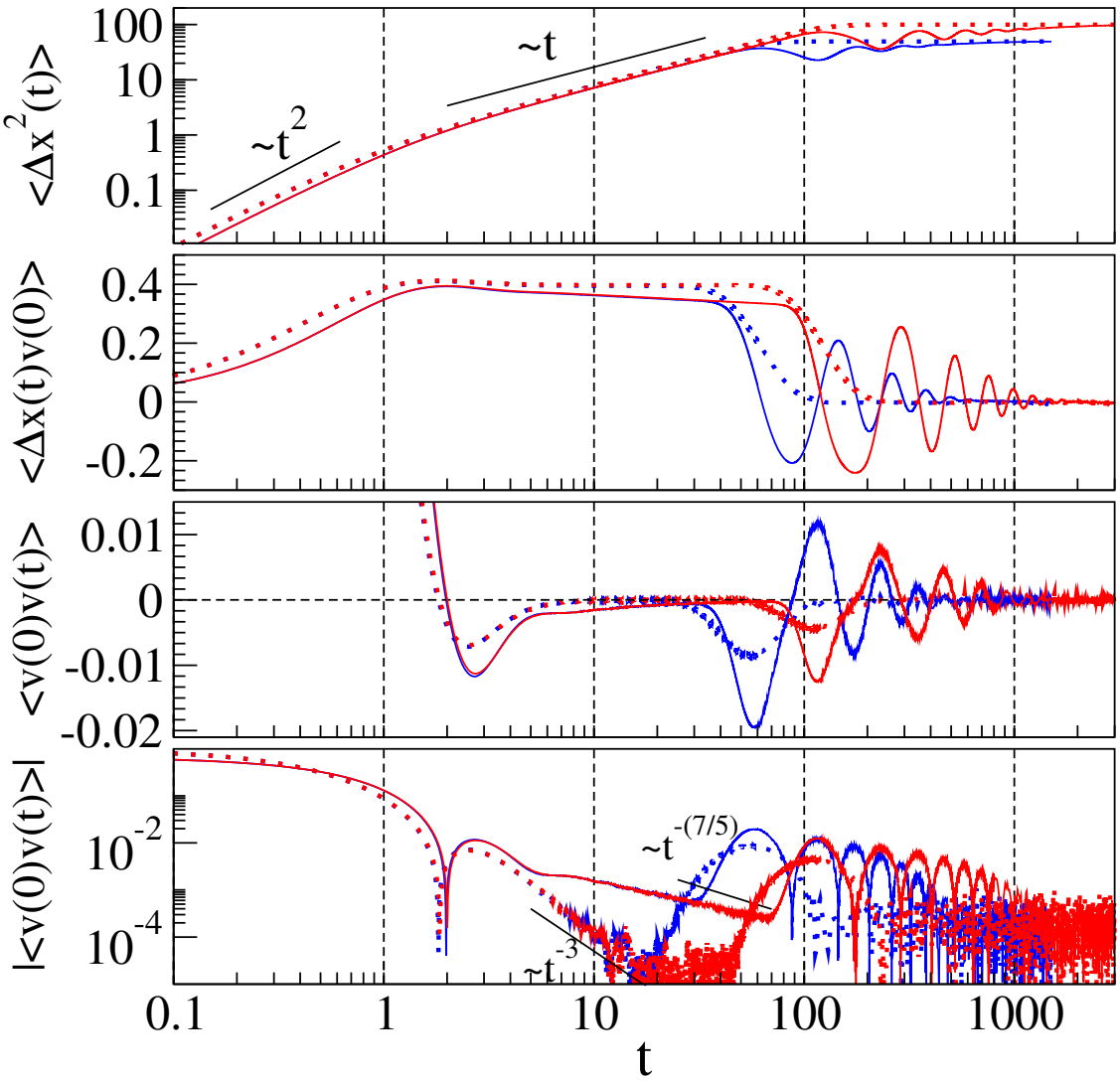

Figure 2.9: Various correlation functions for alternate mass hard particle gas (solid lines) with $N = 101$ (blue) and $N = 201$ (red) particles. The alternate particles have masses 1.5 and 0.5 and in this simulation, the middle particle had mass 1.5. The data is obtained by averaging over 10^9 equilibrium initial conditions. A better approach to the $t^{-7/5}$ for the VAF can be seen in Fig. (5.5) for larger system sizes, see also Fig. (2.10). For comparison, the correlation functions for an equal mass gas with masses 1 is also shown (dotted lines). In all the above simulations we have taken $\rho = 1$ and $k_B T = 1$.

particle is the lighter one. On collision, the colliding particles emerge with modified velocities given by Eq. (2.3).

In Fig. (2.9) we show the various correlation function of the alternate mass gas in comparison to the equal mass case of Fig. (2.8). We see that the short time mean square displacement seems

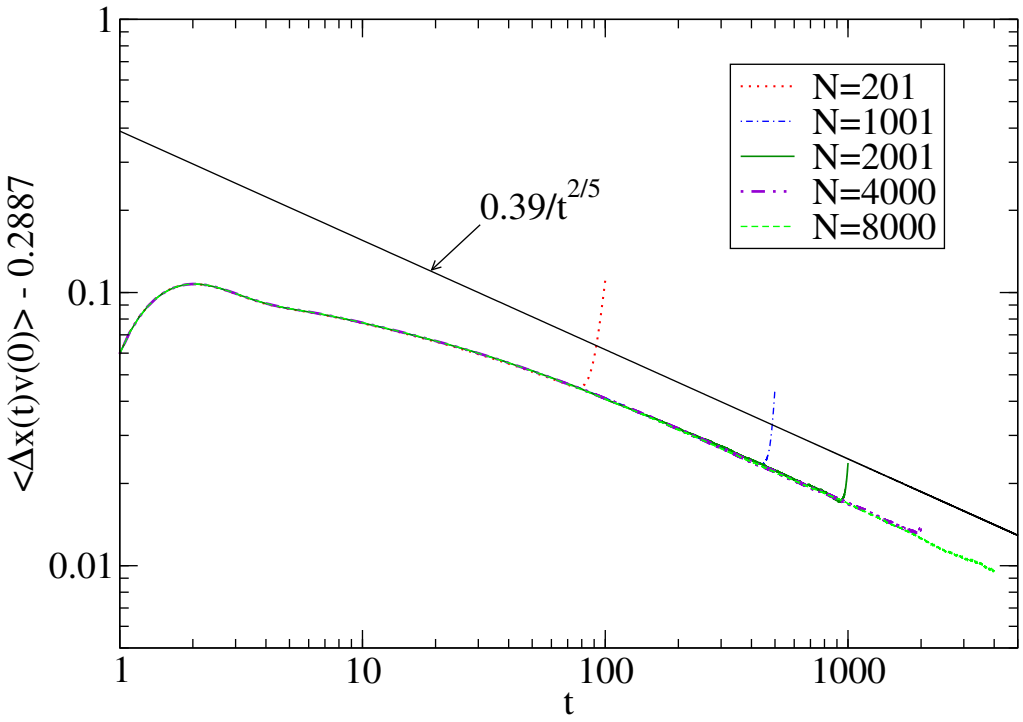

FIGURE 2.10: Alternate mass hard particle gas: plot of $D(t) = \langle \Delta x(t) v(0) \rangle$ for systems of different sizes. The solid line is the prediction of mode-coupling theory [92] and gives a slow power-law decay to the asymptotic diffusion constant $D = k_B T/(2\rho_m c) = 0.2886\ldots$. In these simulations we used periodic boundary conditions since these give better statistics.

to be similar for the two cases; after the expected initial ballistic regime, it grows approximately linearly with time, indicating roughly diffusive motion. It is easier to notice any deviations from diffusive behavior in the plot of $\langle \Delta x(t) v(0) \rangle$, where diffusive or super/sub-diffusive behavior would correspond to (after the ballistic regime) a horizontal or rising/declining straight line respectively. Fig. (2.9) seems to show that $\langle \Delta x(t) v(0) \rangle$ *decreases* as t is increased beyond the ballistic regime, implying sub-diffusive behavior. However, on simulations on larger system sizes [Fig. (2.10)], we find deviation from this short time decay and convergence to a constant value. We also see that these large system simulation results are consistent with the prediction from mode coupling

theory [92] of

$$\langle \Delta x(t) v(0) \rangle = 0.2887 + 0.39 t^{-2/5}. \tag{2.46}$$

This indicates that the system is diffusive, with diffusion constant given by $D = k_B T/(2\rho_m c) = 0.2887$, where ρ_m is the mass density and c is the speed of sound (see chapter 4 and the paragraph below). This power law is also demonstrated by the velocity auto-correlation function as can be seen in the fouth subplot [see Fig. (5.5) for better convergence to this power law decay at longer times, for larger system sizes].

In Fig. (2.9) we also see how the effect of finite size of the box sets in, with onset time depending on the system size. The mean square displacement saturates to the the same value of Eq. (2.11), independent of the particle masses in the gas. The main difference between the equal mass and the alternate mass systems is that the MSD for the equal mass case approaches its saturation value without oscillations, while for alternate mass case there are damped oscillations as saturation is approached, *while always remaining below* the MSD for the equal mass case. The oscillations in the alternate mass system also show up in the other two correlation functions. The time at which these oscillations start showing up is given by $t_{\rm sat} \sim L/c$, where $c = \sqrt{3P/\rho_m}$ is the adiabatic sound velocity in the alternate mass hard point particle gas with P being the pressure. For our numerical simulations, $P = \rho k_B T = 1$ and $\rho_m = 1$, which gives $c = \sqrt{3}$.

The oscillations in the mean square displacement are seen more clearly in Fig. (2.11), where the data is plotted differently. The period of oscillation is proportional to N, in agreement with our ascribing them to sound waves reflecting from the boundary, which takes a time $\sim 2L/c$. However, the amplitude of the oscillations does not show a simple scaling with N; it is clear from the figure that they are damped out in fewer cycles for smaller N, making it impossible to collapse the data onto a single curve by re-scaling the vertical axis.

2.4 Discussions and conclusions

In this chapter we studied two main cases of the hard particle gas, one in which all particles are of same mass m and the other in which the particle masses alternate between m_1 and m_2. For the case where the masses of all the particles are equal we obtained analytic results for the finite-size

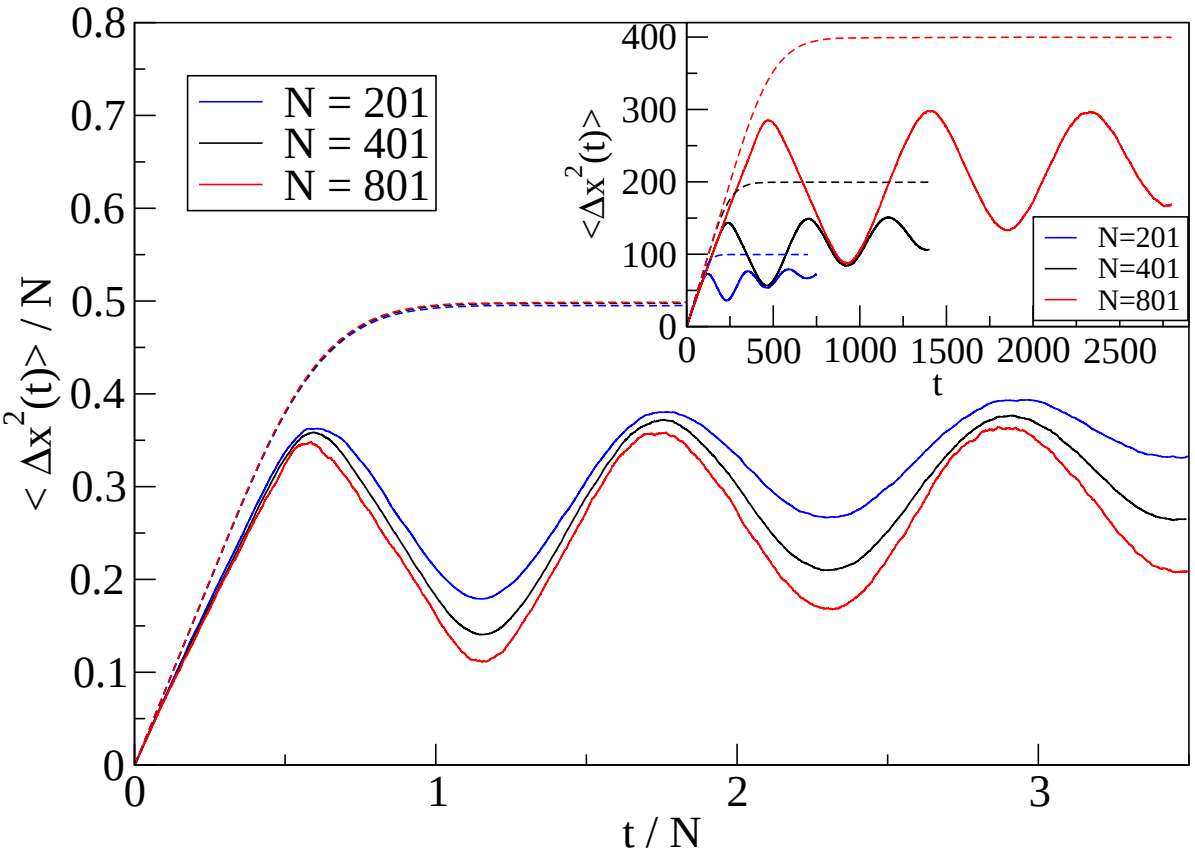

FIGURE 2.11: Scaled plot of MSD as a function of time for three system sizes $N = 201, 401, 801$ for the alternate mass case with fixed number and mass densities $\rho = \rho_m = 1$ and other parameters as in Fig. (2.9). The inset shows the unscaled data. The saturation value for the scaled plot is at 0.5.

velocity auto-correlation function using an approach similar to that of Jepsen. However, our calculation is simpler and we obtained closed form expressions for the velocity auto-correlation function valid at both short times (including the ballistic and diffusive regimes) and long times (when boundary effect shows up). While here we have presented results only for the velocity auto-correlation function, it is straightforward to obtain other correlation functions using our approach.

We then presented simulation results for the various correlation functions of the two cases. We saw that the tagged particle eventually shows normal-diffusion in both the cases even though the detailed correlation functions are different. This gives the first concrete example of non-integrability not affecting the normal-diffusive behaviour of the tagged particle in one-dimensional

systems. We saw the diffusion constant in the equal mass case is obtainable from Jepsen result while the expression given for the alternate mass case will be obtained in chapter 4. It must however be noticed that this normal-diffusion is very different from the normal-diffusion of a tagged particle undergoing Langevin dynamics with white noise. In that case the velocity auto-correlation function decays exponentially in contrast to the power laws observed here. As will be seen in chapter 5, this exponential decay will be recovered for the case when the tagged particle is much heavier than the rest of the particles, which are all of equal masses. In that chapter we will also study the random mass case and mass ratio dependence in the alternate mass gas, among other things.

We also saw how reflecting boundary effect manifests itself in the two cases with the onset time of this boundary effect depending on the system size. We saw that the value to which the mean square displacement saturates is independent of particle masses. However, the way it saturates is very different for the two cases. We calculated the adiabatic sound velocity in the alternate mass hard point particle gas and found it to describe the oscillations seen in the long-time correlation functions of the alternate mass gas. The equal mass gas, as is known, doesn't support sound waves under continuous velocity distributions like the equilibrium distribution [64], and hence doesn't show such oscillations.

3

Oscillator Chain Systems

3.1 Introduction

In the previous chapter we saw how breaking the integrability in the alternate mass hard particle gas didn't effect the asymptotic infinite system behaviour of normal-diffusion of the tagged particle, even though the diffusion constant and the detailed form of the correlation functions were very different. We also saw how the boundary effect sets in differently for the two systems. The long-time oscillations obtained for alternate mass case were attributed to the system supporting sound propagation. In this chapter we study some standard oscillator chain systems [see Fig. (3.1)], to see if and how the infinite system diffusive behaviour and the boundary effect differs in these oscillator chains. The oscillator chains we study are the harmonic chain (Sec. 3.2), the anharmonic Fermi-Pasta-Ulam (FPU) chain (Sec. 3.3) and the Lennard-Jones (LJ) chain (Sec. 3.4).

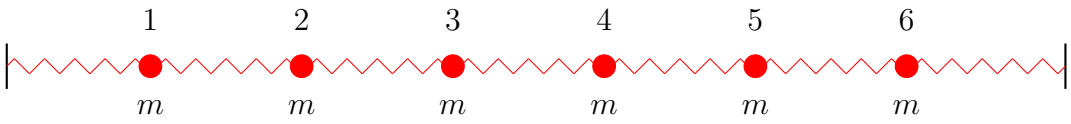

FIGURE 3.1: Schematic diagram of an oscillator chain with $N = 6$ particles and fixed boundary conditions.

In Sec. 3.2 we study the harmonic chain. The problem has been studied for an infinite harmonic chain by Montroll and Mazur [60] where they obtained the velocity auto-correlation function (VAF) to be $\sim \sin(\omega_0 t)/\sqrt{t}$ at large times. This implies fast enough decay of the VAF to give an asymptotic normal-diffusion. Finite size effects, however, have not been studied. Here we present exact results for the various correlation functions, through normal mode analysis, valid over the entire regime: both the diffusive $t << N$ regime and $t >> N$ regime when boundary effect sets in. In particular, we re-obtain the functional form of VAF obtained in [60] for the short time regime, while in the long time regime we again see size dependent oscillations. The speed of sound in the system describes well the onset time and period of these oscillations as in the previous chapter. However, as we will see, nature of these oscillations are different from those seen in the previous chapter. We also see that, apart from the long time sound dependent oscillations, there are short time size-independent oscillations too. These are due to the elastic nature of the system in the microscopic scale, in contrast to the hard particle gas. Next, we perform velocity-verlet molecular dynamics simulations on the system to obtain the various correlation functions and confirm that they match the analytic results.

In Sec. 3.3 we study the anharmonic Fermi-Pasta-Ulam (FPU) chain. This paradigmatic and the most basic example of an anharmonic chain has surprisingly been completely overlooked in the context of tagged-particle diffusion. Note that in the context of heat conduction, studies on these nonlinear systems gave lots of insights into the nature of 1-dimensional Hamiltonian systems [88]. This system, being nonlinear, cannot be handled exactly. Hence, here we study it through velocity-verlet molecular dynamics simulations and obtain the correlation functions valid for both short and long time regime. We will see how the correlation functions for this anharmonic system are qualitatively similar to those of harmonic chain, in the sense that they also show normal-diffusion and that there are both short time and long time oscillations. The

decay of these oscillations, however, will be found to be very different between these two cases. We study both the β and the $\alpha - \beta$ FPU model to see whether the difference one observes between these two models in the context of heat conduction, manifests itself in the context of tagged-particle diffusion too.

In Sec. 3.4 we study the anharmonic Lennard-Jones (LJ) chain. For this system few studies exist. Bishop et. al. and Bagchi et. al. studied the problem, for a LJ gas, through molecular dynamics simulations and obtained the VAF $\sim -1/t^3$ [84–86], which seems like a hard particle result. However, density dependence and finite size effects were not considered thoroughly in these studies. In this section we study the LJ chain extensively for different densities through velocity-verlet molecular dynamics simulations, and we obtain the correlation functions in both short and long time regimes. We make the interesting observation that the nature of the correlation functions for a LJ chain is highly density dependent. At high densities it looks like those of an anharmonic chain while at low densities it looks like those of a hard particle gas, thereby recovering the $\sim -1/t^3$ decay of the velocity auto-correlation function found in [86].

As in the previous chapter, we study the three correlation functions $\langle[\Delta x(t)]^2\rangle, \langle\Delta x(t)v(0)\rangle$ and $\langle v(0)v(t)\rangle$ which are related to each other through Eq. (1.10). The dynamics of the oscillator chain systems studied in this chapter is also completely deterministic and hence the averaging $\langle\cdots\rangle$ is done over the equilibrium initial distribution.

3.2 Harmonic chain

Analytic results for the harmonic chain

We consider a harmonic chain of N particles labeled $l = 1, \ldots, N$ in thermal equilibrium at temperature T. The particles of equal masses m are connected by springs with stiffness constant k. Let $\{q_1, \ldots, q_N\}$ denote the displacements of the particles about their equilibrium positions. The equilibrium positions are assumed to be separated by a lattice spacing a so that the mass density is $\rho_m = m/a$. We assume that the particles $l = 0$ and $l = N + 1$ are fixed so that $q_0 = q_{N+1} = 0$. The Hamiltonian of the system is

$$H = \sum_{l=1}^{N} \frac{m}{2}\dot{q}_l^2 + \sum_{l=1}^{N+1} \frac{k}{2}(q_l - q_{l-1})^2 \ , \tag{3.1}$$

with corresponding equation of motion given as

$$m\ddot{q}_l = -k(2q_l - q_{l+1} - q_{l-1}), \qquad \forall\ l. \tag{3.2}$$

Transforming to normal mode coordinates

$$q_l(t) = \sum_p a_p(t)\phi_p(l)\ , \tag{3.3}$$

where $\phi_p(l) = \left[\frac{2}{m(N+1)}\right]^{1/2} \sin(lpa),\ p = \frac{n\pi}{(N+1)a}\ ,\ n = 1, \ldots, N$, brings the Hamiltonian to the form

$$H = \sum_p \frac{\dot{a}_p^2}{2} + \frac{\omega_p^2 a_p^2}{2}\ , \tag{3.4}$$

with $\omega_p^2 = 2k/m(1 - \cos pa)$. The normal mode equations of motion $\ddot{a}_p = -\omega_p^2 a_p$ are easily solved and lead to the following expression:

$$q_l(t) = \sum_p \phi_p(l)\ \left[a_p(0)\cos\omega_p t + \frac{\sin\omega_p t}{\omega_p}\dot{a}_p(0)\right]\ . \tag{3.5}$$

We consider a chain in thermal equilibrium at temperature T, i.e., $\langle \dot{a}_p^2(0)\rangle = \omega_p^2\langle a_p^2(0)\rangle = k_B T$ and $\langle \dot{a}_p(0)a_p(0)\rangle = 0$. For the middle particle, $l = M = (N+1)/2$ (assuming odd N), $\sin(lpa) = \sin(n\pi/2)$ and hence $\phi_p(l) = 0$ for even n. Defining $\Delta q(t) = q_M(t) - q_M(0)$,

$$\langle[\Delta q(t)]^2\rangle = \frac{8k_B T}{m(N+1)} \sum_{n=1,3,\ldots} \frac{\sin^2(\omega_p t/2)}{\omega_p^2}\ . \tag{3.6}$$

Here we have switched from p to n in the summation index, which are related to each other. The correlations $\langle \Delta q(t)v(0)\rangle$ and $\langle v(t)v(0)\rangle$ can be found by differentiating this expression, as in Eqs.(1.10).

Simulation results for the harmonic chain

Next we obtain the correlation functions from molecular dynamics simulations and show them to match the analytic results obtained above. Since the inter-particle potential is continuous we can perform velocity-verlet molecular dynamics simulation on it [93]. In this scheme the simulation proceeds in fixed time steps δt and the positions (x_i), velocities (v_i) and the accelerations (a_i),

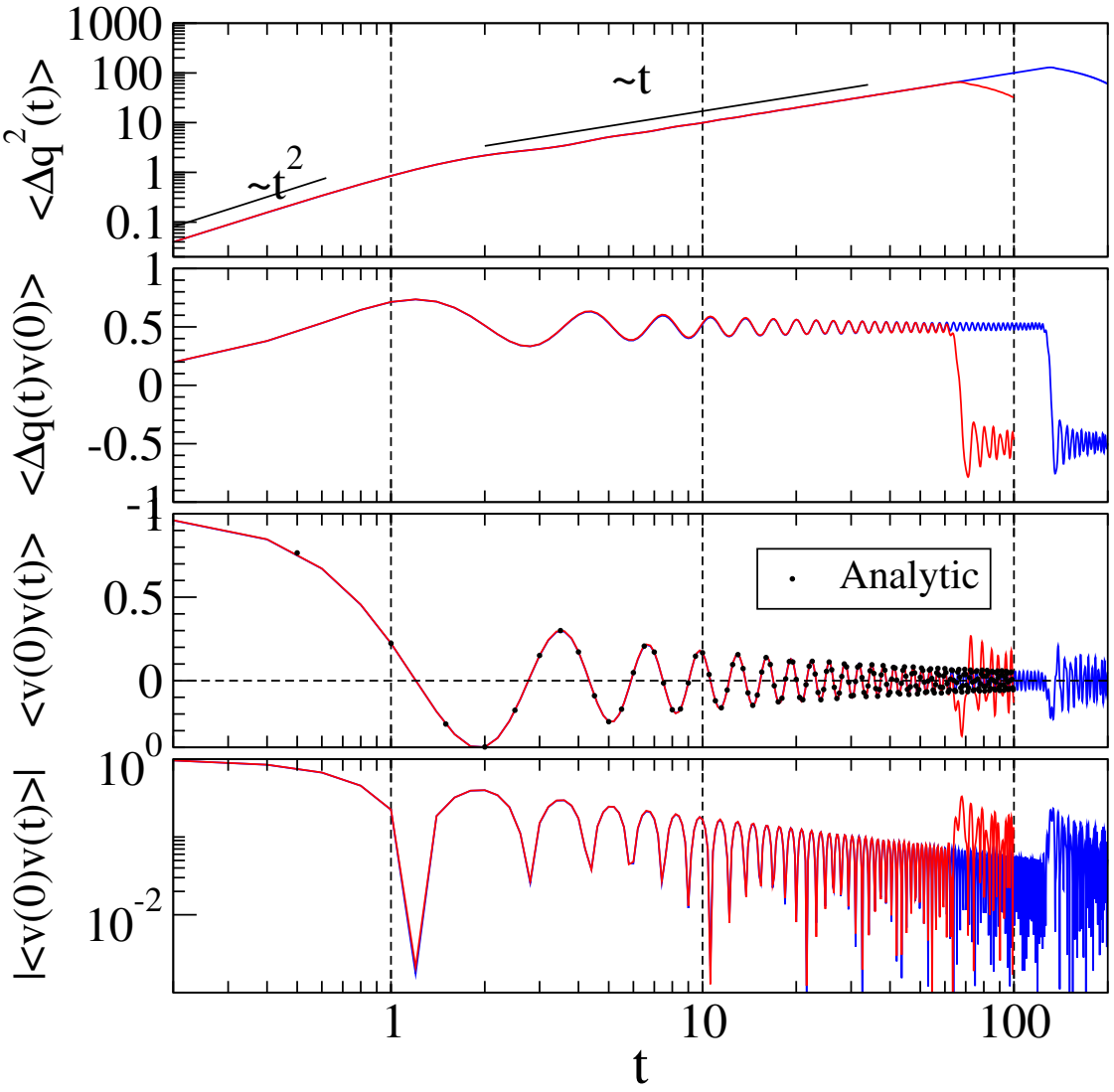

FIGURE 3.2: Harmonic chain: short time correlation functions of the central tagged particle in a system of size $N = 65$ (red) and 129 (blue). Fixed boundary conditions were used and the parameters were taken as $k = 1$, $m = 1$ and $k_BT = 1$. The diffusion constant can be seen to saturate to the expected value $k_BT/(2\rho_m c) = 0.5$ (until boundary effect sets in). For the VAF, we have also plotted the analytic result $\langle v(0)v(t)\rangle = J_0(2t)$

for $i = 1, 2, ..., N$, are evaluated at each time step as

$$x_i(t+\delta t) = x_i(t) + \delta t\ v_i(t) + \frac{1}{2}\delta t^2\ a_i(t),$$
$$v_i(t+\delta t) = v_i(t) + \frac{1}{2}\delta t\ \ [a_i(t) + a_i(t+\delta t)]\,.$$

The system is initially prepared in equilibrium by connecting all particles to Langevin type heat

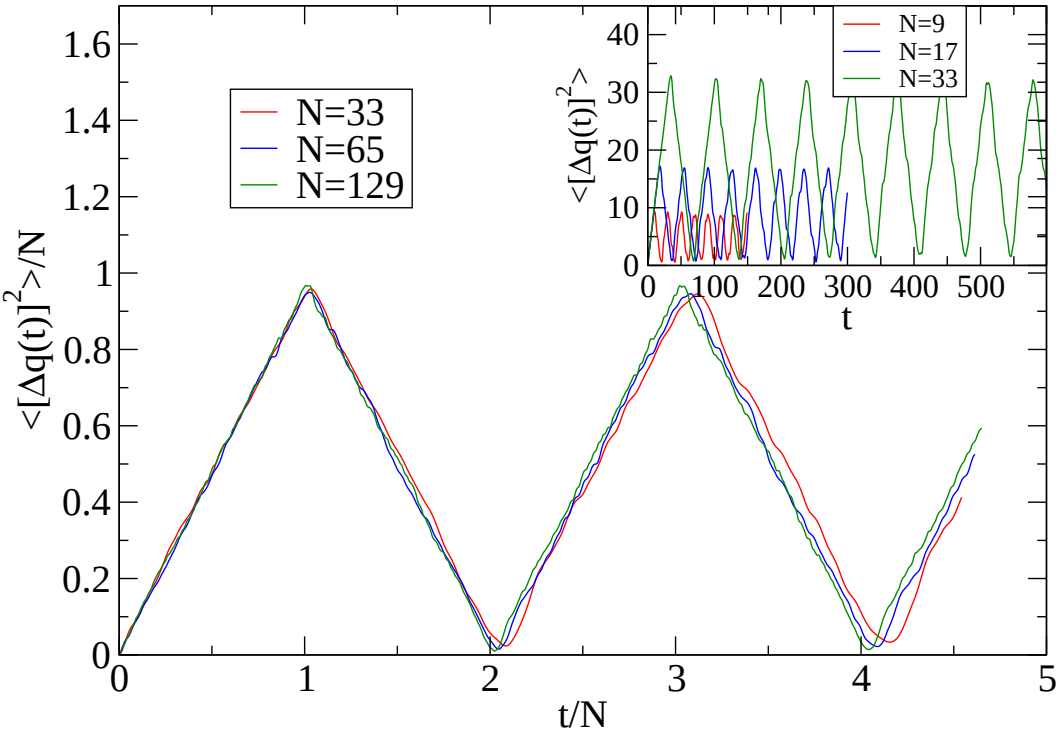

FIGURE 3.3: Harmonic chain: long time MSD of the central tagged particle in systems of different sizes, and with fixed boundary conditions. The parameters here are same as in Fig. (3.2). Note the near recurrent behaviour of the MSD.

reservoirs. The various correlation functions are then obtained from these quantities, at required time intervals, by averaging over a large number of initial conditions.

In Fig. (3.2) and Fig. (3.3) we plot the simulation results for the various correlation functions for different system sizes and find them to match the exact analytic results [Eq.(3.6) and its derivatives]. As seen in Fig. (3.2), an initial $\sim t^2$ growth in $\langle \Delta q^2(t) \rangle$ crosses over to a linear growth, indicating a diffusive regime that is also seen in $\langle \Delta q(t) v(0) \rangle$. After that, boundary effects set in and $\langle (\Delta q)^2 \rangle / N$ is an almost periodic function of t/N [Fig. (3.3)]. This is somewhat surprising for an harmonic chain since we are averaging over an initial equilibrium ensemble with all normal modes, and $\omega_p \approx cp$ (where $c = a\sqrt{k/m}$ is the wave speed) only for small p. Notice

that there are oscillations even before the wall effect sets in. These are indicative of the elastic nature of the system in the microscopic scale.

Further analytic results for the different time regimes of the harmonic chain

The behaviour of $\langle[\Delta q(t)]^2\rangle$ for the harmonic chain can be understood in detail analytically by analyzing the different time regimes of Eq. (3.6) . There are three regimes of t to consider:

(i) When $\omega_N t << 1, \sin^2(\omega_n t/2) \approx \omega_n^2 t^2/4$, (we use ω_n to denote the normal mode frequencies, but with $p = n\pi/[(N+1)a]$), the right hand side of Eq. (3.6) is then equal to $k_B T t^2/m$. This approximation is valid as long as $\omega_N t = 2ct/a$ is small.

(ii) In the second regime, $\omega_N t >> 1 >> \omega_1 t$, and the sum can be replaced by an integral:

$$\frac{4k_BT}{m(N+1)}\int_1^N dn \frac{\sin^2(\omega_n t/2)}{\omega_n^2} \approx \frac{2k_BTat}{\pi mc}\int_0^\infty dy \frac{\sin^2(y)}{y^2\sqrt{1-(ay/ct)^2}} \tag{3.7}$$

where we have changed variables from n to $y = \omega_n t/2$ and used $\omega_N t >> 1 >> \omega_1 t$ to change the limits of the integral. Expanding $[1-(ay/ct)^2]^{-1/2}$ in a binomial series and keeping only the first term of the expansion, we get the leading order behaviour in t as $\langle[\Delta q(t)]^2\rangle \approx (k_BTt/\rho_m c)$. The linear t-dependence implies diffusive behaviour with a diffusion constant $D = k_BT/(2\rho_m c)$.

The VAF in this regime can be obtained by differentiating the first expression in Eq.(3.7), as in Eqs.(1.10):

$$\langle v(t)v(0)\rangle = \frac{k_BT}{m(N+1)}\int_1^N dn \cos(\omega_n t) \ . \tag{3.8}$$

Substituting $z = \omega_n/(2c/a) = \sin(n\pi/2(N+1))$, this is equivalent to

$$\langle v(t)v(0)\rangle = \frac{2k_BT}{\pi m}\int_0^1 dz \frac{\cos(2ctz/a)}{\sqrt{1-z^2}} = \frac{k_BT}{m}J_0(2ct/a) \ \sim \frac{\cos(2ct/a-\pi/4)}{\sqrt{t}} \ \text{ for } t\to\infty, \tag{3.9}$$

using the asymptotic properties of Bessel functions [60]. This is shown in the lower panels of Fig. (3.2).

(iii) In the third regime, the results depend on boundary conditions and our analysis here is for fixed boundary conditions. In this case $\omega_1 t$ is no longer small. As a first approximation, we set ω_n to be equal to $cn\pi/[(N+1)a] \approx cn\pi/Na$. Then Eq. (3.6) becomes

$$\langle[\Delta q(t)]^2\rangle = \frac{8k_BTNa}{\rho_m c^2\pi^2}\sum_{n=1,3,5\ldots}\frac{1}{n^2}\sin^2\left(\frac{cn\pi t}{2Na}\right) \ . \tag{3.10}$$

This is a periodic function in t with a period of $2Na/c$. Since the sum is dominated by $n << N$, we see that our first approximation is a reasonable one. More accurately, we expand ω_n to one order higher:

$$\omega_n = \frac{cn\pi}{Na}[1 - n^2\pi^2/(24N^2) + \cdots] \tag{3.11}$$

and evaluate the sum at $t = 2jNa/c$. We have

$$\langle[\Delta q(t)]^2\rangle = \frac{8k_BTNa}{\rho_m c^2\pi^2} \sum_{n=1,3,\ldots} \frac{1}{n^2[1 - O(n/N)^2]} \sin^2(jn^3\pi^3/(24N^2)). \tag{3.12}$$

Approximating the sum by an integral and changing variables to $y = nj^{1/3}/N^{2/3}$, we get

$$\langle[\Delta q(t)]^2\rangle = \frac{8k_BT(Nj)^{1/3}a}{\rho_m c^2\pi^2} \int_{O(N^{-2/3})}^{O(N^{1/3})} \frac{\sin^2(y^3\pi^3/24)}{y^2[1 - O(y^2/(jN)^{2/3})]} dy. \tag{3.13}$$

As $N \to \infty$, the integral converges to an N-independent value of $0.8046\ldots$, so that the function is $O(Nj)^{1/3}$. We note that this is small compared to the $O(N)$ value of the function at its maxima, but that it increases steadily with j, as expected in a dispersive system. In a more careful analysis, the locations of the minima are taken to be $2jNa/c + \delta_j$ and the δ_j's evaluated to leading order, but this does not change the fact that the minima are $O(Nj)^{1/3}$. A similar analysis shows that the function at its maxima is equal to $k_BTNa/(\rho_m c^2) - O(jN)^{1/3}$.

3.3 Fermi-Pasta-Ulam chain

We now turn to simulation of tagged-particle motion in a chain of nonlinear oscillators. The simulation techniques used are the same as described in the previous section. The Hamiltonian of the Fermi-Pasta-Ulam (FPU) chain we study is taken to be:

$$H = \sum_{l=1}^{N} \frac{m}{2}\dot{q}_l^2 + \sum_{l=1}^{N+1} \left[\frac{k}{2}(q_l - q_{l-1})^2 + \frac{\alpha}{3}(q_l - q_{l-1})^3 + \frac{\beta}{4}(q_l - q_{l-1})^4\right], \tag{3.14}$$

where the q_l's are the displacements from equilibrium positions. We fix the particles at the boundaries by setting $q_0 = 0$ and $q_{N+1} = 0$. The corresponding equations of motion are:

$$m\ddot{q}_l = -k(2q_l - q_{l+1} - q_{l-1}) - \alpha(q_l - q_{l-1})^2 + \alpha(q_l - q_{l+1})^2 - \beta(q_l - q_{l-1})^3 - \beta(q_l - q_{l+1})^3. \tag{3.15}$$

The simulation results are plotted in Fig. (3.4) and Fig. (3.6) for the β chain (where $\alpha = 0$). Comparing to the analogous figures for the harmonic chain, we see that the plots have some

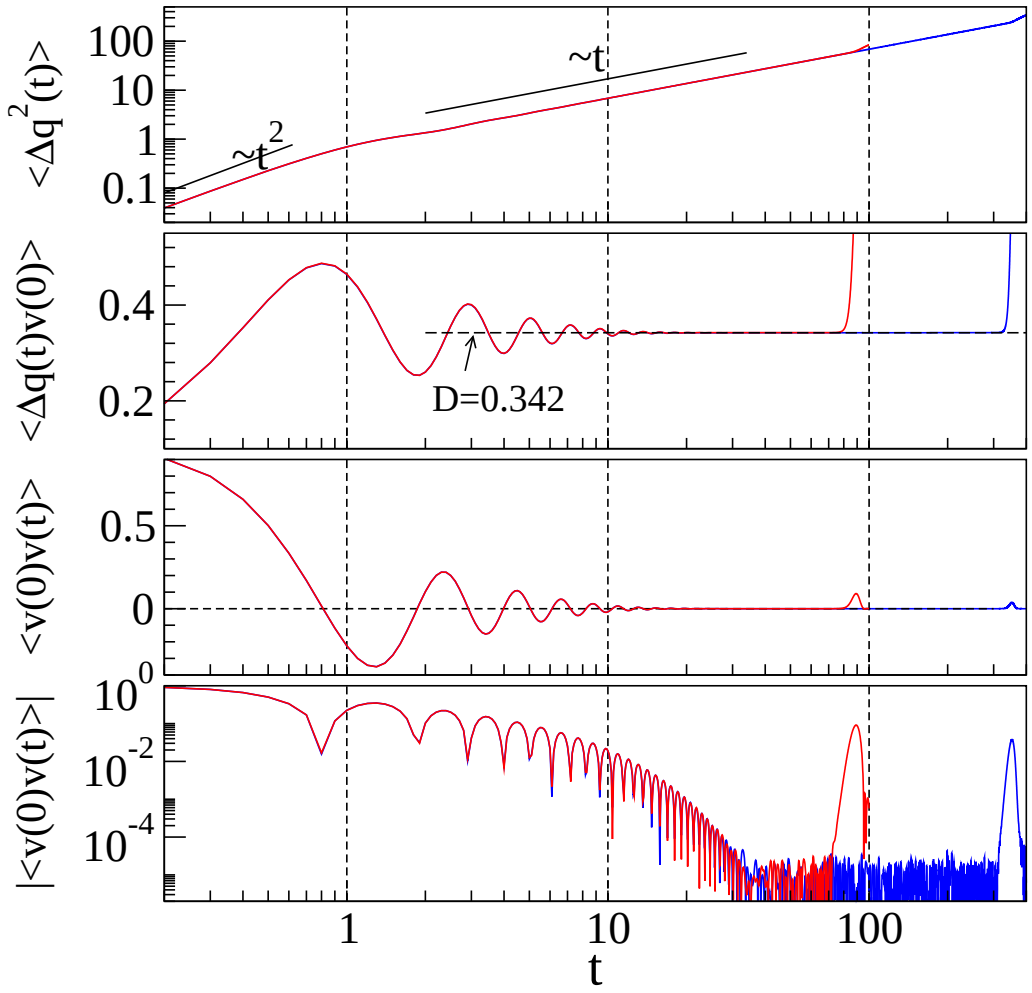

Figure 3.4: FPU β chain: short time correlation functions of the central tagged particle in systems of sizes $N = 129$ (red) and 513 (blue) with periodic boundary conditions. The parameters here were taken as $k = 1, \alpha = 0, \beta = 1, m = 1$ and $k_B T = 1$. We see that there is a fast convergence of $\langle \Delta q(t) v(0) \rangle$ to the expected diffusion constant $D = k_B T / 2\rho_m c = 0.342$. Note that, because of the use of periodic boundaries, the curves go up (positive correlation) when the wall effect sets in, rather than going down [anti-correlation, see Fig. (3.2)].

similarity, as well as significant differences. At short times [Fig. (3.4)], there is again a crossover from ballistic ($\langle \Delta q^2(t) \rangle \sim t^2$) to diffusive ($\langle \Delta q^2(t) \rangle \sim t$) behaviour. As will be discussed in the next chapter, the diffusion constant is again given by the formula $D = k_B T / 2\rho_m c$, where the speed of sound will be determined for a given microscopic model. Moreover, $\langle v(0) v(t) \rangle$ shows oscillatory behavior as in the harmonic case. However, the damping is much faster (exponential)

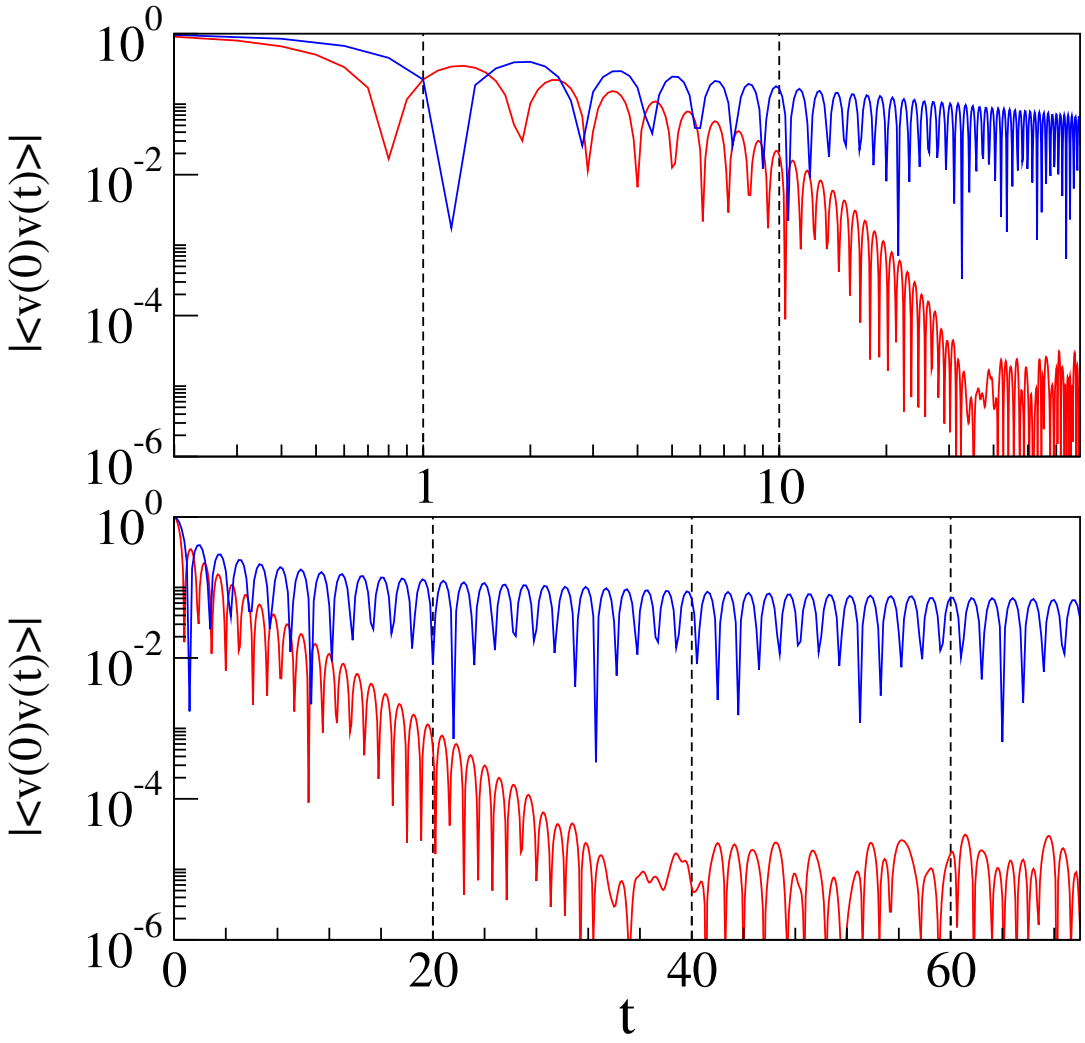

FIGURE 3.5: FPU β chain as compared to the harmonic chain : short time VAF of the central tagged particle in systems of size $N = 129$ with periodic boundary conditions. The upper panel is a log-log plot emphasizing the power-law decay of the VAF for harmonic chain (blue), while the bottom panel is a log-linear plot emphasizing exponential decay for the FPU chain (red).

for the FPU chain than for the harmonic chain (power-law decay) [see Fig. (3.5)]. At long times [Fig. (3.6)], we can see $\langle \Delta q^2(t) \rangle$ converging to the expected equilibrium values, for small system sizes, unlike the harmonic chain. Also notice that these long time damped oscillations are different from the ones seen for the alternate mass hard particle case. Here these are about a mean position while there it was increasing, while always staying below the asymptotic saturation value.

Next, in Fig. (3.7) we compare the β chain with the $\alpha - \beta$ chain, for two values of α. We

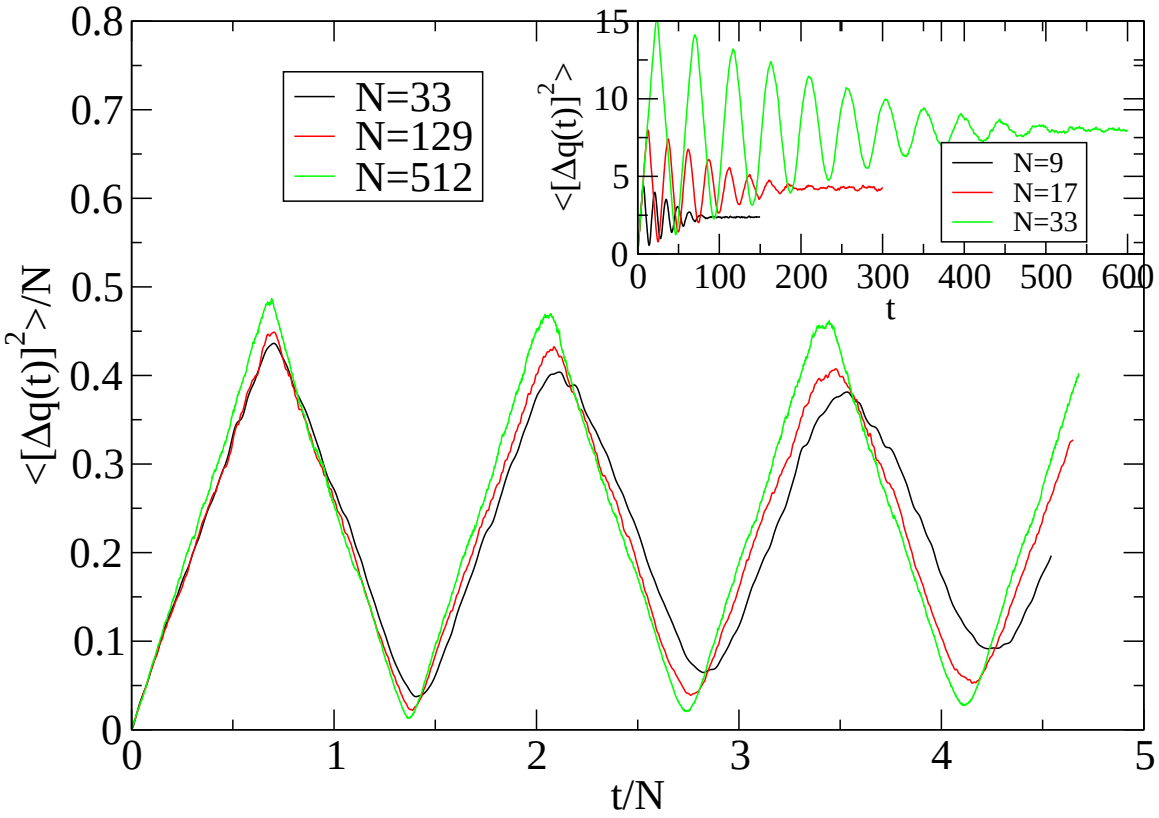

Figure 3.6: FPU β chain: long time MSD of the central tagged particle in FPU chains of different sizes with fixed boundary conditions. The parameters here are the same as in Fig. (3.4).

see that the plots are qualitatively similar, with all of them showing fast convergence to normal-diffusion and exponential decay of velocity auto-correlation function. Thus, there is no apparent significant difference between the β chain and the $\alpha - \beta$ chain, unlike what is seen in recent heat conduction literature [95–97]. However, a hint of difference between them will be seen in the next chapter when we compare them with the linearized model.

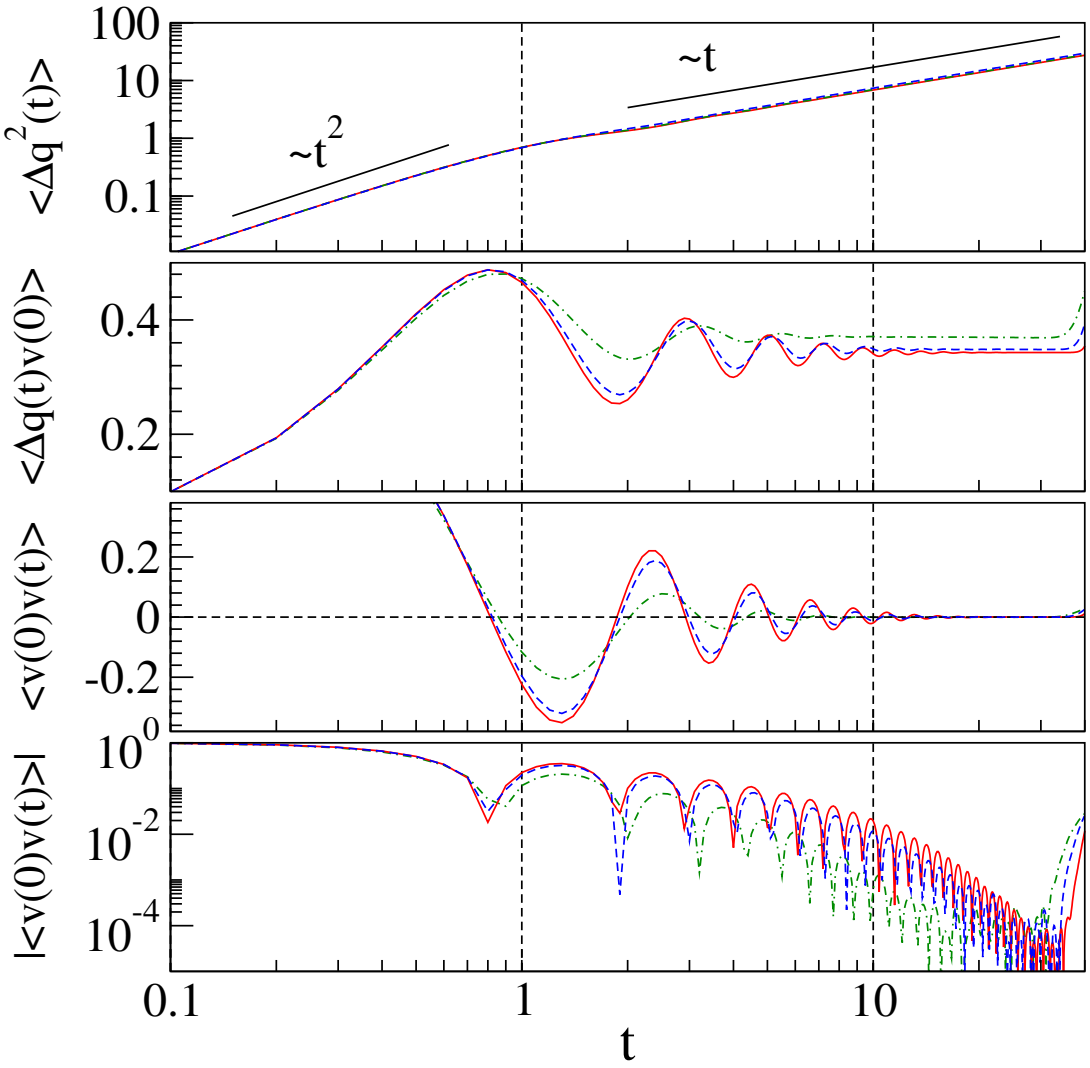

FIGURE 3.7: FPU $\alpha - \beta$ chain as compared to the FPU β chain : short time correlation functions of the central tagged particle in systems of size $N = 65$ with periodic boundary conditions. The three plots correspond to $k = 1, \alpha = 0, \beta = 1$ (red solid line), $k = 1, \alpha = 1, \beta = 1$ (blue dashed line) and $k = 1, \alpha = 2, \beta = 1$ (green dashed-dotted line). Other parameters are same for the three cases, i.e., $m = 1$ and $k_B T = 1$. Same behaviour is seen even for larger system sizes.

3.4 Lennard-Jones chain

The mean-squared displacement $\langle \Delta q^2(t) \rangle$ for the FPU (and harmonic) chain seems to have a similar dependence on t as for a hard particle gas [90], with an initial $\sim t^2$ increase crossing over to a $\sim t$ dependence. However, derivatives of this correlation function, $\langle \Delta q(t) v(0) \rangle$ and $\langle v(0) v(t) \rangle$ show differences. For the FPU chain, $\langle \Delta q(t) v(0) \rangle$ approaches a constant rapidly.

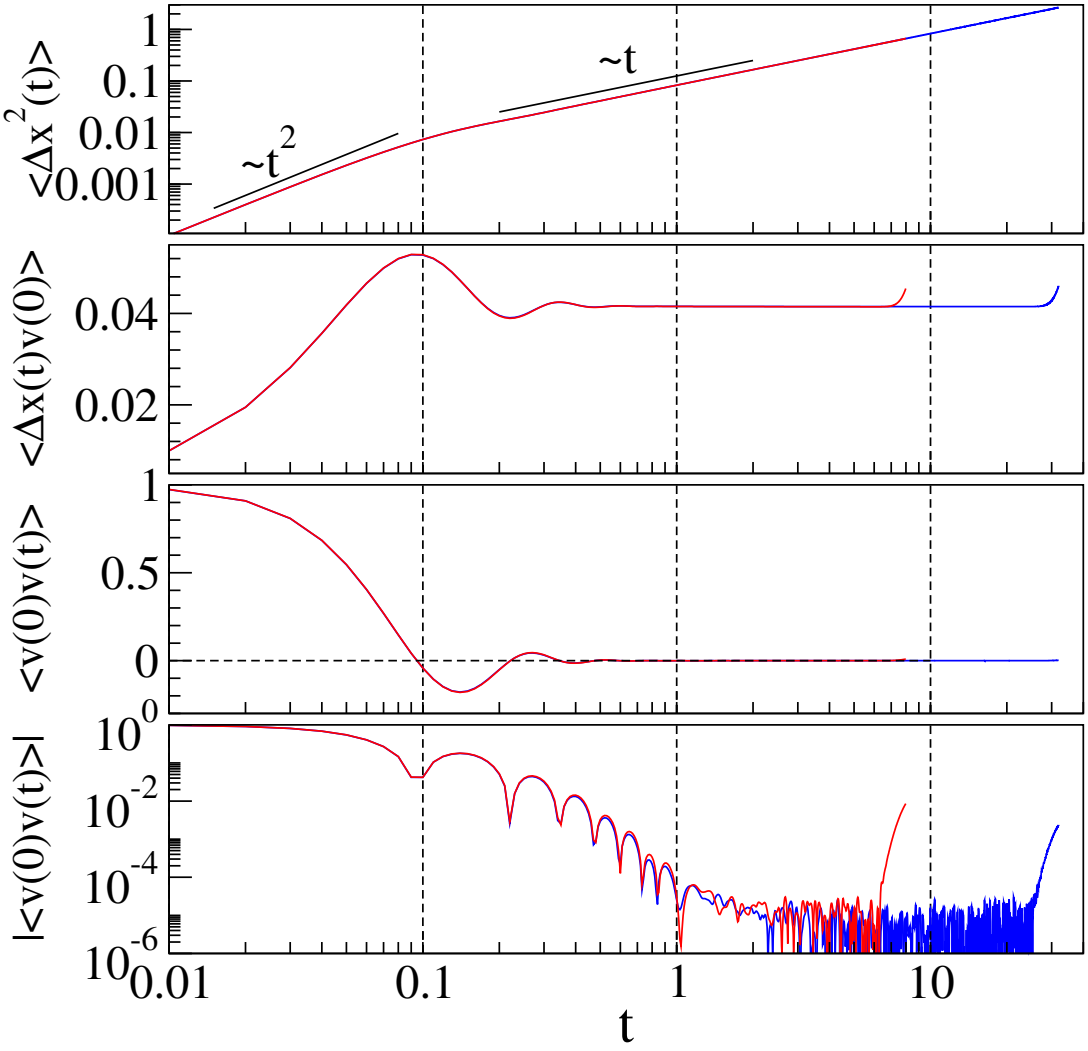

FIGURE 3.8: LJ chain (high density): short time correlation functions of the central tagged particle in systems of sizes $N = 129$ (red) and $N = 513$ (blue) with inter-particle separation 1.0. All the particles are of mass 1.0. Periodic boundary conditions were used here.

Although this is less rapid for a harmonic chain, it is nevertheless clear that the large t limit is a constant. On the other hand, for the alternate mass hard particle gas, $\langle \Delta x(t) v(0) \rangle$ decreases slowly as t increases, with a levelling off at very long times [90] [see also Sec. (2.3)]. Turning to the velocity auto-correlation function, for the FPU chain this has a damped oscillatory behaviour, while there are no — or over-damped — oscillations in the hard particle velocity auto-correlation function.

The hard particle gas may be considered as an extreme case of a non-linear oscillator chain,

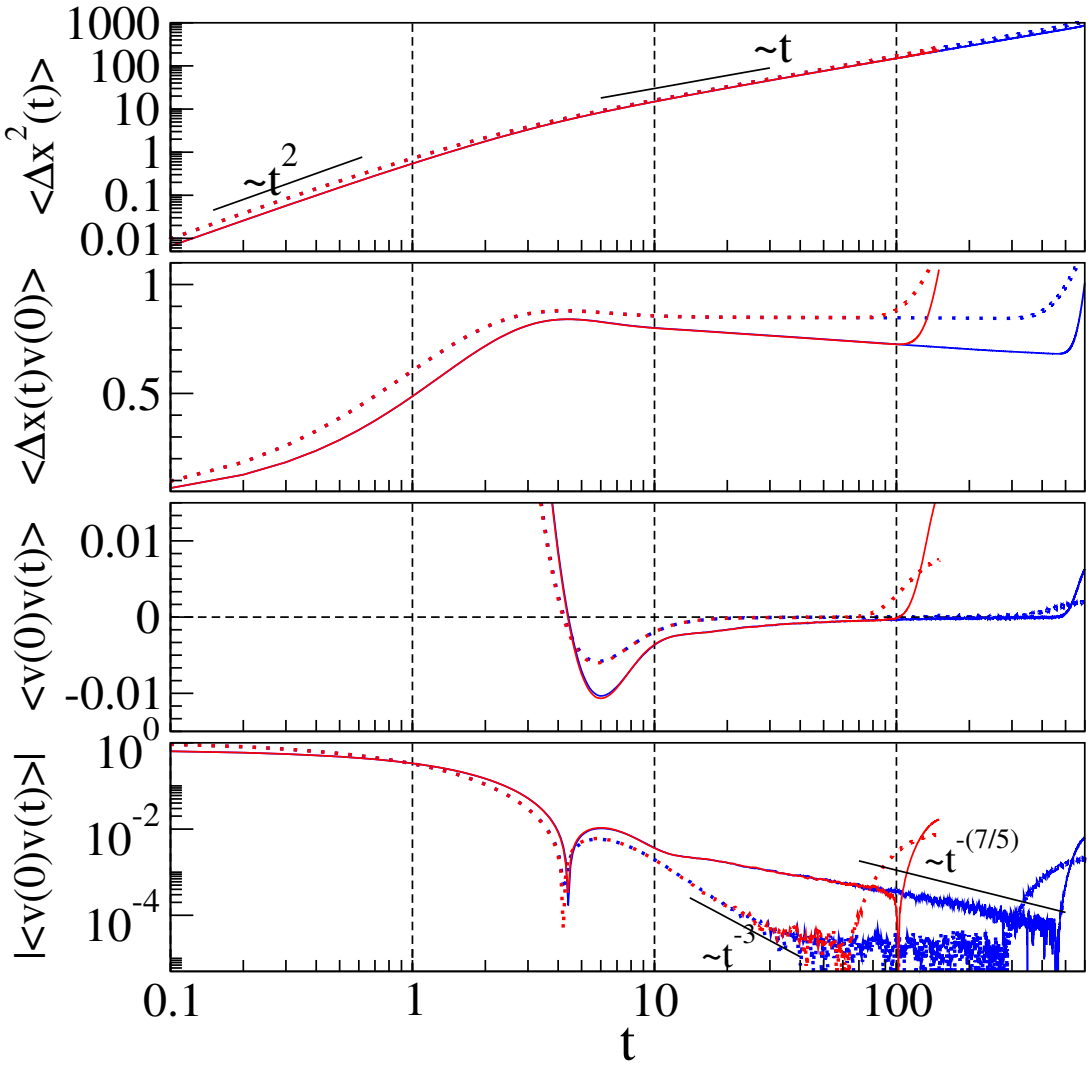

FIGURE 3.9: LJ chain (low density): short time correlation functions of the central tagged particle in systems of sizes $N = 129$ (red) and $N = 513$ (blue) with inter-particle separation 3.0. The equal mass case is represented by dotted lines, while solid lines represent the alternate mass case (with masses 1.5 and 0.5). Periodic boundary conditions were used here.

but it is a singular limit of this family. To see if the differences between the correlation functions for the two cases are significant, we study the Lennard-Jones (LJ) chain. The Hamiltonian of the LJ chain is taken to be

$$H = \sum_{l=1}^{N} \frac{m}{2}\dot{x}_l^2 + \sum_{l=1}^{N+1}\left[\frac{1}{(x_l - x_{l-1})^{12}} - \frac{1}{(x_l - x_{l-1})^{6}}\right] \tag{3.16}$$

where x's are the positions of the particles. At low densities, one would expect the particles to behave approximately like free particles, with a repulsive force between neighbouring particles

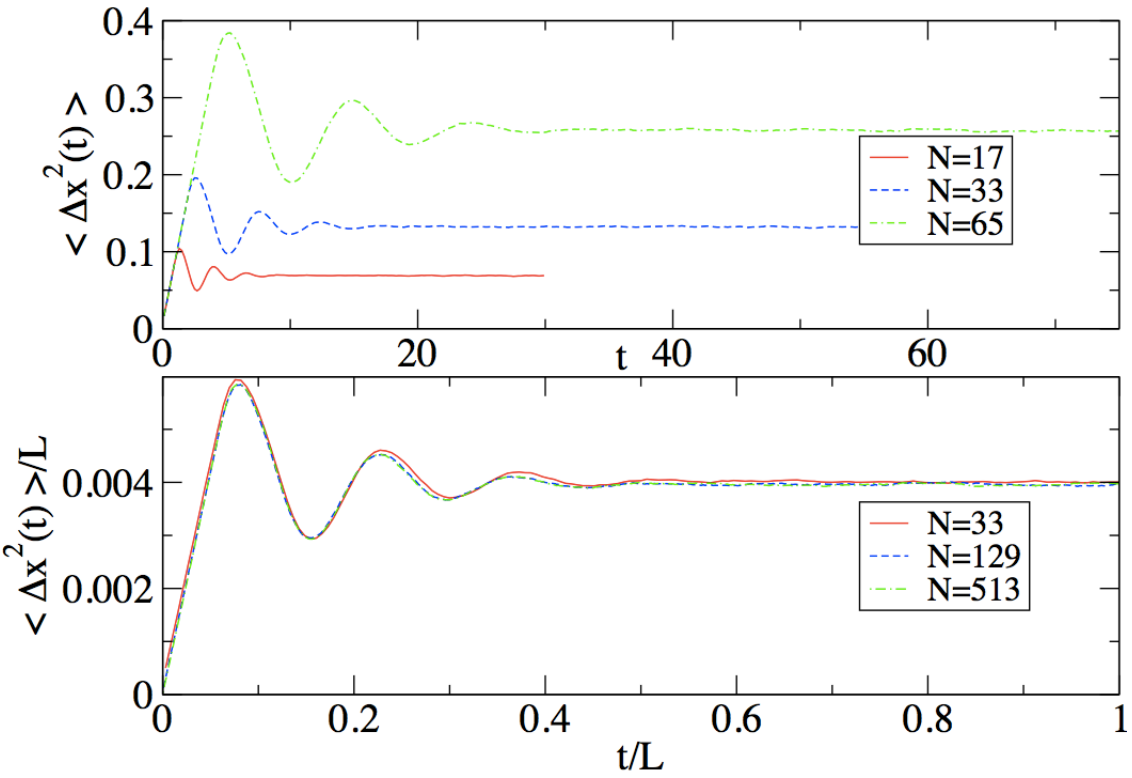

FIGURE 3.10: LJ chain (high density): long time MSD of the central tagged particle in systems of different sizes N with inter-particle separation 1.0 and fixed boundary conditions.

when they come close to each other. Since the repulsion occurs over a distance that is small compared to the mean inter-particle separation, the system is similar to a hard particle gas. On the other hand, at high densities, the particles should remain close to their equilibrium positions with small deviations, resulting in behaviour more like a $\alpha - \beta$ FPU chain, as can also be seen by Taylor expanding the LJ potential about the equilibrium separation.

As in the FPU case we evaluate the correlation functions of the central particle from velocity-verlet molecular dynamics simulations. The particles are inside a box of length L and we fix particles at the boundaries by setting $x_0 = 0$ and $x_{N+1} = L$. The mean inter-particle spacing is thus $a = L/(N+1)$. The simulation results are given in Fig. (3.8) and Fig. (3.9) for short times and Fig. (3.10) and Fig. (3.11) for long times. In these simulations we have taken $k_B T = 1$.

As expected, we observe in Fig. (3.8) and Fig. (3.10) that at high density the behaviour is similar to that of the FPU chain. At low densities, Fig. (3.9) and Fig. (3.11), the behaviour

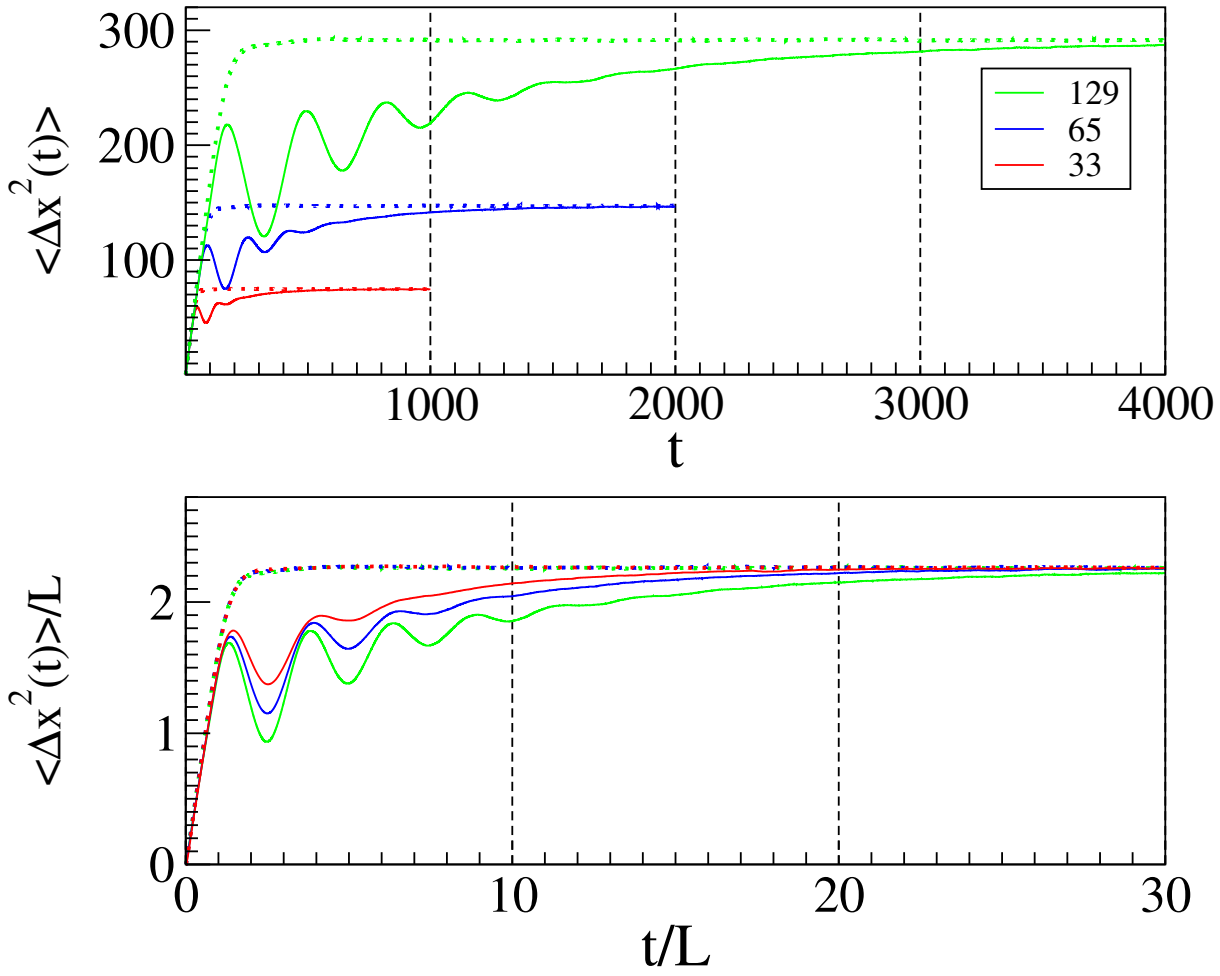

FIGURE 3.11: LJ chain (low density): long time MSD of the central tagged particle in systems of different sizes N with inter-particle separation 3.0 and fixed boundary conditions. The equal mass case is represented by dotted lines, while solid lines represent the alternate mass case (with masses 1.5 and 0.5).

resembles that of the hard particle gas, both for equal and alternate mass cases. The two sets of figures correspond to $a = 1.0$ and $a = 3.0$ respectively. In the next chapter we will estimate the diffusion constant for this case also through the linearized model. Notice that the long time oscillations seen in Fig. (3.10) are also about the equilibrium value, similar to what was seen in the FPU case, while in Fig. (3.11) they are below the saturation value, as was seen in the hard particle case.

3.5 Discussions and conclusions

In this chapter we obtained the tagged-particle correlation functions for various oscillator chains. For the harmonic chain we obtained the correlation functions both analytically and through molecular dynamics simulations. For the nonlinear chains of Fermi-Pasta-Ulam and Lennard-Jones, the correlation functions were obtained through molecular dynamics simulations exclusively. In the next chapter we will study an effective harmonic model and compare its results with the simulation results of the anharmonic systems studied here. Importantly, we saw that here also the tagged particle showed normal-diffusion in all the cases, linear as well as non-linear. As in the previous chapter, this normal-diffusion is very different from the normal-diffusion of a tagged particle undergoing Langevin dynamics with white noise, with the velocity auto-correlation function not being a plain exponential function. The envelop of the decay, though, is an exponential function for the FPU chains.

We also saw how fixed boundary effect manifests itself as long-time oscillations in the various cases, with the onset time being $\sim 2L/c$. For the harmonic chain we saw the period of these oscillations ($2Na/c$) to be determined by the sound speed c. In the next chapter we will obtain the sound speed for various anharmonic chains and compare with the simulation results. We further saw that these long time oscillations for the anharmonic chains were damped, while they were undamped (or minimally damped) for the harmonic chain. Also, the form of these long-time oscillation for the oscillator chain systems were quite different from the alternate mass hard particle gas, except for the low density LJ case, in the sense that they were about a fixed mean position rather than rising ones. We will get some idea behind this difference in the next chapter, where we will also study the effect that periodic boundary condition has on the systems studied here.

4

Effective Harmonic Model

4.1 Introduction

In the previous chapter, we obtained various correlation functions of the tagged particle for different anharmonic chains, through molecular dynamics simulations exclusively. This was due to the non-linearity of the equations of motion. In this chapter, as a simplified model of these systems, we consider an effective harmonic description of the system. The nonlinear terms in Eq. (3.15) normally couple the normal modes of the linear system, and we now assume that they can be replaced by momentum conserving dissipation and noise terms — thus for any mode, all the other modes act as a heat bath. It is important to add *momentum conserving* noise and dissipation since these are generated internally from the systems dynamics and have to preserve the conservation laws. Note that this is different from the effective harmonization technique of [98], where the original dynamics is stochastic, and the noise and dissipation already

exists. We then solve these linear stochastic equations of motion exactly and compare the results obtained from these with the simulation results obtained in the previous chapter.

4.2 The model

Our effective harmonic model with noise and dissipation is described by the following equations of motion:

$$m\ddot{q}_l = -k_{\rm eff}(2q_l - q_{l+1} - q_{l-1}) - \gamma(2\dot{q}_l - \dot{q}_{l+1} - \dot{q}_{l-1}) + (2\xi_l - \xi_{l+1} - \xi_{l-1}) \ , \tag{4.1}$$

where $k_{\rm eff}$ is an effective spring constant, γ a damping constant and ξ_l are noise terms whose properties will be specified later. We consider fixed boundaries condition $q_0 = 0$ and $q_{N+1} = 0$. As for the harmonic oscillator, we transform to normal mode coordinates, $\phi_p(l) = \sqrt{2}/\sqrt{m(N+1)}\sin(lpa)$ with $pa = n\pi/(N+1)$, $n = 1, \ldots, N$, with $\xi_l(t) = \sum_p \tilde{\xi}_p(t)\phi_p(l)$. The normal mode coordinates $a_p(t)$ now satisfy the equation of motion

$$\begin{aligned} \ddot{a}_p(t) + \omega_p^2 a_p(t) &= -\frac{\gamma}{k_{\rm eff}}\omega_p^2\dot{a}_p(t) + \frac{\omega_p^2}{k_{\rm eff}}\tilde{\xi}_p(t) \ , \\ \text{where} \quad \omega_p^2 &= \frac{2k_{\rm eff}}{m}(1 - \cos pa). \end{aligned}$$

To ensure equilibriation of the modes we choose Gaussian noise with zero mean and two point correlations given by

$$\langle \tilde{\xi}_p(t) \ \tilde{\xi}_{p'}(t') \rangle = \frac{2k_{\rm eff}\gamma k_B T}{m\omega_p^2}\delta(t - t') \ \delta_{p,p'} \ .$$

In steady state, $a_p(t) = \omega_p^2 \int_{-\infty}^{t} G(t - t')\tilde{\xi}_p(t')dt'$, where $G(t - t')$ is the Green's function for the equation of motion. After some straightforward computations we finally get

$$\langle q_l(t)q_l(0)\rangle = k_B T \sum_p \frac{\phi_p^2(l)}{\omega_p^2} e^{-\alpha_p t}\left[\cos(\beta_p t) + \frac{\alpha_p}{\beta_p}\sin(\beta_p t)\right], \tag{4.2a}$$

$$\langle q_l(t)v_l(0)\rangle = k_B T \sum_p \frac{\phi_p^2(l)}{\beta_p} e^{-\alpha_p t}\sin(\beta_p t) \ , \tag{4.2b}$$

$$\langle v_l(t)v_l(0)\rangle = k_B T \sum_p \phi_p^2(l) e^{-\alpha_p t}\left[\cos(\beta_p t) - \frac{\alpha_p}{\beta_p}\sin(\beta_p t)\right] \ , \tag{4.2c}$$

$$\text{where} \quad \alpha_p = \frac{\gamma\omega_p^2}{2k_{\rm eff}} \ , \quad \beta_p = (-\alpha_p^2 + \omega_p^2)^{1/2} \ .$$

Taking N to be odd, we get for the middle particle $l = (N+1)/2$

$$\langle q(t)q(0)\rangle = \frac{2k_BT}{m(N+1)} \sum_{n=1,3,\ldots} \frac{e^{-\alpha_p t}}{\omega_p^2} \left[\cos(\beta_p t) + \frac{\alpha_p}{\beta_p}\sin(\beta_p t)\right] , \tag{4.3a}$$

$$\langle q(t)v(0)\rangle = \frac{2k_BT}{m(N+1)} \sum_{n=1,3,\ldots} \frac{e^{-\alpha_p t}}{\beta_p}\sin(\beta_p t) , \tag{4.3b}$$

$$\langle v(t)v(0)\rangle = \frac{2k_BT}{m(N+1)} \sum_{n=1,3,\ldots} e^{-\alpha_p t} \left[\cos(\beta_p t) - \frac{\alpha_p}{\beta_p}\sin(\beta_p t)\right] , \tag{4.3c}$$

If we take the $t \to \infty$ limit first in the middle equation in Eq. 4.3 then we get $D = 0$. As discussed earlier, we need to take the $N \to \infty$ limit before $t \to \infty$ limit, thereby exploring the infinite system diffusive behaviour. In the limit $N \to \infty$, the above equations give:

$$\langle q(t)q(0)\rangle = \frac{k_BTa}{m\pi} \int_0^{\pi/a} dp \frac{e^{-\alpha_p t}}{\omega_p^2} \left[\cos(\beta_p t) + \frac{\alpha_p}{\beta_p}\sin(\beta_p t)\right] , \tag{4.4a}$$

$$\langle q(t)v(0)\rangle = \frac{k_BTa}{m\pi} \int_0^{\pi/a} dp \frac{e^{-\alpha_p t}}{\beta_p}\sin(\beta_p t) , \tag{4.4b}$$

$$\langle v(t)v(0)\rangle = \frac{k_BTa}{m\pi} \int_0^{\pi/a} dp e^{-\alpha_p t} \left[\cos(\beta_p t) - \frac{\alpha_p}{\beta_p}\sin(\beta_p t)\right] . \tag{4.4c}$$

The diffusion constant is obtained as

$$\lim_{t\to\infty} \langle q(t)v(0)\rangle = \frac{k_BTa}{m\pi c} \int_0^\infty dx \frac{\sin(x)}{x} = \frac{k_BT}{2\rho_m c} \tag{4.5}$$

where, as before, ρ_m is the mass per unit length and c is the speed of sound. Thus, we see that our effective damped harmonic model predicts normal-diffusion for the tagged particle. The long time infinite size behaviour of the VAF in Eq. (4.4 c) can be estimated and we find $\langle v(t)v(0)\rangle \sim \exp(-\gamma t/m)\sin(2ct/a)$.

Our effective damped harmonic theory in fact follows from the full hydrodynamic equations discussed in Ref. [99]. Here we briefly outline such a derivation. In the hydrodynamic theory, one starts with equations for the three coarse-grained conserved fields, corresponding to the extension $r_l = q_{l+1} - q_l$, momentum p_l and energy e_l. These are given by

$$\begin{aligned} \frac{\partial r(x,t)}{\partial t} &= \frac{\partial p(x,t)}{\partial x} , \\ \frac{\partial p(x,t)}{\partial t} &= -\frac{\partial P(r,\hat{e})}{\partial x} , \\ \frac{\partial e(x,t)}{\partial t} &= -\frac{\partial P(r,\hat{e})p(x,t)}{\partial x} , \end{aligned} \tag{4.6}$$

where $P(r,\hat{e})$ is the local pressure and is a function of the local extension and energy $\hat{e} = e - p^2/2$. In the above equations we have made the identification $l \to x$ and $\partial/\partial x$ can be thought of as a discrete derivative. Next, one looks at fluctuations of the conserved fields about their equilibrium value and define the fields $u_1 = \delta r = r - \langle r \rangle$, $u_2 = p$ and $u_3 = \delta e = e - \langle e \rangle$, where the angular brackets denote equilibrium averages. Then, expanding the pressure around its equilibrium value, P_{eq}, we get from Eq. (4.6) the following linear equations

$$\begin{aligned}
\frac{\partial \delta r(x,t)}{\partial t} &= \frac{\partial p(x,t)}{\partial x} \ , \\
\frac{\partial p(x,t)}{\partial t} &= -\frac{\partial P_{eq}(r,\hat{e})}{\partial r}\frac{\partial \delta r(x,t)}{\partial x} - \frac{\partial P_{eq}(r,\hat{e})}{\partial e}\frac{\partial \delta e(x,t)}{\partial x}, \\
\frac{\partial \delta e(x,t)}{\partial t} &= -P_{eq}\frac{\partial p(x,t)}{\partial x} \ .
\end{aligned} \tag{4.7}$$

Substituting for $\partial p(x,t)/\partial x$ from the first line into the third line of Eq. (4.7), and operating $\partial/\partial x$ on both sides, we get $\partial \delta e(x,t)/\partial x = -P_{eq}\partial \delta r(x,t)/\partial x$. Substituting this in the second line above, we obtain

$$\frac{\partial p(x,t)}{\partial t} = \left[-\frac{\partial P_{eq}(r,\hat{e})}{\partial r} + P_{eq}(r,\hat{e})\frac{\partial P_{eq}(r,\hat{e})}{\partial e}\right]\frac{\partial \delta r(x,t)}{\partial x}. \tag{4.8}$$

The terms within brackets is precisely the expression for c^2 given in [99], where an expression for it in the constant temperature/pressure ensemble has been given. We now observe that, on adding the momentum conserving noise and damping terms, Eq. (4.8) is equivalent to our Eq. (4.1), upon identifying $c^2 = k_{\rm eff}/m$.

In the next section, we compare the correlation functions given by Eq. (4.3), to the simulation results for the various nonlinear systems studied. We use the expression for sound speed given for a general anharmonic chain in Ref. [99] and use the parameters of our systems to evaluate it. The effective spring constant $k_{\rm eff}$ is then obtained from this sound speed and the damping constant γ is the only free parameter used for fitting.

4.3 Comparison with the nonlinear systems

The sound speed in an anharmonic chain is given, in canonical ensemble described by temperature and pressure, as [99]

$$c^2 = \frac{1}{\Gamma}\left(\frac{1}{2\beta^2} + \langle V + Py; V + Py\rangle\right), \tag{4.9}$$

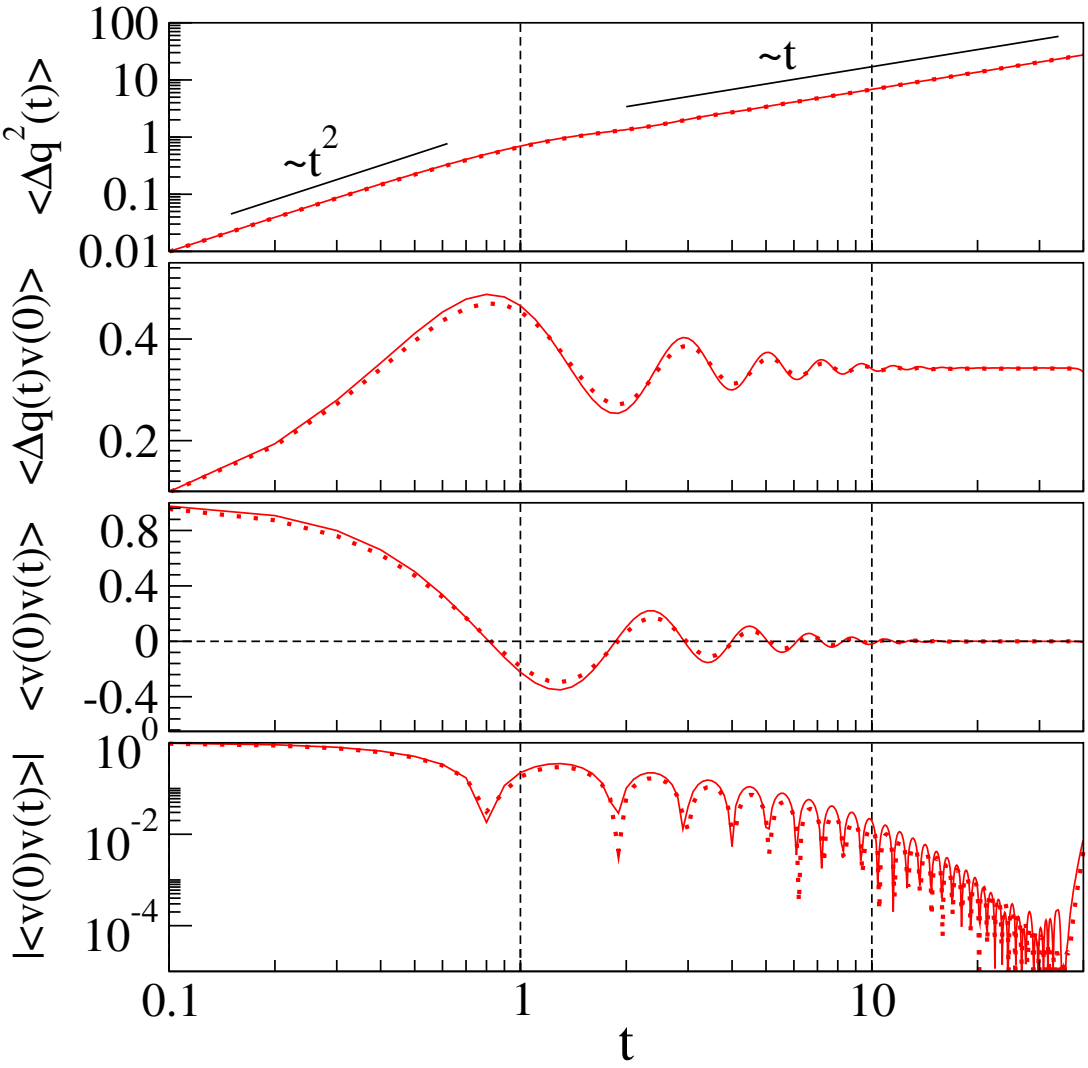

Figure 4.1: Comparison of FPU β chain with the linearized hydrodynamic model: short time correlation functions of the central tagged particle in a chain of size $N = 65$ (solid line) compared with the predictions of the hydrodynamic model (dashed line). The parameters of the chain here are same as in Fig. (3.4). The only fitting parameter of the model is the damping constant γ which is taken to be 0.1 here.

where V is the interparticle pair potential, $\beta = 1/k_B T$, P is the pressure and $\langle y \rangle$ is the average extension between neighbouring particles.

$$\Gamma = \beta \left(\langle y; y \rangle \langle V; V \rangle - \langle y; V \rangle^2 \right) + \frac{1}{2\beta} \langle y; y \rangle , \tag{4.10}$$

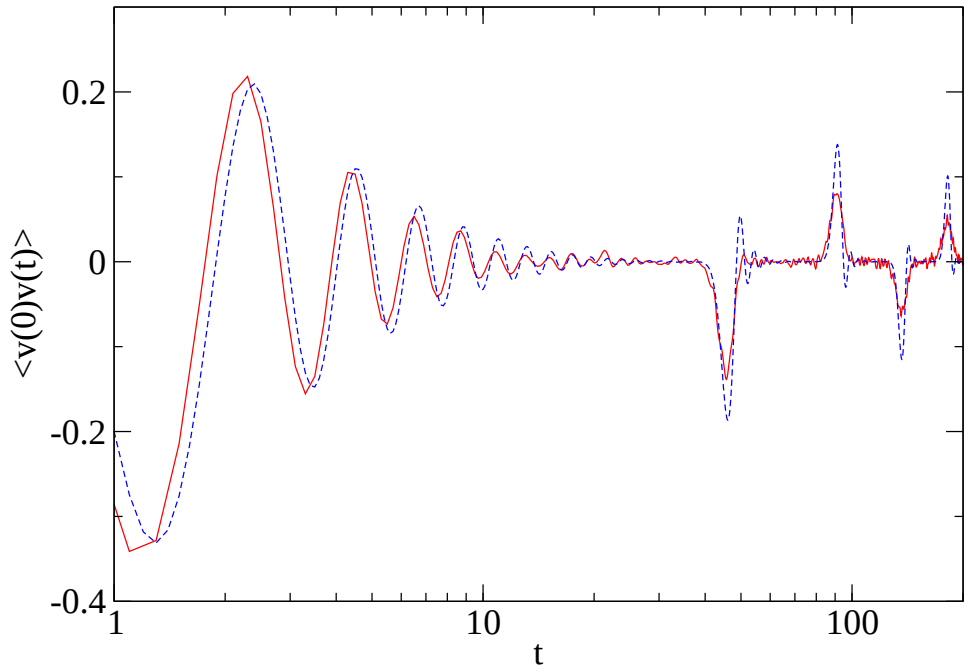

FIGURE 4.2: Comparison of FPU β chain with hydrodynamic model: long time VAF of the central tagged particle in a chain of size $N = 65$ (solid line) compared with the predictions of the hydrodynamic model (dashed line). The parameters of the chain here are again same as in Fig. (3.4). The only fitting parameter of the model is the damping constant γ which was taken to be 0.1.

with the definition $\langle X;Y\rangle = \langle XY\rangle - \langle X\rangle\langle Y\rangle$ and the expectation value of any observable A given as

$$\langle A\rangle = \frac{\int_{-\infty}^{\infty} dy A e^{-\beta(V(y)+Py)}}{\int_{-\infty}^{\infty} dy e^{-\beta(V(y)+Py)}} \quad .$$

In our simulations we have $\beta = 1/k_B T = 1$. The pressure P is evaluated numerically by imposing the condition that the equilibrium extension between neighbouring particles $\langle y\rangle$ is 0 for the FPU chains and a for the LJ chains with inter-particle spacing a.

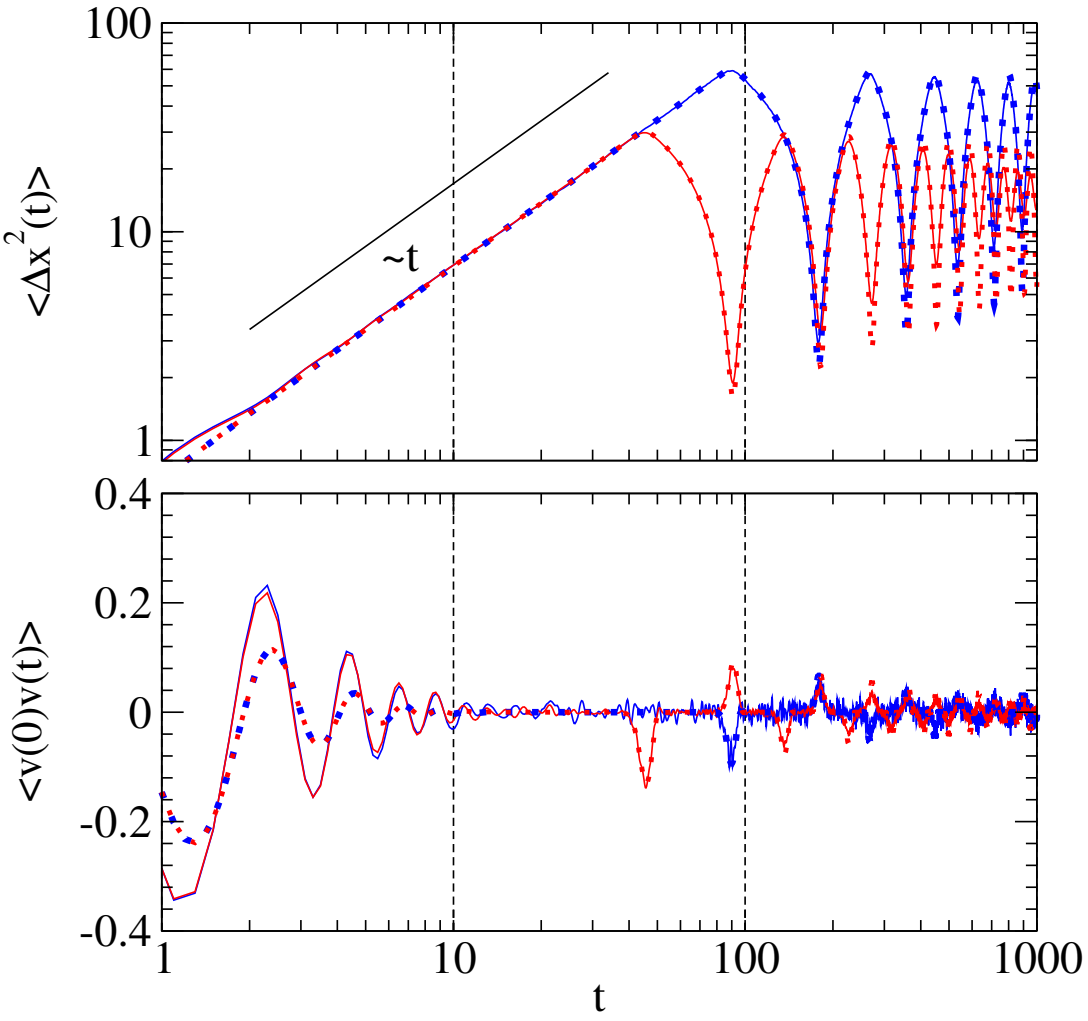

FIGURE 4.3: Comparison of FPU β chain with hydrodynamic model: long time MSD and VAF of the central tagged particle in a chain of sizes $N = 65$ (solid red line) and $N = 129$ (solid blue line) compared with the predictions of the hydrodynamic model (dashed lines of corresponding colours). The parameters of the chain here are again same as in Fig. (3.4). The only fitting parameter of the model being $\gamma = 0.1$.

4.3.1 Comparison with the FPU β chain : $V(y) = y^2/2 + y^4/4$

For the symmetric (even potential) FPU β chain $P = 0$. This gives

$$c = a[k_B T/(m\langle y^2\rangle)]^{1/2} = [1/(\langle y^2\rangle)]^{1/2},$$

$k_B T, m$ and the lattice spacing a being unity in our simulation. Further, we get

$$\langle y^2\rangle = \frac{\int_{-\infty}^{\infty} y^2 e^{-\beta(V(y)+Py)}dy}{\int_{-\infty}^{\infty} e^{-\beta(V(y)+Py)}dy} = \frac{\int_{-\infty}^{\infty} y^2 e^{-\left(y^2/2+y^4/4\right)}dy}{\int_{-\infty}^{\infty} e^{-(y^2/2+y^4/4)}dy} \approx 0.4679 \quad .$$

and hence $k_{\text{eff}} = c^2 \approx 2.137$.

With this k_{eff} Eq. (4.3) is evaluated and compared with the simulation result, in Fig. (4.1) for short time and Fig. (4.2) for long time. In Fig. (4.3) it is plotted for two system sizes. We see a good match between the two by tuning just one parameter γ. Notice that we get an excellent agreement between the diffusion constant D obtained from Eq. (4.5) and the diffusion constant D obtained from simulation.

4.3.2 Comparison with the FPU $\alpha - \beta$ chain :

$$V(y) = y^2/2 + \alpha y^3/3 + \beta y^4/4$$

Case 1 : $\alpha = 1, \beta = 1$

In this case imposing the condition $\langle y \rangle = 0$ gives $P = -0.3904$. Using this P in Eq. (4.9) we get $k_{\text{eff}} = c^2 \approx 2.119$. With this k_{eff} Eq. (4.3) is evaluated and compared with the simulation result in Fig. (4.4). We see that here also there is a good match between the two by tuning just one parameter γ.

Case 2 : $\alpha = 2, \beta = 1$

In this case imposing the condition $\langle y \rangle = 0$ gives $P = -0.86978$. Using this P in Eq. (4.9) we get $k_{\text{eff}} = c^2 \approx 2.003$. With this k_{eff} now, Eq. (4.3) is evaluated and compared with the corresponding simulation result in Fig. (4.5). We now see slight deviations between the correlation functions obtained from simulation and the linearized model. This deviation increases at higher nonlinearities as will be seen next for the LJ system. We believe that this is possibly because of the cubic non-linearity and may be seen as first indication of difference emerging between the $\alpha - \beta$ and β FPU chains. This point will be discussed further later in this chapter.

4.3.3 Comparison with the LJ gas : $V(y) = 1/y^{12} - 1/y^6$

We consider the LJ chain with mean inter-particle spacing taken as $a = 1.0$. Therefore, we impose the condition $\langle y \rangle = 1.0$ and get $P = 12.98$. Using this P we get from Eq. (4.9) $k_{\text{eff}} = c^2 \approx 169.767$. We plot Eq. (4.3) evaluated using this k_{eff} in Fig. (4.6) and compare it with

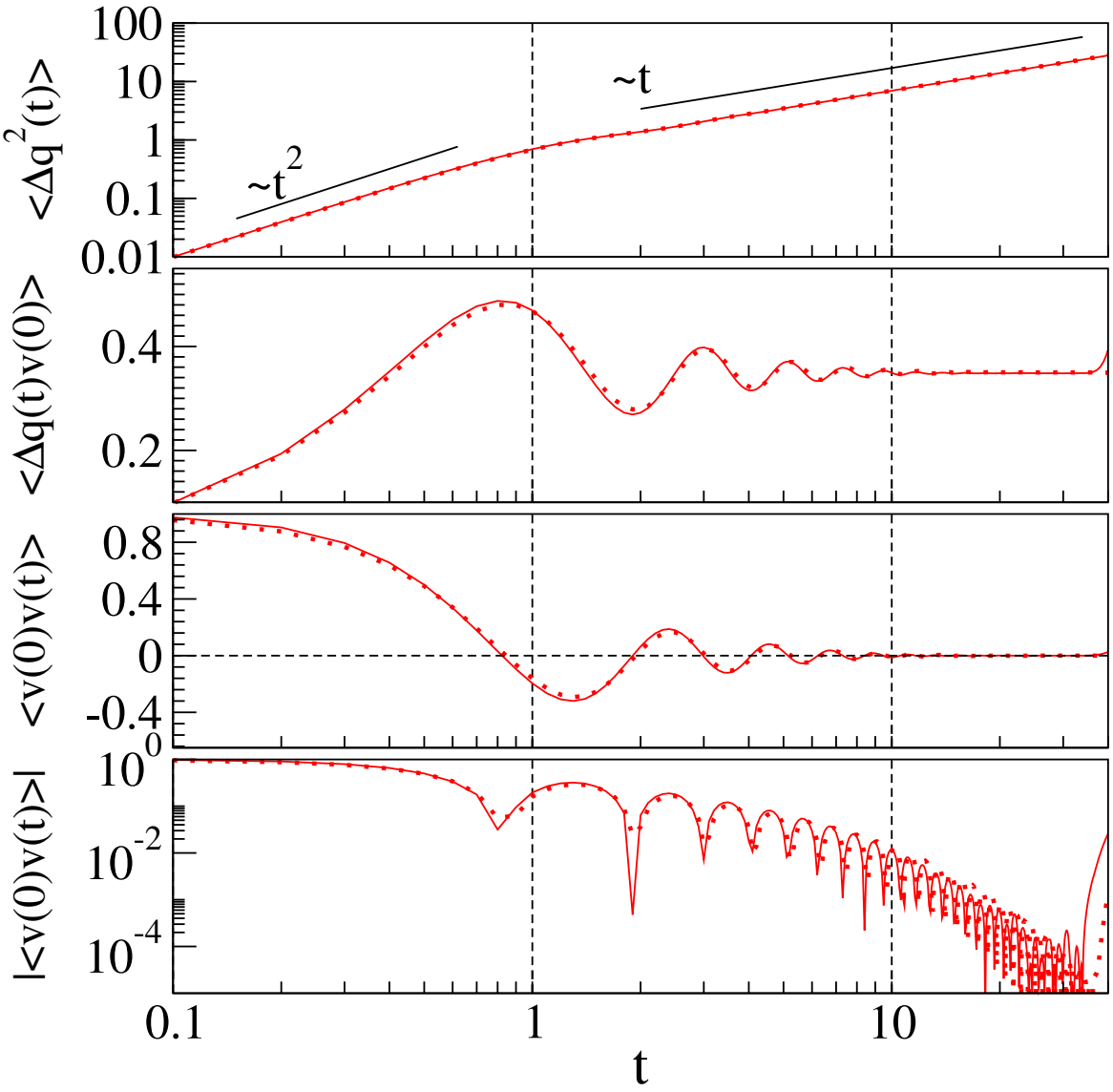

FIGURE 4.4: Comparison of FPU $\alpha - \beta$ chain with hydrodynamic model (Case 1): short time correlation functions of the central tagged particle in a chain of size $N = 65$ (solid line) compared with the predictions of the hydrodynamic model (dashed line). The parameters of the chain here are same as in Fig. (3.7).

the simulation result of corresponding system. We see that the mismatch here increases further. The effective damped harmonic model used for the FPU chains, though works qualitatively for the correlation functions of the high density Lennard-Jones gas, the quantitative agreement, for example with the predicted diffusion constant, is not very good. We believe that this is also because of the cubic non-linearity (in an FPU description valid for small displacements) being

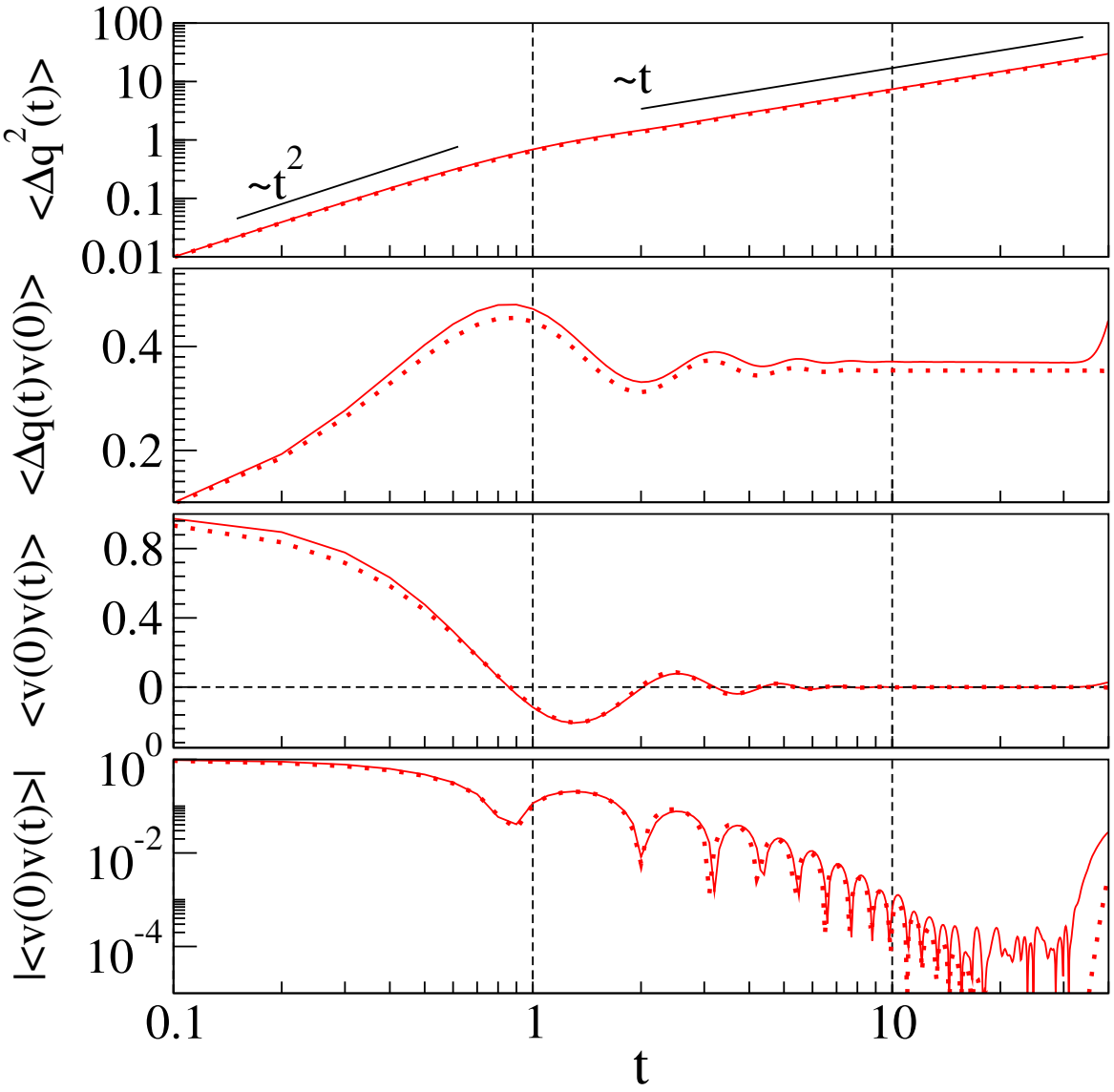

FIGURE 4.5: Comparison of FPU $\alpha - \beta$ chain with hydrodynamic model (Case 2): short time correlation functions of the central tagged particle in a chain of size $N = 65$ (solid line) compared with the predictions of the hydrodynamic model (dashed line). The parameters of the chain here are same as in Fig. (3.7).

significant.

For the low density LJ chain, i.e. the hard-particle like limit, however, this linearized equation completely breaks down. It can neither reproduce the short time power laws of the velocity auto-correlation function nor the long time rising oscillation of the mean square displacement of the low density alternate mass LJ. This and the previous few examples demonstrate that

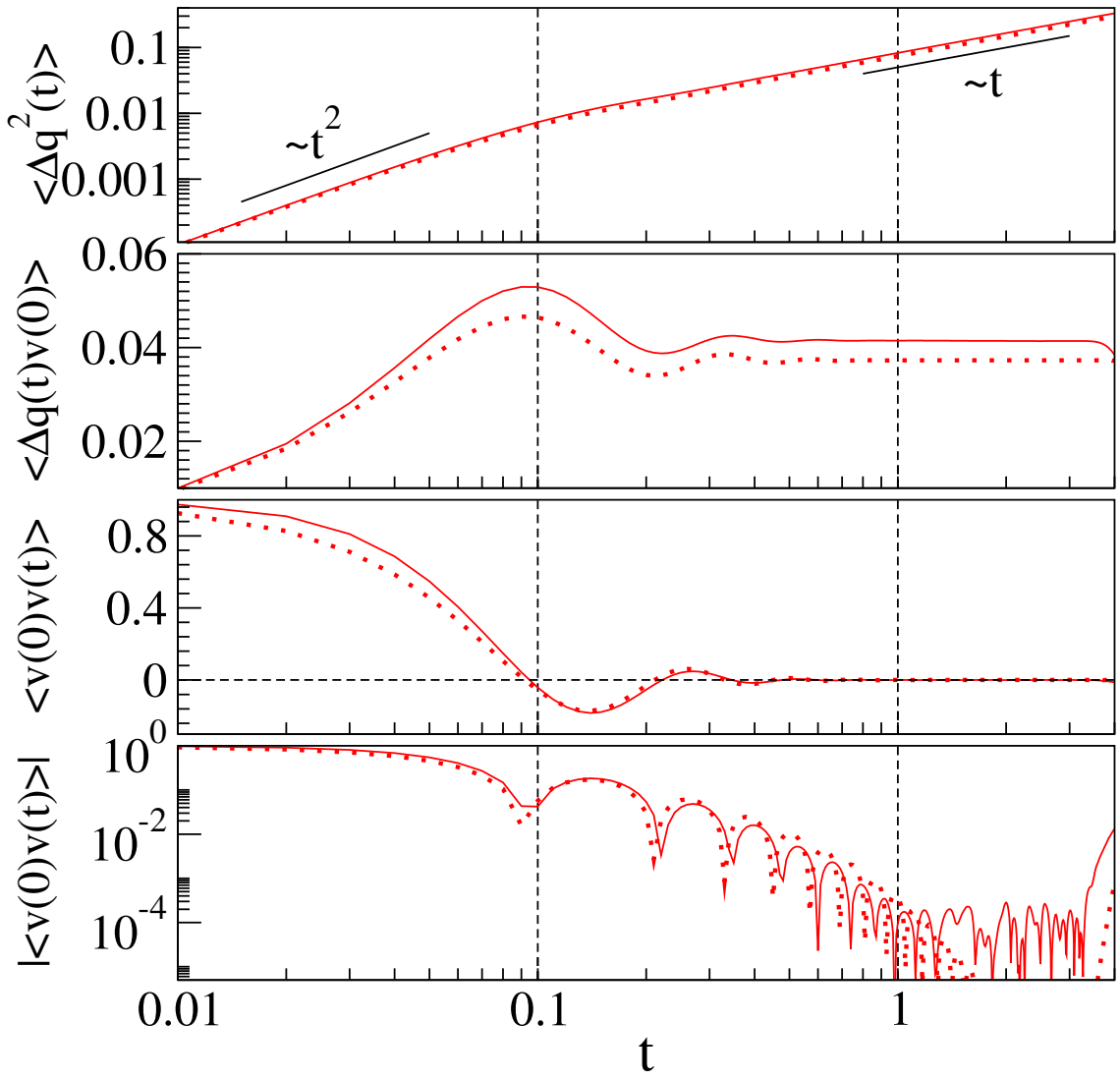

Figure 4.6: Comparison of LJ chain with hydrodynamic model: short time correlation functions of the central tagged particle in chain of size $N = 65$, with inter-particle separation 1.0 (solid line), compared with the predictions of the hydrodynamic model (dashed line). The only fitting parameter of the model is the dissipation constant γ. The parameters of the chain here are same as in Fig. (3.8).

the simple effective damped harmonic model, where we neglect the effect of heat mode, has strong limitations and that the effect of heat mode may actually be important in describing these systems. We believe that a complete description of these 1-dimensional Hamiltonian systems require a calculation based on the full nonlinear hydrodynamic theory which is presumably what Beijeren's calculation (unpublished, [92]) is based on. The origin of the difference in the form of the velocity auto-correlation function between the anharmonic (oscillatory exponential decay)

and the alternate mass hard-particle gas (power law decay) requires further investigation of the nonlinear fluctuating hydrodynamics and appears quite non-trivial to us. It is possible that the effect of non-linearity and coupling between heat and sound modes on the tagged particle correlations are quite different in different parameter regimes.

4.4 Discussions and conclusions

In this chapter we formulated an effective damped harmonic model for the nonlinear chains studied in the previous chapter and solved it analytically for tagged-particle correlation functions. This model, which can be seen as a special case of the full hydrodynamic equations studied by Spohn [99], where the coupling with the heat mode has been neglected, is a first analytic attempt to tackle the problem of tagged-particle diffusion in anharmonic chains. The idea behind the linearization was that the effect of the nonlinearity of the interaction between neighbouring particles may be modeled by an internal heat bath acting on a linear chain. This is done by adding *momentum conserving* noise and damping, which satisfy Fluctuation-dissipation relation among them thereby ensuring equilibriation, to a harmonic chain. This is different from the harmonization technique of [98], where one approximates an anharmonic chain already having noise and dissipation terms. The only fitting parameters of our model are the effective spring constant $k_{\rm eff}$ and the effective damping constant γ, of which $k_{\rm eff}$ is fixed from Spohn's work, leaving only γ as the free fitting parameter. We see that it provides a good description of tagged-particle diffusion in the symmetric FPU chain. We also studied the asymmetric FPU chain, where, though the behaviour of the tagged particle is mostly the same, we find less quantitative agreement with the effective model. This may be indicative of the importance of heat mode that has been neglected in the model. The mismatch is seen to increase further for the LJ chains, especially in the hard-particle like limit. This gives further reason to believe that including coupling of heat mode is necessary. Importance of the heat mode is further appreciated by noting the fact that the mode-coupling result of van-Beijeren presented in Chapter 2 was calculated after inclusion of the heat mode. Therefore further study on tagged-particle diffusion should investigate the full nonlinear fluctuating hydrodynamic equation, incorporating the coupling of sound modes and heat modes and see if the power laws and rising oscillations are obtained.

5

Some special cases

5.1 Introduction

In previous chapters we studied tagged-particle diffusion in various 1-dimensional Hamiltonian systems. We found that the tagged particle shows generic normal-diffusion in all the systems studied, even if the detailed correlation functions are different for different systems. In this chapter we study some more cases of those Hamiltonian systems, with the aim of further exploring the robustness of this normal-diffusion.

In previous chapters we saw that the normal-diffusion persists till the boundary effect shows up and is independent of the boundary conditions before that. In those studies we exclusively concentrated on the reflecting/fixed boundary conditions for studying the long time boundary effect and observed sound speed dependent oscillations in the tagged-particle correlation functions. In Sec. 5.2 we study in some detail, the effect periodic boundary condition has on the long time

behaviour of the tagged-particle correlation functions. We concentrate on the hard particle gas and the harmonic chain and see some expected and also some surprising results.

In Chapter 2 we studied the equal and alternate mass cases of the hard particle gas. In Sec. 5.3 we study the random mass case of the hard particle gas and the mass ratio dependence of the alternate mass hard particle gas. In the subsequent section we study the case where the tagged particle is much heavier than rest of the particles. This problem has some interesting features, both at short and at long times. However, in this thesis we will concentrate on the short time behaviour. In the short time it has been analytically tackled for the hard particle gas ([101]) and the harmonic chain ([102, 103]). Here we present molecular dynamics simulation results demonstrating those findings. In particular, we re-obtain the Langevin exponential decay of the velocity auto-correlation function for the tagged particle, which is characteristic of a Brownian particle.

One interesting thing we saw in this thesis is the absence of the famous single-file diffusion scaling of the tagged particle mean-squared displacement ($\langle \Delta x^2(t) \rangle \sim \sqrt{t}$), observed in various one-dimensional stochastic systems, in any of the one-dimensional Hamiltonian systems studied. Since ultimately stochastic models are supposed to be coarse grained descriptions of deterministic systems, a fundamental important question that remains is whether one can obtain this scaling, in some way, in these deterministic systems. We address this question in Sec. 5.5, by studying a particular configuration of the hard particle gas which may be expected to show the scaling.

5.2 Periodic Vs reflecting boundary conditions : Surprises of the zero mode

In this section we study the effect of implementing periodic boundary condition on the long time behaviour of the tagged particle, first for the hard particle gas and then for the harmonic chain. For the hard particle gas we present results from event driven molecular dynamics simulations, performed as described in Chapter 2. For the harmonic chain we perform velocity-verlet molecular dynamics simulations (Chapter 3), as well as exact analytic calculations. The periodic boundary condition is implemented by identifying the $(N+1)^{th}$ particle with the 1^{st} particle in a N particle

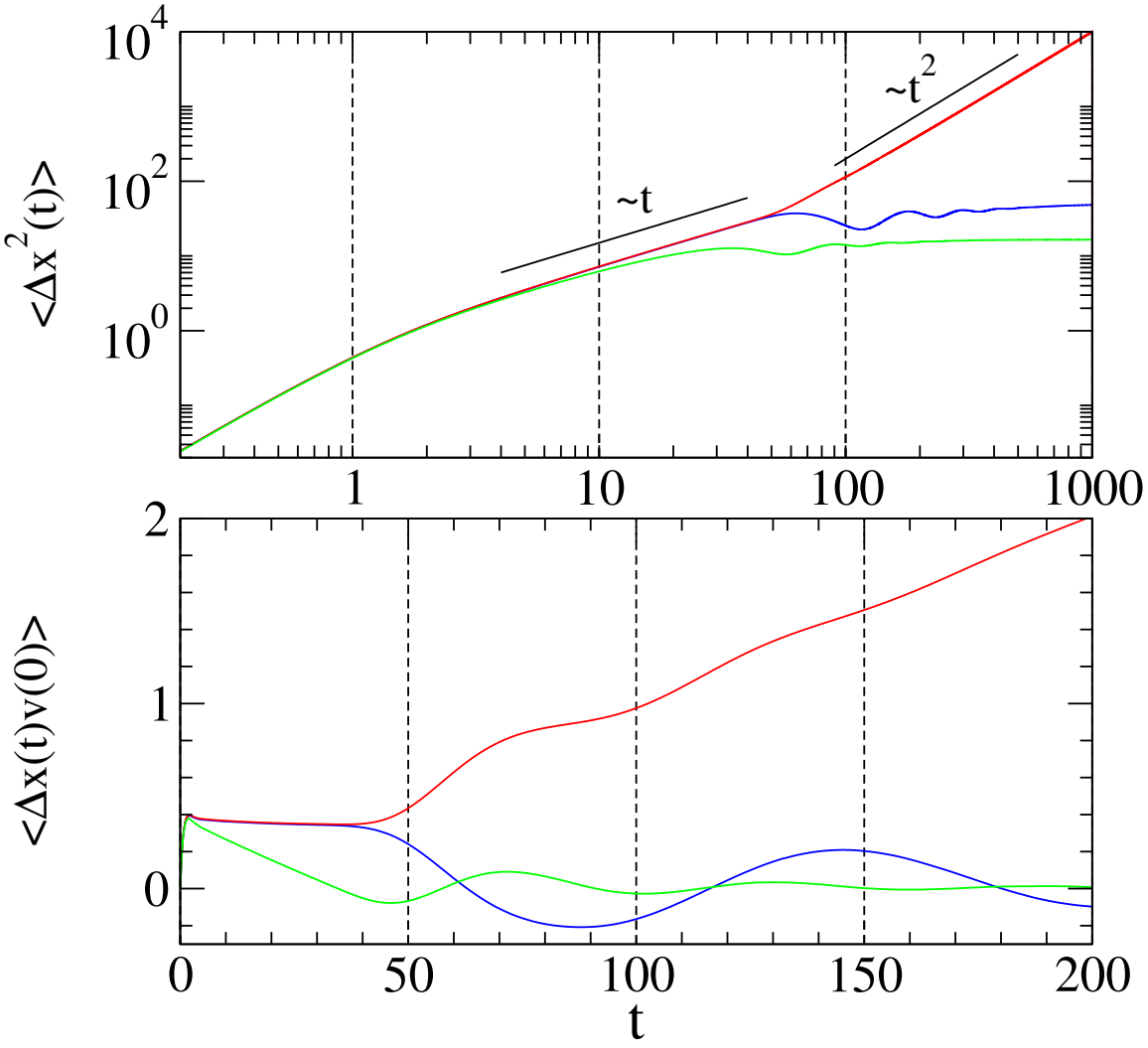

Figure 5.1: Hard particle gas of size $N = L = 100$ with masses of the alternate particles being 1.5 and 0.5. Here we plot the reflecting boundary case (blue) and the periodic boundary case (red) as well as the CoM velocity subtracted periodic boundary case (green). In all the cases $k_BT = 1$.

system. That is, the geometry is taken to be like that of a ring.

Even before beginning our analysis we can make some predictions based on our experience with the reflecting boundary case. In that case we found the period of the long time oscillations, determined by the sound speed, to be given by $2L/c_s$. This was the time it takes for the perturbation generated by the tagged particle fluctuations to propagate to one end, reflect from there, propagate to the other end, reflect back from there and reach the original position in original direction. In this case of periodic boundary we expect the period to be L/c_s, which is

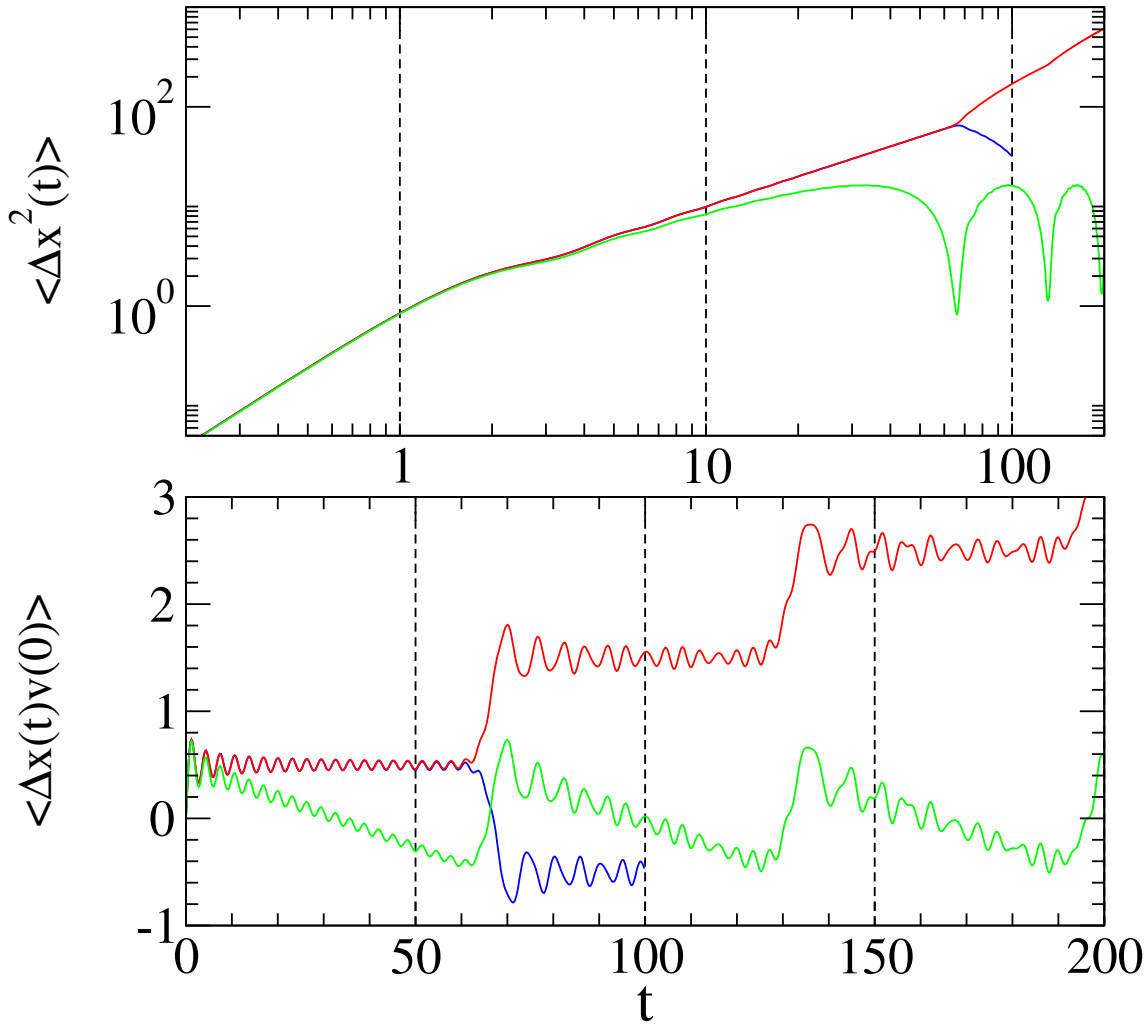

FIGURE 5.2: Harmonic chain of size $N = 65$ and density $\rho = 1$, all the particles are of mass 1. Here also we plot the reflecting boundary case (blue) and the periodic boundary case (red) as well as the CoM velocity subtracted periodic boundary case (green). In all the cases $k_BT = 1$.

the time it takes for the perturbation to propagate to one end, appear at the other end and reach the original position in original direction. Also, the trough of the oscillations in the reflecting boundary case, which appears at L/c_s, is caused by the backward propagating wave after being reflected from one of the ends. Here there are no reflected wave and the troughs would come only from the backaction of the other particles. Hence the amplitude of the oscillations may be expected to be considerably smaller. We also expect any non-zero centre of mass velocity (V_{cm}) in the initial distribution of velocity to persist for all times, in contrast to the reflecting boundary

case where it will average out to zero on reflecting from the walls. Such non-zero centre of mass velocity comes because even though we are choosing the velocities of the particles from a Boltzmann distribution centred around zero, due to finite number of selections fluctuations will always be there in V_{cm}. This non-zero centre of mass velocity is expected to impart an overall drift to the system and give a t^2 crossover for the tagged particle mean squared displacement in the long time. This will be in contrast to saturation seen in reflecting boundary cases.

We see all these features in the simulation plots of Fig. (5.1) for the alternate mass hard particle gas and of Fig. (5.2) for the harmonic chain. Here we plot the figures for reflecting and periodic boundaries as well as for periodic case with centre of mass velocity subtracted from the initial velocities of the particles in each of the realizations, i.e., a zero momentum ensemble. In these simulations k_BT is taken to be 1. Apart from the expected behaviour discussed above we see some surprising results as well. The tagged particle dynamics for the zero momentum ensemble doesn't remain diffusive in the short time. In fact the diffusion constant seems to decrease linearly with time. Such difference in the short time diffusive behaviour between a regular and a zero momentum ensemble can also be seen in simulations of particles interacting through square-shoulder potential [92] and also in study of heat conduction of hard particle gas [100]. Below we investigate these features analytically for a harmonic chain with periodic boundary conditions. Note that even though the equal mass hard particle gas does not support sound waves, it will still show some of the general features of periodic boundary conditions.

We consider a harmonic chain of N particles labeled $l = 1, \ldots, N$ in thermal equilibrium at temperature T, similar to the one studied in Chapter 3. The particles of equal masses m are connected by springs with stiffness constant k. Let $\{q_1, \ldots, q_N\}$ denote the displacements of the particles about their equilibrium positions. The equilibrium positions are assumed to be separated by a lattice spacing a so that the mass density is $\rho = m/a$. The Hamiltonian of the system is

$$H = \sum_{l=1}^{N} \frac{m}{2}\dot{q}_l^2 + \sum_{l=1}^{N+1} \frac{k}{2}(q_l - q_{l-1})^2 \ , \tag{5.1}$$

with corresponding equation of motion given as

$$m\ddot{q}_l = -k(2q_l - q_{l+1} - q_{l-1}), \qquad \forall\ l. \tag{5.2}$$

However, in contrast to fixed boundary case studied in Chapter 3, here we consider $q_{N+1} = q_1$.

We now transform to normal mode coordinates

$$q_l(t) = \sum_p a_p(t)\phi_p(l) \ . \tag{5.3}$$

The normal modes for periodic boundary conditions are given by

$$\phi_p(l) = \left[\frac{1}{mN}\right]^{1/2} \exp(ilpa) \ , \tag{5.4}$$

with $p = \frac{2n\pi}{Na}$, $n = 0, \ldots, N-1$. Normal mode transformation brings the Hamiltonian to the form

$$H = \sum_p \frac{\dot{a}_p^2}{2} + \sum_p \frac{\omega_p^2 a_p^2}{2} \ , \tag{5.5}$$

with $\omega_p^2 = 2k/m(1-\cos pa)$. The normal mode equations of motion are $\ddot{a}_p = -\omega_p^2 a_p$. These equations are easily solved and lead to the following expression:

$$q_l(t) = \sum_{p\neq 0} \phi_p(l) \left[a_p(0)\cos(\omega_p t) + \frac{\sin(\omega_p t)}{\omega_p}\dot{a}_p(0)\right] + \phi_0(l)\left[\dot{a}_0(0)t + a_0(0)\right] \ . \tag{5.6}$$

Defining $\Delta q_l(t) = q_l(t) - q_l(0)$,

$$\Delta q_l(t) = \sum_{p\neq 0} \phi_p(l) \left[a_p(0)(\cos(\omega_p t) - 1) + \frac{\sin(\omega_p t)}{\omega_p}\dot{a}_p(0)\right] + \phi_0(l)\left[\dot{a}_0(0)t\right] \ . \tag{5.7}$$

Since the chain is in thermal equilibrium at temperature T, $\langle \dot{a}_p^2(0)\rangle = \omega_p^2\langle a_p^2(0)\rangle = k_B T$ and $\langle \dot{a}_p(0)a_p(0)\rangle = 0$.

$$\left\langle \Delta q_l^2(t)\right\rangle = 4k_B T \sum_{p\neq 0} \phi_p^2(l)\frac{\sin^2(\omega_p t/2)}{\omega_p^2} + k_B T \ \phi_0^2(l) \ t^2 \ . \tag{5.8}$$

For the middle tagged particle, we have

$$\langle [\Delta q(t)]^2\rangle = \frac{8k_B T}{mN} \sum_{n=1,\ldots,\frac{N-1}{2}} \frac{\sin^2(\omega_p t/2)}{\omega_p^2} \ + \ \frac{k_B T}{mN} \ t^2 \ . \tag{5.9}$$

The CoM velocity can be obtained as,

$$V_{cm} = \frac{1}{N}\sum_{l=1\ldots N} \dot{q}_l(0) = \frac{1}{N}\sum_{l=1\ldots N}\left[\sum_{p\neq 0} \phi_p(l) \ \dot{a}_p(0) + \phi_0(l)\dot{a}_0(0)\right] = \frac{\dot{a}_0(0)}{\sqrt{mN}}$$

$$\Rightarrow \quad \langle V_{cm}^2\rangle = \frac{k_B T}{mN}. \tag{5.10}$$

Thus, we see that the zeroeth mode contributes for the centre of mass velocity and that the mean squared displacement of the tagged particle can be written as

$$\langle [\Delta q(t)]^2 \rangle = \frac{8k_BT}{mN} \sum_{n=1,\ldots,\frac{N-1}{2}} \frac{\sin^2(\omega_p t/2)}{\omega_p^2} \; + \; \langle V_{cm}^2 \rangle \; t^2. \tag{5.11}$$

The correlations $\langle \Delta q(t) v(0) \rangle$ and $\langle v(t) v(0) \rangle$ can be found by differentiating this expression, as in Eqs.(1.10). Evaluating the above equation numerically, we see that plotting just the first term produces the curve corresponding to centre of mass velocity subtracted periodic boundary case (green), while plotting the complete expression produces the curve corresponding to the periodic boundary case (red) of Fig. (5.2). Notice that in the limit $N \to \infty$, Eq. (5.11) goes to Eq. (3.6); the $1/N$ term in this centre of mass velocity makes it go to zero as $N \to \infty$. However, for a general N, both the first term, which corresponds to the mean squared displacement of the tagged particle in the zero momentum ensemble, and the second centre of mass velocity term remains. This is interesting because this not only shows that the expected and observed long time diffusive to ballistic crossover is caused by the centre of mass velocity (zero mode) but also that it is important for the short time normal diffusion. It is also surprising because it implies that the tagged particle's dynamics in the zero momentum ensemble depends on the system size even at short times, which is contrary to the other two cases where the tagged particle correlations are independent of the system size till boundary effect is seen.

5.3 Special cases of the hard particle gas

In Chapter 2 we studied the equal and alternate mass cases of the hard particle gas exclusively. To check for the robustness of our results as a function of mass configurations, here we study some more cases. In particular, we study the random mass case and also the mass ratio dependence of the alternate mass gas, with emphasis on mass ratio $\to 1$.

5.3.1 Random mass hard particle gas

We simulate a gas of hard point particles with random distribution of masses. Each particle is assigned a mass from a uniform distribution between 0.5 and 1.5. We look at tagged-particle

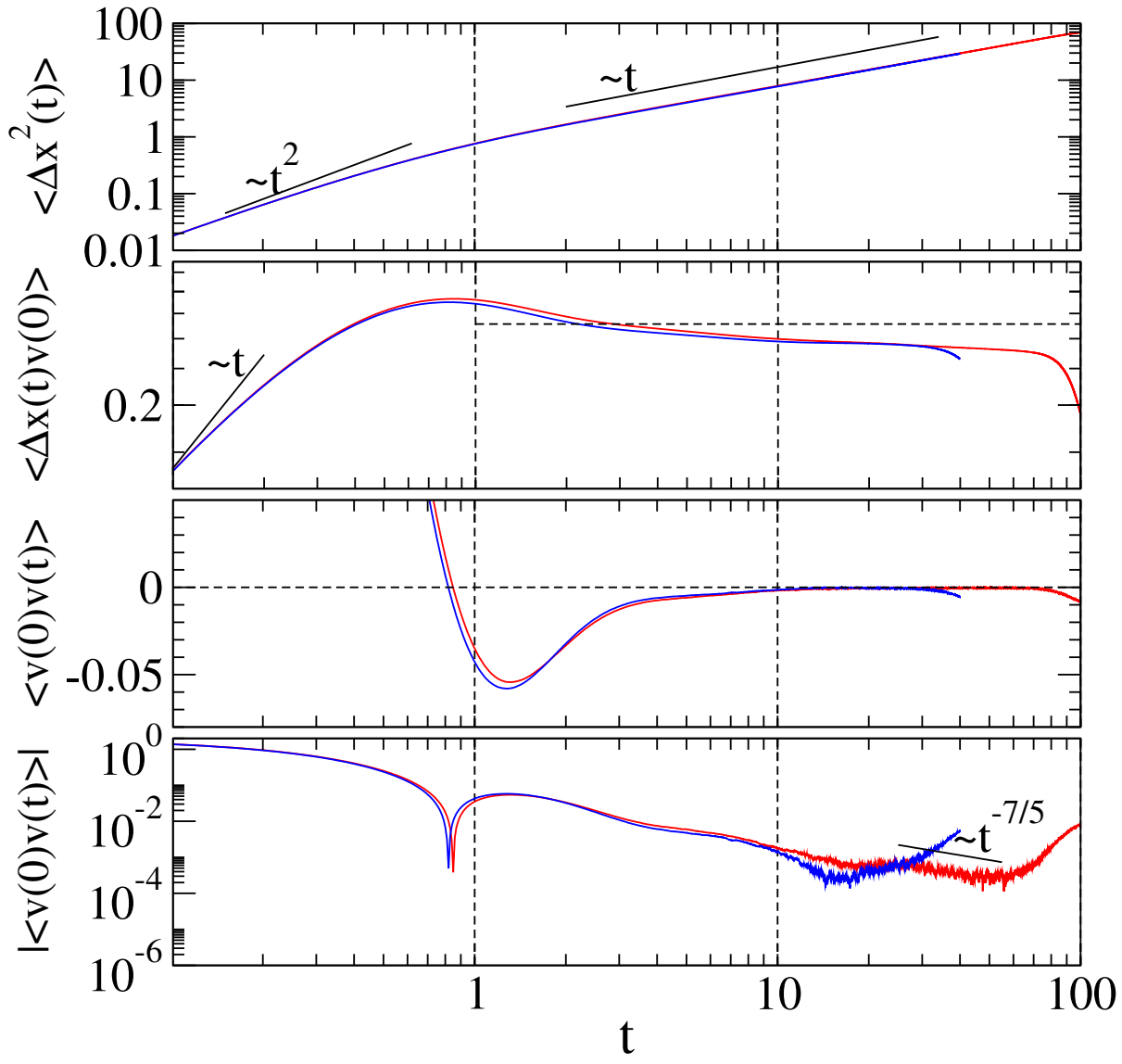

FIGURE 5.3: Various correlation functions (in the short-time regime) for random mass hard particle gas with N = 101 (blue) and N = 201 (red) particles and density $\rho = 1$. The mass of the middle particle is always 0.5 and the results are an average over 32 different random mass realizations. In all the cases $k_B T = 1$ and reflecting boundary conditions are used.

correlations of the central particle whose mass is fixed at 0.5. The correlations fluctuate between different mass realizations and we take an average over 32 realizations. The results are plotted in Fig. (5.3) where we see the same qualitative features as for the alternate mass case. Thus we conclude that the random mass hard particle gas shows normal-diffusion for the tagged particle.

5.3.2 Mass ratio dependence of the alternate mass hard particle gas

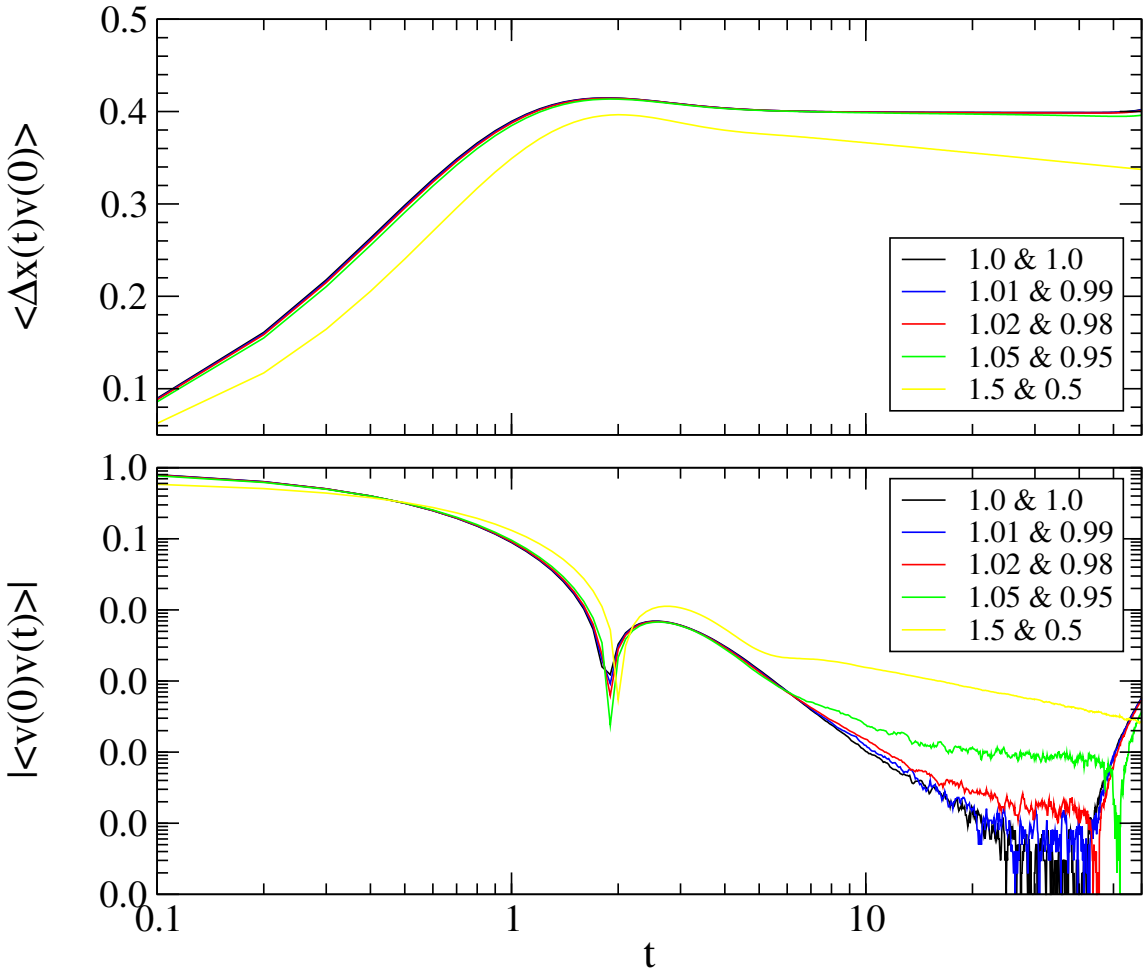

Figure 5.4: Mass ratio dependence (in the short-time regime) in alternate mass hard particle gas. The figure is for small mass ratios in the gas of size N=L=200. In all the cases $k_BT = 1$ and periodic boundary conditions are used.

Next, we perform simulations for various mass ratios of the alternate masses in the hard particle gas. In particular, we are interested in the transition from $1/t^3 \to 1/t^{7/5}$ as the mass ratio is increased from 1. It was demonstrated in [81] that any mass ratio $\neq 1$ is ergodic, in the sense that, starting with an arbitrary distribution for the velocities, it reaches a Maxwellian distribution. However they could not study the transition due to limited statistics [82]. In Fig. (5.4) we plot the results for various mass ratios and observe the transition. Note that even though the transition seems gradual, we expect to see a $\sim 1/t^{7/5}$ decay in the long time regime, for any

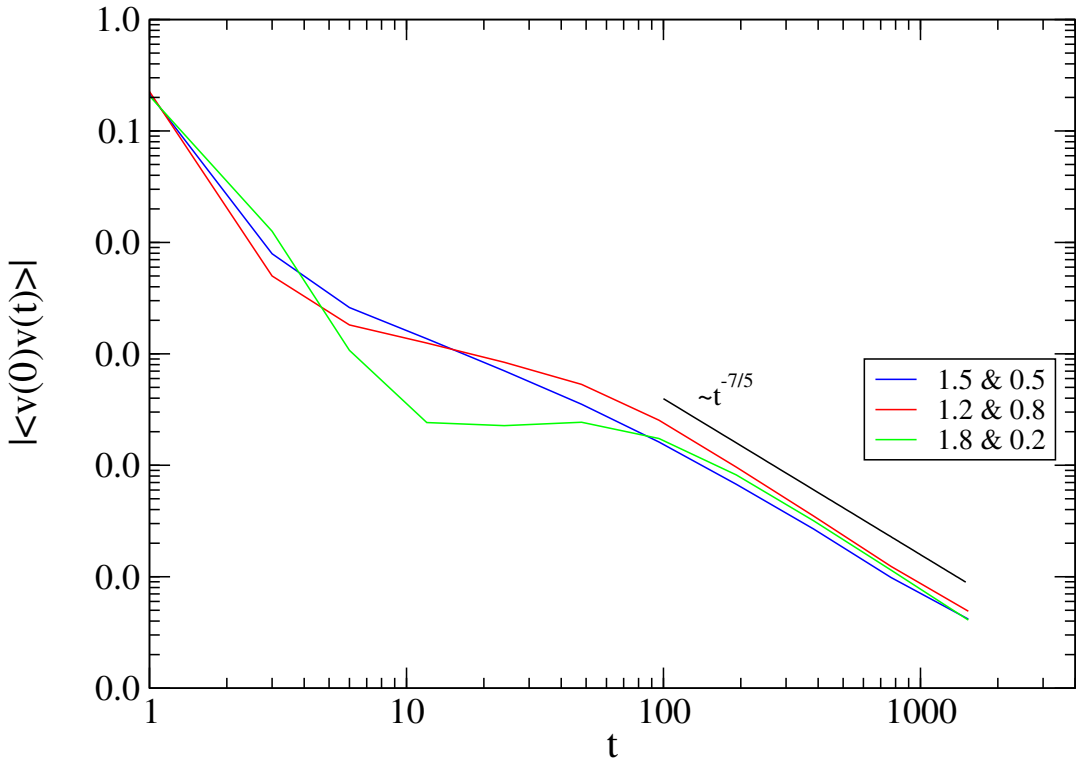

FIGURE 5.5: Mass ratio dependence (in the short-time regime) in alternate mass hard particle gas. The figure is for intermediate mass ratios in the gas of size N=L=8000. In all the cases $k_BT = 1$ and periodic boundary conditions are used.

mass ratio $\neq 1$. This expectation is borne out in Fig. (5.5) where we see plots of three different mass ratios converging to $\sim 1/t^{7/5}$ in the long time.

5.4 Dynamics of a heavy particle in a 1-dimensional gas of light equal mass particles

The problem of one heavy hard particle in the middle of a large number of lighter hard particles of equal masses, separating the system into two halves, is a long studied problem and has been studied extensively in $3-, 2-$ and $1-$dimensions [104–120]. It goes by the name of Rayleigh piston or the adiabatic piston problem and has evoked lots of interests and controversies.

Another interesting feature of this system is that, in equilibrium, the velocity of the heavy tagged particle has been shown to follow an Ornstein-Uhlenbeck process at short times [101],

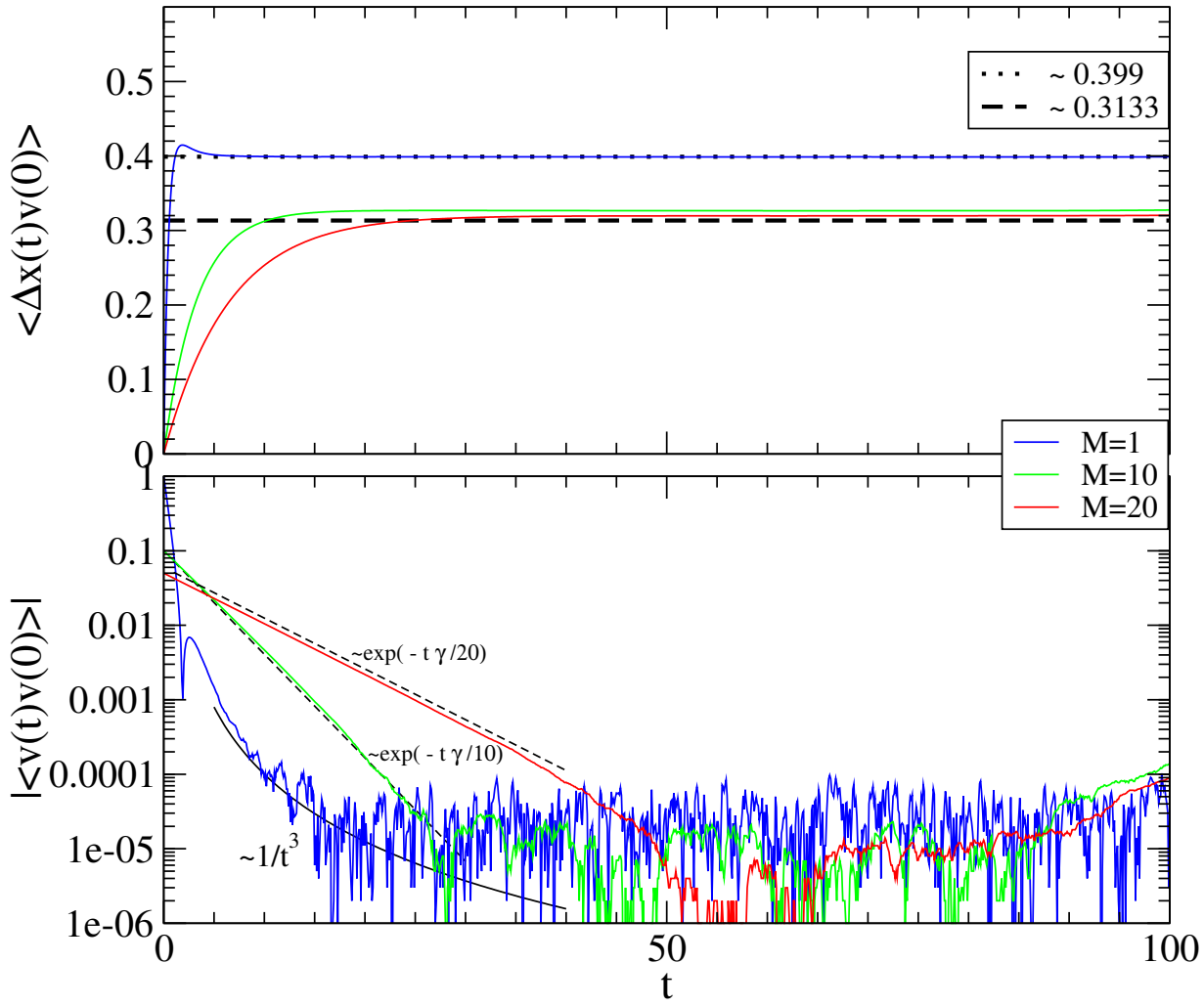

Figure 5.6: Short time behaviour of a 1-D hard particle gas with one heavy particle of mass $M = 10$ (green) and $M = 20$ (red) respectively, in the middle of light equal mass particles of mass $m = 1$, as compared to the equal mass hard particle gas (blue). Here $\gamma = 3.19$ (see main text). $N = L = 400, k_B T = 1$ and periodic boundary conditions are used.

i.e., the tagged particle dynamics at short times is not only normal-diffusive, but its velocity auto-correlation function is also exponentially decaying. It was shown that, the diffusion constant of the tagged particle of mass M in an ideal gas of hard particles of mass $m = 1$ and density unity, is bound between $(\pi/32)^{1/2} < D < (1/2\pi)^{1/2}$ [121, 122], where the upper bound of $(1/2\pi)^{1/2} \approx 0.399$ is for $M = 1$ and the lower bound of $(\pi/32)^{1/2} \approx 0.313$ is for $M = \infty$. In Fig. (5.6) we demonstrate this through simulations, for the hard particle system described above. Note that in the figure $\gamma = k_B T/D \approx 1/0.313 \approx 3.19$. Also note the convergence of D to the

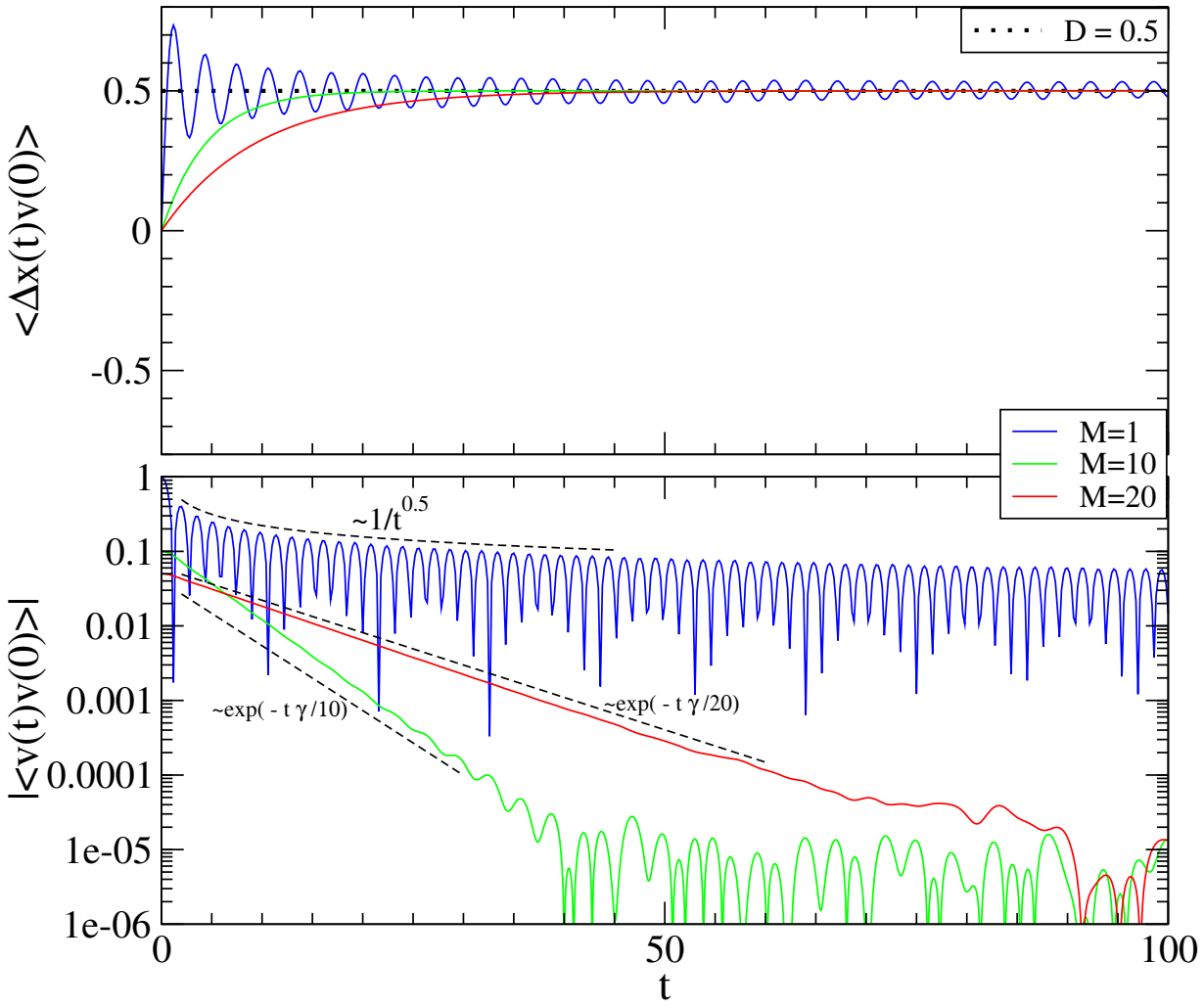

FIGURE 5.7: Short time behaviour of a 1-D harmonic chain with one heavy particle of mass 10 (green) and $M = 20$ (red) respectively, in the middle of light equal mass particles of mass $m = 1$, as compared to that of the regular equal mass harmonic chain (blue). Here $\gamma = 2$ (see main text). $N = L = 129, k_B T = 1$ and periodic boundary conditions are used.

expected lower bound as M increases.

In fact such a result of velocity of the tagged particle being Ornstein-Uhlenbeck process exists even for a heavy particle in a harmonic chain of light equal mass particles [102, 103]. It was shown that, in the heavy mass limit, the velocity auto-correlation function decays as $C(t) \approx exp(-mt/Mt_0)$, where $1/t_0 = \sqrt{4K/m}$. In our simulations, where $K = 1$ and $m = 1$, we have $1/t_0 = 2 \Rightarrow \gamma = m/t_0 = 2$. We demonstrate this in Fig. (5.7) through simulations on such a harmonic system. Here also, we see convergence to the expected behaviour as M increases.

It is interesting, that none of the other Hamiltonian systems we studied till this point in the thesis showed the Langevin diffusion, but the case of one heavy particle seems to generically show it. In fact, we have tested this to be true in all other anharmonic chains as well (figures not shown). This points to the fact that the Langevin description assumes separation of time scales between the tagged and the fluid molecules, for which their masses need to be significantly different. This can be seen as the difference between self and Brownian diffusion.

5.5 Widely separated heavy particles : Transition to single-file diffusion ?

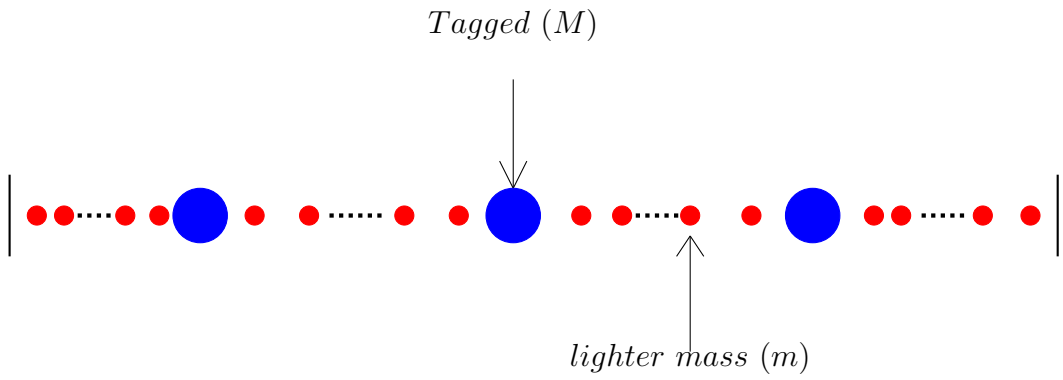

Figure 5.8: Schematic diagram of an arrangement where many heavy particles of mass M are placed in a sea of lighter particles of equal masses m.

In all the Hamiltonian systems studied throughout this thesis we saw that the tagged-particle diffusion is generically normal-diffusive. This is in striking contrast to the stochastic systems like interacting Brownian walkers or the symmetric exclusion process, where the tagged particle mean squared displacement is shown to demonstrate single-file diffusion scaling, i.e. $\langle \Delta x^2(t) \rangle \sim \sqrt{t}$. However, stochastic systems are supposed to be coarse grained description of real classical systems which are ultimately deterministic. This suggests that we should get the single-file diffusion scaling even from deterministic systems. In this section we study this problem for the hard particle gas.

In the previous section we saw that the motion of a heavy particle in the middle of a system of light equal mass particles shows normal-diffusion and its velocity is well approximated by an

Ornstein-Uhlenbeck process. What happens when we have many such heavy particles in a sea of smaller particles [Fig. (5.8)]? This should be equivalent to the picture of Brownian walkers interacting with each other and should give the transition to single-file diffusion. In Fig. (5.9) we present the simulation results for such a hard particle gas. Note that the heavy particles are placed far enough so that it reaches the normal-diffusive regime before seeing other heavy particles. We study various values of the heavy mass and various separations between the heavy masses but don't find the single-file diffusion scaling. In fact, as can be seen from the plot of $\langle \Delta x(t) v(0) \rangle$, it has the functional form of the alternate mass hard particle gas; i.e., we still find normal-diffusion for the tagged particle.

Our failure to see single-file diffusion scaling even in this set-up lends itself to some important questions. Firstly, what is the requirement for obtaining the sub-diffusive scaling? Is it momentum conservation, will breaking it lead to SFD scaling? Another important question is whether such normal-diffusion can be seen in experimental setup. We note that historically there have been reports of normal-diffusion in 1-dimensional atomistic and zeolitic systems [43, 45]. These findings were however rejected citing particle crossings, which are difficult to avoid in such systems, to be the reason. Success of various stochastic models encouraged even experimentalists to concentrate on demonstrating single-file diffusion scaling. Our work may motivate experimentalists to design experiments which may observe these findings.

5.6 Discussions and conclusions

In this chapter we studied some special cases of the various Hamiltonian systems that we studied in the preceding chapters. Our main aim has been to further explore the robustness of normal-diffusion in classical Hamiltonian systems. We found that it persisted under various mass configurations. It also persisted for different boundary conditions. However, we also found the surprising deviation from this normal-diffusion for the zero momentum ensemble, which seems to be a generic feature. Further, we made the interesting observation about the generic nature of the Ornstein-Uhlenbeck diffusive behaviour for a heavy particle in the bath of lighter particles.

We also explored the possibility of observing the single-file diffusion scaling in Hamiltonian system. However, we failed to obtain it even in a system where one would naively expect it to be

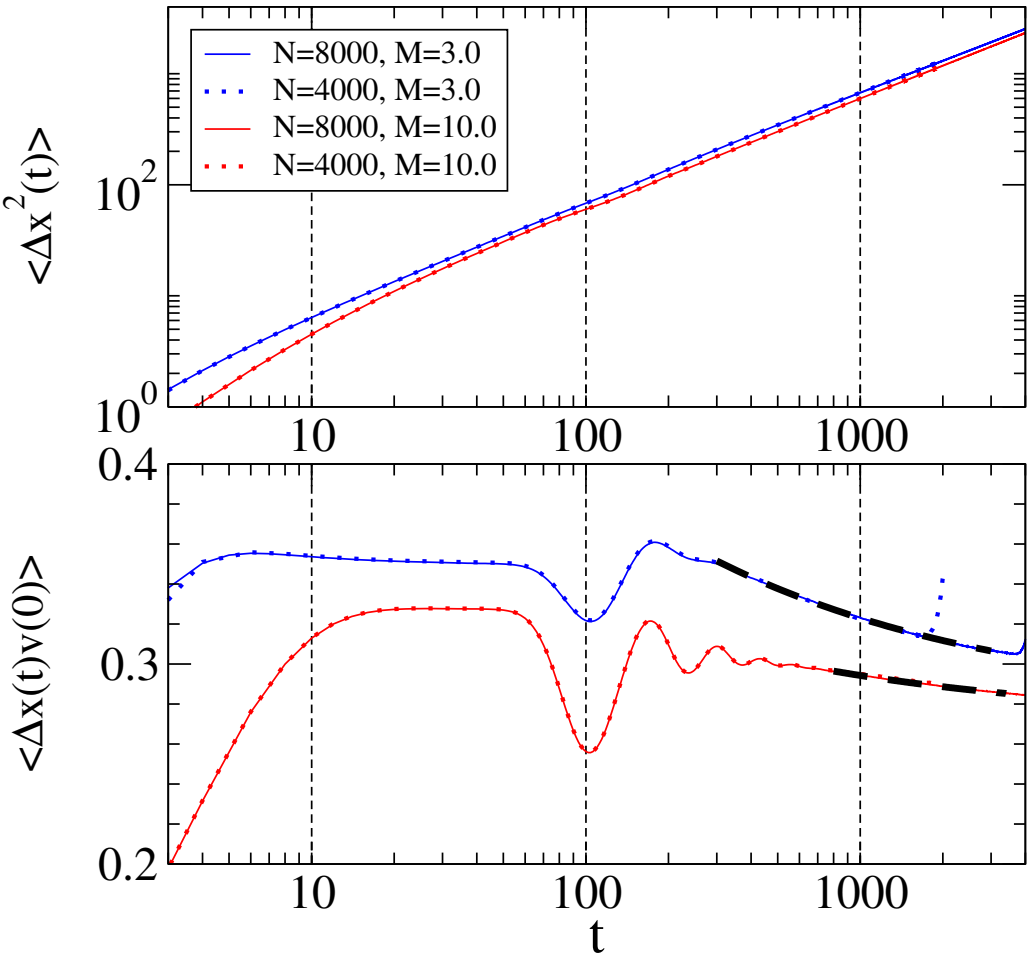

Figure 5.9: Search for Single-File Diffusion : Short time behaviour of a 1-D hard particle gas with heavy particles of mass $M = 3$ (blue) and $M = 10$ (red) respectively, placed among light equal mass particles of mass $m = 1$. The heavy particles are placed equidistant, with a spacing of 100 light particles in-between them for all the cases shown here. Note that the heavy tagged particle reaches normal-diffusion, as can be seen in the lower panel of the graph, before seeing the effect of others. After that $\langle \Delta x(t) v(0) \rangle$ approaches the functional form of the alternate mass hard particle gas, viz. $a + b\, x^{-2/5}$ (black dashed lines) with $a = 0.2767, b = 0.733$ for $M = 3.0$ and $a = 0.271, b = 0.369$ for $M = 10.0$. Two systems sizes are $N = L = 4000$ (dotted) and $N = L = 8000$ (solid), where we are counting both the species. In all the cases we have $k_B T = 1$ and use periodic boundary conditions.

seen. We saw that the tagged particle diffusion still remains normal. The problem of finding the diffusion constant in this case, however, remains an open theoretical problem. We then suggested further ways of exploring it, to see the transition from normal to sub-diffusion in these systems, both through computer and laboratory experiments.

Our studies indicate that one will get normal diffusion as long as the conservation laws (of

energy, momentum) are maintained, irrespective of whether the dynamics is Hamiltonian or stochastic. Indeed our results in Sec. 4.2 for the effective harmonic model shows that stochastic dynamics with the correct conservation laws leads to normal diffusion. On the other hand we know that for interacting Brownian particles (where momentum is not conserved) one gets subdiffusive tagged particle motion.

6

Conclusions

The main results of this thesis are summarised in the following table:

Equal mass hard particle gas	**Short times:** Normal-diffusion, $D = a\sqrt{k_B T/2m\pi}$, $\langle v(0)v(t)\rangle \sim -1/t^3$; **Long times:** $\langle \Delta x^2(t)\rangle$ saturates, no oscillations.
Alternate mass hard particle gas	**Short times:** Normal-diffusion, $D = k_B T/2\rho_m c$, $\langle v(0)v(t)\rangle \sim -1/t^{7/5}$; **Long times:** $\langle \Delta x^2(t)\rangle$ saturates after oscillations, starting time and period of oscillations $\sim L/c$.

Harmonic chain	**Short times:** Normal-diffusion, $D = k_B T/2\rho_m c$, $\langle v(0)v(t)\rangle \sim \sin(\omega_0 t)/\sqrt{t}$; **Long times:** $\langle \Delta x^2(t)\rangle$ keeps oscillating, starting time and period of oscillations $\sim L/c$.
Fermi-Pasta-Ulam chain	**Short times:** Normal-diffusion, $D = k_B T/2\rho_m c, \langle v(0)v(t)\rangle \sim \sin(2ct/a)\exp(-\gamma t/m)$; **Long times:** $\langle \Delta x^2(t)\rangle$ shows damped oscillations, starting time and period of oscillations $\sim L/c$.
Lennard-Jones chain	**Short times:** Normal-diffusion, $D = k_B T/2\rho_m c, \langle v(0)v(t)\rangle \sim \sin(2ct/a)\exp(-\gamma t/m)$; **Long times:** $\langle \Delta x^2(t)\rangle$ shows damped oscillations, starting time and period of oscillations $\sim L/c$.
Heavy tagged particle in hard particle gas	**Short times:** Normal-diffusion, $(\pi/32)^{1/2} < D < (1/2\pi)^{1/2}$, Langevin decay of $\langle v(0)v(t)\rangle \sim \exp(-\gamma t/M)$.
Heavy tagged particle in harmonic chain	**Short times:** Normal-diffusion, $D = k_B T/\gamma$, Langevin decay of $\langle v(0)v(t)\rangle \sim \exp(-\gamma t/M)$.
Widely separated heavy hard particles	**Short times:** Normal-diffusion, $D = k_B T/2\rho_m c$?, $\langle v(0)v(t)\rangle \sim -1/t^{7/5}$.

References

[1] "De rerum natura", under the title "The Nature of Things", translated by A. E. Stallings. Penguin Books, 2007.

[2] Ingenhousz, Jan. "Vermischte schriften physisch medicinischen inhalts." Wappler, Vienna, vol. 2, pp. 123-126, 1784.

[3] Brown, Robert. "XXVII. A brief account of microscopical observations made in the months of June, July and August 1827, on the particles contained in the pollen of plants; and on the general existence of active molecules in organic and inorganic bodies." The Philosophical Magazine, or Annals of Chemistry, Mathematics, Astronomy, Natural History and General Science 4.21 (1828): 161-173.

[4] Einstein, Albert. "On the movement of small particles suspended in stationary liquids required by the molecular-kinetic theory of heat." Annalen der Physik 17.549-560 (1905): 16.

[5] Einstein, Albert. "Zur theorie der brownschen bewegung." Annalen der physik 324.2 (1906): 371-381.

[6] Von Smoluchowski, Marian. "Zur kinetischen theorie der brownschen molekularbewegung und der suspensionen." Annalen der physik 326.14 (1906): 756-780.

[7] Chandrasekhar, Subrahmanyan. "Stochastic problems in physics and astronomy." Reviews of modern physics 15.1 (1943): 1.

[8] L. Onsager, "Reciprocal relations in irreversible processes, 1.," Phys. Rev. 37, 405426 (1931).

[9] H. B. Callen and T. A. Welton, "Irreversibility and generalized noise," Phys. Rev. 83, 3440 (1951).

[10] M. S. Green, "Markov random processes and the statistical mechanics of time-dependent phenomena," J. Chem. Phys. 20, 12811295 (1952).

[11] M. S. Green, "Markov random processes and the statistical mechanics of timedependent phenomena, 2., Irreversible processes in fluids," J. Chem. Phys. 22, 398413 (1954).

[12] R. Kubo, "Statistical-Mechanical Theory of Irreversible Processes, 1., General Theory and Simple Applications to Magnetic and Conduction Problems," J. Phys. Soc. Japan 12, 570586 (1957).

[13] R. Kubo, "Fluctuation-dissipation theorem," Rep. Prog. Phys. 29, 255284 (1966).

[14] R. Kubo, "Brownian motion and nonequilibrium statistical mechanics," Science 233, 330334 (1986).

[15] W. Sutherland, "A dynamical theory of diffusion for non-electrolytes and the molecular mass of albumin," Phil. Mag. (6-th Series) 9, 781785 (1905).

[16] A. Pais, "Subtle is the Lord....The Science and the Life of Albert Einstein," (Oxford Univ. Press, Oxford and New York, 1982), p. 92.

[17] Hänggi, Peter, and Fabio Marchesoni. "100 years of Brownian motion." arXiv preprint cond-mat/0502053 (2005).

[18] A. Einstein, "Elementare Theorie der Brownschen Bewegung," Z. f. Elektrochemie 14, 235239 (1908).

[19] N. Wiener, "The average of an analytic functional and the Brownian movement," Proc. Natl. Acad. Sci. USA 7, 294298 (1921).

[20] N. Wiener, "Differential Space," J. Mathematical and Physical Sci. 2, 131174 (1923).

[21] J. B. Perrin, "Mouvement brownien et réalité moléculaire," Ann. de Chimie et de Physique (VIII) 18, 5114(1909).

[22] J. Perrin, "Atoms," translated by D. Ll. Hammick (London: Constable), and reprinted by (Ox Bow Press, Woodbridge, 1990).

[23] Langevin, Paul. "Sur la thorie du mouvement brownien." CR Acad. Sci. Paris 146.530-533 (1908).

[24] Hellriegel, Christian, et al. "Diffusion of single streptocyanine molecules in the nanoporous network of sol-gel glasses." The Journal of Physical Chemistry B 108.38 (2004): 14699-14709.

[25] Schmidt, Th, et al. "Imaging of single molecule diffusion." Proceedings of the National Academy of Sciences 93.7 (1996): 2926-2929.

[26] Machán, Radek, and Martin Hof. "Lipid diffusion in planar membranes investigated by fluorescence correlation spectroscopy." Biochimica et Biophysica Acta (BBA)-Biomembranes 1798.7 (2010): 1377-1391.

[27] Wachsmuth, Malte, Waldemar Waldeck, and Joérg Langowski. "Anomalous diffusion of fluorescent probes inside living cell nuclei investigated by spatially-resolved fluorescence correlation spectroscopy." Journal of molecular biology 298.4 (2000): 677-689.

[28] Banks, Daniel S., and Cécile Fradin. "Anomalous diffusion of proteins due to molecular crowding." Biophysical journal 89.5 (2005): 2960-2971.

[29] Upadhyaya, Arpita, et al. "Anomalous diffusion and non-Gaussian velocity distribution of Hydra cells in cellular aggregates." Physica A: Statistical Mechanics and its Applications 293.3 (2001): 549-558.

[30] Joo, Chirlmin, et al. "Advances in single-molecule fluorescence methods for molecular biology." Annu. Rev. Biochem. 77 (2008): 51-76.

[31] Moerner, W. E., and David P. Fromm. "Methods of single-molecule fluorescence spectroscopy and microscopy." Review of Scientific Instruments 74.8 (2003): 3597-3619.

[32] Bouchaud, Jean-Philippe, and Antoine Georges. "Anomalous diffusion in disordered media: statistical mechanisms, models and physical applications." Physics reports 195.4 (1990): 127-293.

[33] Metzler, Ralf, and Joseph Klafter. "The random walk's guide to anomalous diffusion: a fractional dynamics approach." Physics reports 339.1 (2000): 1-77.

[34] Nägle, Gerhard. "On the dynamics and structure of charge-stabilized suspensions." Physics Reports 272.5 (1996): 215-372.

[35] Hodgkin, A. L., and R. D. Keynes. "Active transport of cations in giant axons from Sepia and Loligo." The Journal of physiology 128.1 (1955): 28-60.

[36] Lea, E. J. A. "Permeation through long narrow pores." Journal of theoretical biology 5.1 (1963): 102-107.

[37] Rickert, Hans. "Zur Diffusion durch eine lineare Kette (Single-File-Diffusion)." Zeitschrift für Physikalische Chemie 43.3 (1964): 129-139.

[38] Levitt, David G. "A new theory of transport for cell membrane pores. I. General theory and application to red cell." Biochimica et Biophysica Acta (BBA)-Biomembranes 373.1 (1974): 115-131.

[39] Rosenberg, Paul A., and A. L. A. N. Finkelstein. "Water permeability of gramicidin A-treated lipid bilayer membranes." The Journal of general physiology 72.3 (1978): 341-350.

[40] Hernandez, J. A., and Jorge Fischbarg. "Kinetic analysis of water transport through a single-file pore." The Journal of general physiology 99.4 (1992): 645-662.

[41] Hahn, Kärger, J. Kärger, and V. Kukla. "Single-file diffusion observation." Physical review letters 76.15 (1996): 2762.

[42] Kukla, Volker, et al. "NMR studies of single-file diffusion in unidimensional channel zeolites." Science 272.5262 (1996): 702-704.

[43] Hahn, K., and J. Kärger. "Deviations from the normal time regime of single-file diffusion." The Journal of Physical Chemistry B 102.30 (1998): 5766-5771.

[44] Sholl, David S., and Kristen A. Fichthorn. "Concerted diffusion of molecular clusters in a molecular sieve." Physical review letters 79.19 (1997): 3569.

[45] Jobic, Hervé, et al. "Unidirectional and single-file diffusion of molecules in one-dimensional channel systems. A quasi-elastic neutron scattering study." The Journal of Physical Chemistry B 101.30 (1997): 5834-5841.

[46] Wei, Q-H., Clemens Bechinger, and Paul Leiderer. "Single-file diffusion of colloids in one-dimensional channels." Science 287.5453 (2000): 625-627.

[47] Lutz, Christoph, Markus Kollmann, and Clemens Bechinger. "Single-file diffusion of colloids in one-dimensional channels." Physical review letters 93.2 (2004): 026001.

[48] Lin, Binhua, et al. "From random walk to single-file diffusion." Physical review letters 94.21 (2005): 216001.

[49] Das, Anindya, et al. "Single-file diffusion of confined water inside SWNTs: an NMR study." ACS nano 4.3 (2010): 1687-1695.

[50] Harris, T. E. "Diffusion with "collisions" between particles." Journal of Applied Probability 2.2 (1965): 323-338.

[51] Levitt, David G. "Dynamics of a single-file pore: non-Fickian behavior." Physical Review A 8.6 (1973): 3050.

[52] Richards, Peter M. "Theory of one-dimensional hopping conductivity and diffusion." Physical Review B 16.4 (1977): 1393.

[53] Fedders, Peter A. "Two-point correlation functions for a distinguishable particle hopping on a uniform one-dimensional chain." Physical Review B 17.1 (1978): 40.

[54] van Beijeren, Henk, K. W. Kehr, and R. Kutner. "Diffusion in concentrated lattice gases. III. Tracer diffusion on a one-dimensional lattice." Physical Review B 28.10 (1983): 5711.

[55] Arratia, Richard. "The motion of a tagged particle in the simple symmetric exclusion system on Z." The Annals of Probability (1983): 362-373.

[56] Alexander, S., and P. Pincus. "Diffusion of labeled particles on one-dimensional chains." Physical Review B 18.4 (1978): 2011.

[57] Kollmann, Markus. "Single-file diffusion of atomic and colloidal systems: Asymptotic laws." Physical review letters 90.18 (2003): 180602.

[58] Hemmer, P. Chr., "Dynamic and Stochastic Types of Motion in the Linear Chain." Thesis, Trondheim (1959).

[59] Turner, R. E. "Motion of a heavy particle in a one dimensional chain." Physica 26.4 (1960): 269-273.

[60] Mazur, Peter, and Elliott Montroll. "Poincar cycles, ergodicity, and irreversibility in assemblies of coupled harmonic oscillators." Journal of mathematical physics 1.1 (1960): 70-84.

[61] Ullersma, P. "An exactly solvable model for Brownian motion: I. Derivation of the Langevin equation." Physica 32.1 (1966): 27-55.

[62] Jepsen, D. W. "Dynamics of a Simple ManyBody System of Hard Rods." Journal of Mathematical Physics 6.3 (1965): 405-413.

[63] Lebowitz, J. L., and J. K. Percus. "Kinetic equations and density expansions: Exactly solvable one-dimensional system." Physical Review 155.1 (1967): 122.

[64] Lebowitz, J. L., J. K. Percus, and J. Sykes. "Time evolution of the total distribution function of a one-dimensional system of hard rods." Physical Review 171.1 (1968): 224.

[65] Lebowitz, J. L., and J. Sykes. "The velocity autocorrelation function of a finite model system." Journal of Statistical Physics 6.2-3 (1972): 157-171.

[66] Evans, J. W. "Velocity correlation functions for finite one-dimensional systems." Physica A: Statistical Mechanics and its Applications 95.2 (1979): 225-251.

[67] Kasperkovitz, P., and J. Reisenberger. "Finite hard-rod systems and their thermodynamic limit: Survey of methods and results." Physical Review A 31.4 (1985): 2639.

[68] Alder, B. J., and T. E. Wainwright. "Velocity autocorrelations for hard spheres." Physical review letters 18.23 (1967): 988.

[69] Alder, B. J., and T. E. Wainwright. J. Phys. SOC. Japan. Suppl. 1968 (1968): 26-267.

[70] Alder, B. J., and T. E. Wainwright. "Decay of the velocity autocorrelation function." Physical review A 1.1 (1970): 18.

[71] Van Beijeren, H. "Fluctuations in the motions of mass and of patterns in one-dimensional driven diffusive systems." Journal of statistical physics 63.1-2 (1991): 47-58.

[72] Kärger, Jörg. "Straightforward derivation of the long-time limit of the mean-square displacement in one-dimensional diffusion." Physical Review A 45.6 (1992): 4173.

[73] Kärger, Jörg. "Long-time limit of the self-correlation-function of one-dimensional diffusion." Physical Review E 47.2 (1993): 1427.

[74] Hahn, K., and J. Kärger. "Propagator and mean-square displacement in single-file systems." Journal of Physics A: Mathematical and General 28.11 (1995): 3061.

[75] Rödenbeck, Christian, Jörg Kärger, and Karsten Hahn. "Calculating exact propagators in single-file systems via the reflection principle." Physical Review E 57.4 (1998): 4382.

[76] Gupta, Shamik, et al. "Tagged particle correlations in the asymmetric simple exclusion process: Finite-size effects." Physical Review E 76.2 (2007): 021112.

[77] Lizana, Ludvig, and Tobias Ambjörnsson. "Single-file diffusion in a box." Physical review letters 100.20 (2008): 200601.

[78] Lizana, Ludvig, and Tobias Ambjörnsson. "Diffusion of finite-sized hard-core interacting particles in a one-dimensional box: Tagged particle dynamics." Physical Review E 80.5 (2009): 051103.

[79] Barkai, E., and R. Silbey. "Theory of single file diffusion in a force field." Physical review letters 102.5 (2009): 050602.

[80] Barkai, E., and R. Silbey. "Diffusion of tagged particle in an exclusion process." Physical Review E 81.4 (2010): 041129.

[81] Marro, Joaqun, and Masoliver, Jaume. "Kinetics of a finite one-dimensional mixture of hard rods with different masses." Journal of Statistical Physics 31.3 (1983): 565-575.

[82] Marro, Joaqun, and Masoliver, Jaume. "Long-time tails in the velocity autocorrelation function of hard-rod binary mixtures." Physical review letters 54.8 (1985): 731.

[83] Percus, J. K. "On Tagged Particle Dynamics in Highly Confined Fluids." Journal of Statistical Physics 138.1-3 (2010): 40-50.

[84] Bishop, Marvin, Marie Derosa, and Joanne Lalli. "Molecular dynamics simulations of one-dimensional Lennard-Jones systems." Journal of Statistical Physics 25.2 (1981): 229-235.

[85] Srinivas, Goundla, and Biman Bagchi. "Understanding the anomalous $1/t^3$ time dependence of velocity correlation function in one dimensional Lennard-Jones systems." Journal of Chemical Physics 112.17 (2000): 7557-7563.

[86] Pal, Subrata, et al. "Intermittency, current flows, and short time diffusion in interacting finite sized one-dimensional fluids." The Journal of chemical physics 116.14 (2002): 5941-5950.

[87] Lepri, Stefano, Roberto Livi, and Antonio Politi. "Thermal conduction in classical low-dimensional lattices." Physics Reports 377.1 (2003): 1-80.

[88] Dhar, Abhishek. "Heat transport in low-dimensional systems." Advances in Physics 57.5 (2008): 457-537.

[89] Narayan, Onuttom, and Sriram Ramaswamy. "Anomalous heat conduction in one-dimensional momentum-conserving systems." Physical review letters 89.20 (2002)

[90] Roy, Anjan, et al. "Tagged particle diffusion in one-dimensional gas with Hamiltonian dynamics." Journal of Statistical Physics 150.5 (2013): 851-866.

[91] Roy, Anjan, et al. "Tagged particle diffusion in one-dimensional systems with Hamiltonian dynamics-II." arXiv preprint arXiv:1405.5718 (2014).

[92] H.van Beijeren, unpublished work.

[93] Allen, Mike P., and Dominic J. Tildesley. "Computer simulation of liquids." (1987).

[94] Grassberger, Peter, Walter Nadler, and Lei Yang. "Heat conduction and entropy production in a one-dimensional hard-particle gas." Physical review letters 89.18 (2002): 180601.

[95] Das, Suman G., Abhishek Dhar, and Onuttom Narayan. "Heat Conduction in the Fermi-PastaUlam Chain." Journal of Statistical Physics 154.1-2 (2014): 204-213.

[96] Das, Suman G., et al. "Numerical test of hydrodynamic fluctuation theory in the Fermi-Pasta-Ulam chain." arXiv preprint arXiv:1404.7081 (2014).

[97] Zhong, Yi, et al. "Normal heat conduction in one-dimensional momentum conserving lattices with asymmetric interactions." Physical Review E 85.6 (2012): 060102.

[98] L. Lizana, T. Ambjörnsson, A. Taloni, E. Barkai, and M. A. Lomholt, "Foundation of fractional Langevin equation: harmonization of a many-body problem." Phys. Rev. E 81(5), 051118 (2010).

[99] H. Spohn, J. Stat. Phys. 154, 1191 (2014).

[100] Brunet, E., Bernard Derrida, and Antoine Gerschenfeld. "Fluctuations of the heat flux of a one-dimensional hard particle gas." Europhysics Letters 90.2 (2010): 20004.

[101] Holley, Richard. "The motion of a heavy particle in an infinite one dimensional gas of hard spheres." Probability Theory and Related Fields 17.3 (1971): 181-219.

[102] Ullersma, P. "An exactly solvable model for Brownian motion: III. Motion of a heavy mass in a linear chain." Physica 32.1 (1966): 74-89.

[103] Zwanzig, Robert. "Nonequilibrium statistical mechanics. Oxford University Press," 2001.

[104] Gruber, Ch, and J Piasecki. "Stationary motion of the adiabatic piston." Physica A: Statistical Mechanics and its Applications 268.3 (1999): 412-423.

[105] Gruber, Christian. "Thermodynamics of systems with internal adiabatic constraints: time evolution of the adiabatic piston." European journal of physics 20.4 (1999): 259.

[106] Piasecki, J., and Ch Gruber. "From the adiabatic piston to macroscopic motion induced by fluctuations." Physica A: Statistical Mechanics and its Applications 265.3 (1999): 463-472.

[107] Lebowitz, J. L., J. Piasecki, and Ya Sinai. "Scaling dynamics of a massive piston in an ideal gas." Hard ball systems and the Lorentz gas. Springer Berlin Heidelberg, 2000. 217-227.

[108] Kestemont, Edouard, C. Van den Broeck, and M. Malek Mansour. "The "adiabatic" piston: And yet it moves." Europhysics Letters 49.2 (2000): 143-149.

[109] Munakata, Toyonori, and Hideki Ogawa. "Dynamical aspects of an adiabatic piston." Physical Review E 64.3 (2001): 036119.

[110] Chernov, N., and J. L. Lebowitz. "Dynamics of a massive piston in an ideal gas: Oscillatory motion and approach to equilibrium." Journal of Statistical Physics 109.3-4 (2002): 507-527.

[111] White, J. A., et al. "The adiabatic piston at equilibrium: Spectral analysis and time-correlation function." Europhysics Letters 59.4 (2002): 479-485.

[112] Morriss, G. P., and Ch Gruber. "Strong and weak damping in the adiabatic motion of the simple piston." Journal of Statistical Physics 109.3-4 (2002): 549-568.

[113] Neishtadt, A. I., and Ya G. Sinai. "Adiabatic piston as a dynamical system." Journal of statistical physics 116.1-4 (2004): 815-820.

[114] Brito, R., M. J. Renne, and Christian Van den Broeck. "Dissipative collapse of the adiabatic piston." EPL (Europhysics Letters) 70.1 (2005): 29.

[115] Mansour, M. Malek, Christian Van Den Broeck, and Edouard Kestemont. "Hydrodynamic relaxation of the adiabatic piston." EPL (Europhysics Letters) 69.4 (2005): 510.

[116] Mansour, M. Malek, Alejandro L. Garcia, and Florence Baras. "Hydrodynamic description of the adiabatic piston." Physical Review E 73.1 (2006): 016121.

[117] Cencini, Massimo, et al. "Macroscopic equations for the adiabatic piston." Physical Review E 76.5 (2007): 051103.

[118] Gislason, Eric A. "A close examination of the motion of an adiabatic piston." American Journal of Physics 78.10 (2010): 995-1001.

[119] Fruleux, Antoine, Ryoichi Kawai, and Ken Sekimoto. "Momentum transfer in nonequilibrium steady states." Physical review letters 108.16 (2012): 160601.

[120] Foulaadvand, M. Ebrahim, and M. Mehdi Shafiee. "One-dimensional Brownian motion in hard rods: The adiabatic piston problem." EPL (Europhysics Letters) 104.3 (2013): 30002.

[121] Szász, Domokos, and Bálint Tóth. "A dynamical theory of Brownian motion for the Rayleigh gas." Journal of Statistical Physics 47.5 (1987): 681-693.

[122] Ya. G. Sinai and M. R. Soloveychik, "One-dimensional classical massive particle in the ideal gas," Commun. Math. Phys. 104:423-443 (1986).